Final Project Report

Project Term: 7/1/06 to 12/31/2011
Project Title: A non-point source of contaminants to the estuarine food web: Mobilized particles from the intertidal zone.
Amount Funded: $790,000

Contractor/Grant recipient contact information

Program Administrator

NAME: Raymond Torres
INSTITUTION: University of South Carolina Department of Earth and Ocean Sciences
PHONE: 803-777-4506
EMAIL: torres@geol.sc.edu

Principal Investigator/Lead Principal Investigator

NAME: Raymond Torres
INSTITUTION: University of South Carolina Department of Earth and Ocean Sciences
ADDRESS: 701 Sumter St. EWS 617, Columbia, SC 29208
PHONE: 803-777-4506
EMAIL: torres@geol.sc.edu

Granting program contact information

Technical Contact

NAME: Marina Brand
TITLE: Science Program Technical Grant Manager
AGENCY: Delta Stewardship Council
ADDRESS: 980 Ninth Street, Suite 1500 Sacramento, CA 95814
PHONE: (916)445-5031
EMAIL: marina.brand@deltacouncil.ca.gov

1. Project Summary

The San Francisco Bay and Sacramento-San Joaquin Delta (Bay-Delta) region (Figure 1) is a highly urbanized and contaminated estuary with a valuable commercial and recreational fishery (Nichlos et al., 1986; SFEI, 2004). Many fish and birds in the San Francisco Estuary exhibit high levels of contaminants (metals and organic pollutants), which have been shown to affect their behavior and reproductive success, yet routes of exposure and assimilation pathways remain unclear. A number of physiological and behavioral effects on biota have been reported such as the loss of reproductive success due to high metal stress in clams, invertebrates, fish and birds (Brown and Luoma, 1999; Brown et al., 2003; Weiner et al., 2003; Schwartzbach et al., 2005). Understanding the pathways by which contaminants are exposed to and assimilated by biota is essential to appropriately manage Bay-Delta resources and habitats to reduce the threat to the foodweb. The interplay of physical, chemical and biological processes in intertidal habitats provide one potentially significant pathway.

The processes in the intertidal habitats leading to biological activation also activate sediments with respect to contaminant exposure. First, these aggregated sediments have been shown to be elevated in contaminants, particularly metals. Second, the presence of labile organic material in contact with sediments will facilitate the processes that can increase bioavailability, such as partitioning and methylation. Also, highly energetic events – either wind- or rain-storms – are necessary to resuspend the cohesive sediments in these systems, which will preferentially concentrate them spatially and temporally. This could lead to enhanced exposure and assimilation in valuable brooding habitats at an important time for reproduction and maturation.

Understanding where, when, how, and why these processes occur is particularly important to managers and planners in the Bay-Delta region so that the proper preparations can be made for system-wide environmental changes brought on by anticipated (climate change, restoration activities) and

unanticipated (earthquakes) events. Therefore, a quantitative understanding of the combined physical, chemical, and biological processes driving local and system-wide biotic contamination is necessary to inform decision makers of future threats and remedial actions available to protect and preserve the Bay-Delta ecosystem.

The overarching hypothesis driving this study is that weather events local to the Bay-Delta area facilitate the cycling of mercury and other metals that are sorbed to intertidal zone sediments. Erosion by rainfall during low tide and wind waves at high tide may activate non-point sources of previously deposited metals (Torres et al., 2004; Torres and Fulton, submitted). Hence, wind- or rainstorms may resuspend contaminated cohesive sediments, and sediment redistribution processes may spatially concentrate them, increasing faunal exposure to metal contaminants. Several project objectives were developed to provide structure for investigating the hypothesis. These objectives are:

1. Quantify the relationship between wind and rain intensity and the elevated concentration of aggregated sediments.

2. Investigate the extent to which dissolved contaminant concentrations are influenced by resuspension of sediment aggregates containing elevated contaminant concentrations.

3. Characterize properties of particle and dissolved constituents that govern elevated contaminant load released through the mobilization process
    a. Source of particles (benthic polymers, algal, mineral, detrital, etc)
    b. Particle character (OM content, nutrients, grain and aggregate size)
    c. Partitioning

4. Estimate contribution of this mobilization process on biotic contaminant burden relative to the system background

5. Improve our ability to monitor for contaminant transport in restoration and regional settings by developing *in situ* methods for determination of contamination exposure potential using optical characterization of particulate and dissolved constituents.

To address the objectives of this study, observations and samples were collected in winter and summer of 2011 in two areas of the Bay-Delta: Liberty Island and Grizzly Bay. In-situ optical measurements of water quality parameters were complemented by the collection and analysis of

meteorological data, intertidal bulk sediment samples, and water samples during wind, rain, and fair-weather events.

Suspended sediment concentration was elevated during rain events occurring near low tide, and during wind events exceeding about 8 m s^{-1}. Suspended sediment concentrations were higher after low-tide rain events than both wind events and fair-weather background measurements. One example of each was selected for further analyses. Concentrations of selected leachable metals (^{111}Cd, ^{133}Cs, ^{208}Pb, ^{53}Cr, ^{55}Mn, ^{57}Fe, ^{60}Ni, ^{63}Cu, ^{66}Zn, ^{107}Ag, ^{89}Y and ^{146}Nd) were higher during the rain event than during the wind event. Concentrations during both events were higher than concentrations during the tidal cycle only for Cd, Cu, Ni, Zn, and Y. The weakly-bound fraction of total leachable metals differed little between rain and wind events, with the exception of Pb and Mn. The relationship between metal content and suspended sediment concentration varied widely between different metals, but indicated that rainfall mobilizes sediments from a different source than is available to wind and tidal resuspension. Particulate organic carbon, particulate nitrogen, percent organic carbon, percent nitrogen, and the carbon to nitrogen ratio were all much higher during the rain event than during both the wind event and the tidal cycle. All organic parameters increased during pulses of rainfall, and decreased steadily after rainfall ended. By contrast, the parameters varied little during the wind and tidal cycle events.

To better understand the behavior of mercury locally, two sites in the San Francisco Bay Delta, Grizzly Bay and Liberty Island were chosen to collect sediment (sampling depth: 0 – 2 and 2 – 4 cm) and water samples in winter and spring 2008. Laboratory-scale experiments were performed to investigate the impact of dissolved organic matter, especially fulvic acid, and divalent cations, i.e. calcium and magnesium on mercury release from these sediments. Total mercury concentrations in the sediments from Grizzly Bay and Liberty Island ranged between 0.12 and 0.18 mg Hg kg^{-1} sediment, and were particularly associated with organic matter (56 to 72 %). The positive correlation between the

total mercury concentration and amount of clay minerals, and total organic carbon, which are both supposed to act as sorbents for mercury, indicated that their distribution in the environment is controlled by the same factors, and explains the observed spatial variability. The highest concentration of total mercury in Grizzly Bay sediments was found in the fine sand fraction (250 – 106 μm) where the clay mineral and total organic carbon content was also the highest in comparison to all other particle size fractions. Batch extraction experiments revealed that divalent cations especially calcium and magnesium exert strong control on the mercury release from these sediments. In the presence of calcium or magnesium (0.2 mM), mercury release was significantly inhibited regardless of whether additional dissolved organic matter (5 mg C L^{-1}), which typically increase the release by forming complexes with mercury, was also present in the solution or not. A reason could be that calcium or magnesium in solution sorbs on to colloidal surfaces -- clay minerals or aggregated organic matter -- blocking the active surface sites against other dissolution agents, as well as influencing the mobilization of colloids by reducing electrostatic repulsion, favoring aggregation and inhibiting mercury release. Filtration was performed to investigate the distribution of released mercury between various size fractions (0.45, 0.1 and 0.025 μm). Results supported this idea. Thus, changes in the water chemistry in an estuarine system with regard to divalent cations and, in general, salinity which were also investigated in the present, study for the San Francisco Bay Delta could have a significant impact on mercury release; the presence of elevated amounts of calcium in the system could prevent or at least decrease the mercury release and, thus, the potential of methylation and bioaccumulation of mercury.

A combination of in situ marine optics (light absorption, attenuation and scattering), velocimeters and wave gauges provided continuous surrogates for dissolved and particulate organic matter (DOM and POM) and physical/hydrodynamic forcings due to wind and gravity waves. Calibration of the high frequency in situ surrogates was accomplished by laboratory analyses of discrete

samples collected concurrently with the instrument readings. The laboratory measurements were correlated to the in situ measurements, providing high frequency timeseries for DOM, POM, filtered mercury species, suspended sediment concentrations and particle size distribution. The time series provided the temporal scales necessary to identify and explore relationships between wind and tide driven constituents in the water column. Observed wind events at both study sites increased suspended sediment concentration, and had minor effects on particle chlorophyll-A and dissolved constituents. Filter-passing mercury concentrations were strongly related to optical measurements and ranged from 0.5 to 3.5 ng L^{-1}, while filtered methyl mercury ranged from 0.02 to 0.2 ng L^{-1}. Mercury concentration on particles ranged from 150 to 250 ng g^{-1} and were well correlated with suspended sediment concentrations ($r^2 \sim 0.75$- 0.96). Methyl mercury on particles were measured lower in winter (0.6 to 1.8 ng g^{-1}) and higher in summer (1.6 to 4.2 ng g^{-1}), possibly related to higher median particle size and algal activity found in the summer. A 1-D model of resuspension processes suggests that resuspension of intertidal sediment by wind occurs frequently.

Although rain falling during low tide does mobilize marsh sediments, with associated organic matter and metals, into the adjacent tidal creek, the effect on the nearby larger shallow waters is relatively minor. Winds, while of minor importance in the tidal creek, are a more important driver of benthic sediment resuspension in the large shallow bays but of low importance to the mobilization of contaminant metals. The overall importance of metals input to Grizzly Bay and Liberty Island by rainfall mobilization seems to be minor, but further research into the place of rainfall mobilization in local metals budgets would help to clarify the situation.

2. Budget Summary

Pending receipt of final invoices.

EXPENSE	AMOUNT INVOICED (1ST YEAR)	AMOUNT INVOICED (2ND YEAR)	AMOUNT INVOICED (3RD YEAR)	AMOUNT INVOICED TO DATE (ALL YEARS)
Salaries and Wages				
Employee Benefits				
Equipment & Facilities				
Supplies, Materials & Services				
Travel				
Subcontracts				
Indirect Costs				
Overhead				
Totals				

3. List of Tasks and Activities Performed

Data collection occurred at two study sites, Liberty Island and Grizzly Bay (Figure 1). Grizzly Bay is a shallow subembayment of Suisun Bay, in the San Francisco Bay complex. It covers 24 km^2 and is less than 2 meters in depth in most areas (Warner et al., 2004). Tides in Grizzly Bay are mixed semidiurnal with a range of approximately 2 m (Warner et al., 2004). Flooding tides enter Grizzly Bay from a deep extension of the main channel and propagate as a partial standing wave across the shallows (Cuetara et al., 2001). Suisun bay connects to San Pablo Bay via Carquinez Strait, and the freshwater input is predominantly from the Sacramento River with some discharge from the San Joaquin River.

Salinity is usually minimal during the winter rainy season, but periodic stratification may develop during the summer dry season (Cuetara et al., 2001). Liberty Island is a 5,209 acre former agricultural field complex on the Sacramento River. The area was farmed until 1998, when the levees breached and were not repaired. The site has been converting back to intertidal habitat since, and currently has marsh and mudflat areas to the north and open water to the south. It is also the southernmost part of the Yolo Bypass, a flood control diversion for the Sacramento River.

Known sources of metals into San Francisco Bay waters include historical contamination from gold, mercury, zinc, and copper mining (Nichols et al., 1986; Hornberger et al., 1999), acid mine drainage from the same (Alpers et al., 2000a; 2000b), outflows from wastewater treatment and various industrial plants (Nichols et al., 1986; Hornberger et al., 1999; Flegal et al., 2005), resuspension of contaminated bottom sediments (Ritson et al., 1999; Squire et al., 2002), runoff from agricultural fields and urban areas (Alpers et al., 2000a; 2000b), erosion of natural source rocks (Hornberger et al., 1999), and groundwater seepage (Spinelli et al., 2002). The temporal and spatial patterns in metals concentrations are controlled by a variety of physical factors. The strong rainfall seasonality in the area causes inputs of metals and fine-grained suspended sediment from urban runoff and fluvial transport from landward portions of the watershed to be greatest during winter (Cloern and Nichols, 1985; Conaway et al., 2007). Resuspension of bottom sediments and consequent remobilization of relict contaminants, however, is greatest in summer when winds and wind-wave-induced mixing are strongest (Cloern and Nichols, 1985; Conaway et al., 2003). Bottom sediment contamination tends to be higher in areas of deposition, such as mudflats, in areas of concentrated industrial activity, such as near wastewater treatment plants, and near rivers that drain historical mining areas (Conaway et al., 2003).

The field work for this project took place in winter 2011 for the rainy season deployment, and summer 2011 for the dry, windy season deployment. Winter field work was conducted between 17

December 2010 and 14 February 2011 at Liberty Island, and 15 February and 30 March 2011 at Grizzly Bay. Summer field work was conducted between 26 May and 20 June at Liberty Island, and 26 June and 14 July at Grizzly Bay. An additional deployment of weather data at Liberty Island was performed between 15 and 25 July, 2011. Personnel from the US Geological Survey (USGS) performed field and laboratory work of all water-related data, and personnel from the University of South Carolina (USC) and University of Oregon (UO) performed field and laboratory work for sediment-related data. Field and laboratory activities associated with each project task are detailed below.

3.1 Task 1: Project Administration.

Project administration was performed by Raymond Torres at USC.

3.2 Task 2: Physical, hydrodynamic, and meteorological field measurements.

A suite of equipment was deployed at each location during the winter rainy season and the summer dry season. Liberty Island deployments were between 5 January and 14 February 2011 for winter, and 26 May to 20 June 2011 followed by 15 July to 25 July 2011 for summer. Instruments were deployed at Grizzly Bay between 15 February and 30 March 2011 for winter, and 26 June to 14 July 2011 for summer. The equipment was located in shallow intertidal areas near salt marsh and mudflat (Figure 2).

Event sample collection

The wintertime equipment package included an ISCO automatic water sampler and a weather station. The ISCO sampler was triggered by a tipping bucket rain gauge and programmed to take one liter of water every five minutes, with a total of 24 samples per event. The trigger was initially set to

0.05 inches of rainfall in 15 minutes, and decreased to 0.03 inches in 15 minutes. The intake hose of the ISCO sampler was located at the water surface and kept approximately in place with a small anchor and buoy. The weather station was located on non-intertidal ground nearby. The weather station consisted of a Campbell Scientific CR1000 data logger, a Setra 278 barometer, another rain gauge, a Met One wind sensor set, and a Parsivel laser disdrometer to measure the rain drop size and velocity distribution. Measurements were recorded every 1 minute, but the Parsivel was programmed to turn on and record only when the rain gauge tipped.

During summer, the ISCO sampler was located in the same locations as during winter, but the weather stations were brought closer. The rain gauges and Parsivel were not used during summer. Instead of the rain gauge, the ISCO sampler was triggered by wind speed exceeding a changeable threshold, between 5 and 8 m s^{-1}.

Bulk sample collection

Bulk sediment samples were collected from Grizzly Bay in April 2011 and Liberty Island in July 2011. Samples were taken from marsh, mudflat, bay bottom, and levee-top (at Grizzly Bay) areas near the water sampler at both field locations. Sediments from the top approximately 2 cm were scooped into plastic bags using a plastic spoon or a spackling blade according to sediment texture and wetness. Bay bottom samples from Grizzly Bay near the sensor location were collected with a plastic push-corer in July 2011. Samples were tested for grain size distribution and concentration of adsorbed metals. Additional analyses of subaqueous sediment samples were performed as described under Task 6 below.

Data mining was performed in summer and fall of 2010 to examine extant SSC, water level, discharge, and meteorological records. Particular attention was given to the relationships between SSC and tides, winds, discharge, and rain.

3.3 Task 3: Laboratory physical and chemical characterization of sediments.

Water samples were retrieved within 18 hours of the end of sampling and refrigerated. Wintertime samples were tested with a YSI and returned to the bottle. Samples were filtered by vacuum through one Pall SUPOR PES membrane filter with 0.4 μm pore size and as many precombusted glass fiber filters with pore size of 0.45 μm as necessary to process the whole bottle. Filters were weighed before use, and dried overnight at 50°C. After weighing again, filters were stored under refrigeration until shipping in dry ice to South Carolina for further analysis. Selected rain and wind events were tested for organic and metal content.

Organic content analysis

Organic content analysis was performed by the University of Oregon, and comprised total organic carbon and nitrogen (POC, PN; mg g^{-1} sed), %OC, %N (mg g^{-1} sed), and carbon to nitrogen ratio (C:N). The diameter of the filtered area on each filter was measured with a caliper and recorded, and a punch-hole was used to subsample each filter. Three clippings were made per filter and placed into 5x9 mm silver (Ag) capsules, which were in turn placed in two labeled Teflon trays placed into a desiccator. The diameter of 10 clippings was measured with a caliper and an average value determined, to calculate the average surface area of the filter subsamples. A drop of DI water was added to the samples and a small crucible of trace metal clean 12N $HCl_{(l)}$ was placed into the desiccator. The water insured a good diffusion of the HCl fumes into the sample for IC removal. The desiccator was closed and the samples were fumed for 36-48hrs under a fume-hood. When done, the HCl crucible was removed and the desiccator lid left cracked open to allow the remaining HCl fumes to escape for 15 min. The desiccator was then covered with a piece of Al foil and placed into a drying oven for 24-36hrs at 60ºC. The Ag capsules were carefully closed using tweezers and placed into a 5x9 mm tin (Sn)

capsule. The latter was then folded into a rounded pellet and stored in labeled sample trays in desiccators until analyzed.

The analysis of POC and PN was performed by flash combustion at 1020ºC using a NC2500 elemental analyzer (CE Instruments) controlled by the EAS Clarity software (Costech Analytical Technologies Inc). Throughout the analysis, a series of six standards (L-Cystine N: 11.66%, C: 29.99%, Atropine N: 4.84%, C: 70.56% and GoniLab 2^{ndary} low C standard N: 0.119%, C: 1.298%) and two blanks were run to calibrate the analyzer response, along with four other blanks (duplicates of two different blank types) for data correction.

The C and N signal output (mV s^{-1}) of each sample was converted to mg of C and N contained in the three clippings making up the sample using the run's calibration and further corrected for blank values. Assuming a homogeneous distribution of the particles and water throughout the 47mm filter area during filtration, the mass of sediment contained in the analyzed sub-sampled filter clippings and the volume of water filtered through it were calculated, and the C and N concentration in mg L^{-1} and mg g^{-1} sediment determined.

Metals analysis

Metals analysis was performed on filtered sediments at the University of South Carolina in a metal-clean lab. Filters were quartered with ceramic scissors. One quarter of each membrane filter was subjected to sequential leaching with 25% cold acetic acid followed by 7.5N hot nitric acid. The acetic leach removed weakly-sorbed metals most likely to be bioavailable, and the nitric acid leach removed the more strongly bound metals not liberated by the acetic acid. The leachates from each process were analyzed on a Thermo Scientific Element 2 HR-ICP mass spectrometer. Total metal content was derived as the sum of the acetic leach and the nitric leach. Resulting metal content per processed sample was converted to mass of metal per gram of dry sediment.

3.4 Task 4: Laboratory physical and chemical characterization of mobilized particles and dissolved constituents.

Laboratory characterization of mobilized particles and dissolved constituents proceeded in conjunction with Task 5, and used samples collected as described in Task 5 below.

Sample processing

Bulk samples (9-12 L) were processed within 24 hours of collection (on 2 occasions = 48hrs). The sample was poured into a 20 L teflon-lined churn and subsampled for SSC analysis at the USGS lab in Marina, CA. Following the SSC, other raw samples were collected. Mercury samples were collected according to WMRL filtration procedures using a vacuum chamber and clean Teflon filter tower loaded with pre-combusted glass fiber filters (Olson and Dewild, 1999). Approximately 250 to 1000 mL of sample was passed through each filter for TSS, pTHg and pMeHg analyses. Each filter was placed in a teflon (Hg) or plastic (TSS) petri dish and frozen until analysis. The filtrate was collected in the appropriate bottle for fTHg, fMeHg, DOC, and optical analyses.

Particulate analyses

Suspended sediment concentration was measured according to work done in Gray et al. (2000). Total suspended sediment concentration was measured gravimetrically on pre-weighed filter pads at the CAWSC.

All THg and MeHg analyses were performed at the USGS Mercury Research Laboratory in Middleton, Wisconsin (http://wi.water.usgs.gov/mercury-lab/). Total Hg analysis followed U.S. EPA Method 1631. Aqueous samples were pretreated by the addition of 1–2 percent (v/v) 0.2 N Bromine monochloride (BrCl) to solubilize and oxidize all forms of Hg to reactive mercuric ion (Hg2+).

Samples were placed in an oven at 50°C for a minimum of 12 h to accelerate the oxidation reaction. Oxidation was considered complete when excess BrCl was present, detectable by a faint yellow color. Immediately prior to analysis, a small amount of hydroxylamine hydrochloride (NH2OH–HCl) was added to each sample until the residual color from added BrCl disappeared. Approximately 10 min after BrCl reduction, 0.5 ml of stannous chloride (SnCl2) was added to the sample within the bubbling flask to reduce the Hg2+ to Hg(0). The Hg(0) was purged from samples with Hg-free N2 gas and concentrated onto a gold-coated, glass bead trap. Finally, gold traps were heated and the Hg(0) thermally desorbed into an Argon gas stream and quantified by cold vapor atomic fluorescence spectroscopy (CVAFS). The daily detection limit (DDL) for these specific analytical runs during total Hg analysis was 0.02 ng L^{-1} and the precision, measured as the relative percent difference (RPD) between analytical duplicates, averaged 10% (n = 7).

Methylmercury analyses were performed using USEPA method 1631 following standard distillation and ethylation procedures described in detail elsewhere *(*DeWild et al, 2002; Horvat et al., 1993*)*. MeHg isotope ($Me^{199}Hg$; 30 pg) was added to all samples to assess recoveries on an individual basis. Briefly, this method calls for isolation of all ambient MeHg and amended $Me^{199}Hg$ from the sample matrix by atmospheric pressure water vapor distillation. The MeHg in the distillates was derivatized using sodium tetraethylborate and preconcentrated onto a Carbo trap column. Detection and quantification was after thermodesorption, isothermic GC separation, and detection by ICP/MS [Hintelmann and Evans, 1997] which permitted independent quantification of ambient MeHg and added $Me^{199}Hg$. Hg masses were corrected on the basis of the internal standard recovery. Across all samples, recoveries averaged 101 ± 5%. The daily detection limit using the combined method with isotope dilution was 0.01 ng L^{-1}. Precision, measured as the relative percent difference (RPD) between analytical duplicates, averaged 12% (n = 7 pairs).

Dissolved analyses

DOC was measured by high-temperature combustion oxidation using a Shimadzu TOC-VCPH total organic carbon analyzer. Reported DOC concentrations are the averages of duplicate analyses. Standard deviation for the DOC measurement was ± 0.2 mg L^{-1}, and the method detection limit was 0.2 mg L^{-1}. Reported DOC concentrations are the averages of duplicate analyses. Standard deviation for the DOC measurement was± 0.2 mg L^{-1}, and the MDL was 0.2 mg L^{-1}. Absorbance at 254 nm (A254) was determined using a photo-diode array UV-Visible spectrophotometer with a 1 cm path length (Model 8453, Agilent). Specific ultraviolet absorbance (SUVA254) values were determined by dividing the UV absorbance measured at λ = 254 nm by the DOC concentration and are reported in the units of liter per milligram carbon per meter (Weishaar et al., 2003). SUVA254 is commonly used as an indicator of DOC aromaticity (Chin et al., 1994; Weishaar et al., 2003).

3.5 Task 5: Physical, chemical, and optical characterization of mobilized particles and dissolved constituents in the field.

In situ instrumentation was deployed in Grizzly Island and Liberty Island for multi-week periods in Winter 2010, and Summer 2011, and left unattended except for weekly service visits to download data, clean optical sensors and replace filter cartridges. Sampling periods of at least two weeks were chosen in order to resolve spring-neap frequency of the tides. Discrete samples were collected during service breaks and over the sampling period, usually during the time of greatest tidal range to capture the maximum variability in constituent concentration (DOC, Hg species) and character. Laboratory optical measurements (absorption and fluorescence) and DOC were cross-calibrated with the accompanying in situ optical measurements.

Moored instrumentation system

The moored instrument package consisted of a stainless steel cage containing submersible sampling pumps, membrane filters, underwater batteries, optical, acoustic and hydrographic sensors (Figure 3). Measurements were collected over multiple weeks at 30 min intervals via two simultaneously pumped flowpaths; a filtered flowpath for measurement of optical properties related to dissolved constituents and an unfiltered flowpath for characterization of particulates. Pumps and instruments were controlled and most data logged using an in situ data and power handler (DH-4, WET Labs). Other ancillary measurements were collected using their onboard dataloggers. All data was merged and corrected to Pacific standard time (PST) using MATLAB scientific software.

Fluorometers: DOM and Chlorophyll-A fluorescence

The fluorescent fraction of the DOM pool (FDOM) was measured in situ using a WETLabs WETStar single-band excitation-emission in situ fluorometer (370 nm excitation, 10 nm full width half max, FWHM; 460 nm emission, 120 nm FWHM). The fluorometer was installed in the filtered path after the ac-9 spectrophotometer. The fluorometer was cleaned using lens papers, 0.5% solution of Liquinox®, and organic-free water, plus a final rinse of organic-free water as described in the users' guide provided by WET Labs. Blank water offsets were collected before every field deployment and subtracted from the field measurements. Raw data collected from the WETStar fluorometer were converted from volts DC (VDC) to quinine sulfate units (QSU) using the factory-supplied QSU scale factor (units of $\mu g\ L^{-1}$). A WETLabs WETStar chlorophyll–A fluorometer was used to measure the fluorescence of chlorophyll containing phytoplankton, which absorbs light of wavelengths between 400 and 520 nm and fluoresces light between 670 and 730 nm.

Photometers: Absorption, Scattering and Attenuation

In situ optical measurements of absorbance (a), scattering (b), and attenuation (c) measurements were completed using two WETLabs ac-9 model spectrophotometers (WETLabs, Inc., Philomath, OR, USA) designed to measure absorbance and attenuation in visible wavelengths ranging from blue to red (412 to 715 nm). Dissolved optical measurements were acquired using one of the ac-9 meters, with the flow cells pumped through a 0.2 um membrane filter. Particulate optical measurements were acquired simultaneously using a separate pump flow path, using a 2.5mm Teflon screen to prevent large debris from plugging the flow tubes of the particulate ac-9. The ac-9 flow cells and detectors (absorption flow cell and attenuation flow cell) were cleaned using a combination of lens papers, 0.5% solution of Liquinox®, and organic-free water, plus a final rinse of organic-free water. Blank water (>18.0 MOhm) offsets were checked in the lab before and after each field deployment, and monitored in the field by logging air reading before and after weekly service.

Dissolved absorption (a_g) and particulate absorption (c_p) were corrected for scattering errors using spectral scattering measured value at 715 nm and that value subtracted from the remaining spectra. Particulate scattering is computed from the difference between attenuation and absorption ($b_p = c_p - a_p$) thus, removing any effects of dissolved absorption (mainly chromophoric) from the particulate absorption fraction. This is relatively important as the fraction of the dissolved absorption in the total attenuation can be significant.

Photometric parameters: Spectral Slope (a_g, c_p slopes)

Spectral slope (S_{ag} , S_{cp}), known to be a relative indicator of composition, was calculated from ac-9 data using a non-linear least squares curve fitting technique (Del Vecchio and Blough, 2002). The absorption (a_g) data from 440 to 650 nm were used to determine S_{ag} with higher values related to lower molecular weight or fresher organic materials of microbial or algal origin (Twardowski et al., 2004).

Similarly, particulate attenuation (c_p) spectrum from 440 to 650 nm were used to determine the slope of c_p (S_{cp}), using a nonlinear least squares (power) fit, which is related to the shape of the particle size distribution, with lower values related to a higher median bulk particle size (Boss et al., 2004).

Temperature, Specific Conductance, pH, Dissolved oxygen and Turbidity

Two YSI model 6920 V2 instrument (YSI, Inc., Ohio, USA), equipped with sensors for specific conductance, temperature, depth, pH, dissolved oxygen (DO) and turbidity, were deployed on the main instrumentation package. The instrument was retrieved weekly for cleaning and data retrieval, as well as calibration checks with known standards. The turbidity sensor reports output in formazin nephelometric units (FNU). Because optical characteristics of sediment vary with particle size and composition, water samples must be collected to calibrate the sensor for local sediment characteristics. Water samples were collected to relate FNU to suspended-sediment concentrations (SSC), in milligrams per liter (mg L^{-1}) of suspended sediment.

Nitrate (Satlantic ISUS)

Filtered water was pumped through an ISUS optical nitrate sensor (Satlantic Inc., Halifax, Novia Scotia, Canada), which calculated NO3 concentrations using the absorption spectrum from 217-240 nm. A linear baseline correction of the raw ISUS data was required to correct for a constant offset relative to lab NO3- concentrations ($y = 1.194 * ISUS_{NO3} - 0.068$). Instrument precision is ± 0.5 μM and accuracy is reported at ± 2 μM.

Particle Size Distribution (LISST)

A Laser In-Situ Scattering and Transmissometer (LISST-100x, type C) from Sequoia Instruments (Sequoia Scientific, Bellevue, WA, USA) was utilized to measure the particle size distribution (PSD) of particles 2.5 to 400 microns in diameter and total volume concentration. The open

path LISST used the compute_mean.m MATLAB script available from Sequoia Scientific (Hill et al., 2000; Mikkleson et al., 2006).

The PSD data was further processed to analyze particle dynamics over the time period sampled. Three size fractions have been identified to analyze flocculation in estuaries, 2.5-36 μm represents single grain fraction, 36-133 μm represents microfloc fraction, and >133 μm represents the macrofloc fraction (Eisma, 1986; Mikkelsen et al., 2006). Flocs that aggregate and de-aggregate have been identified as potential transport mechanisms for heavy metal contaminants and are also an indicator of organic matter, since organic matter is a necessary constituent needed to form flocs (Eisma, 1986).

Waves/Tides

Wave statistics were measured with a Seabird Electronics SBE-26 Wave and Tide Gauge. The SBE26 was setup to measure short period wind waves (< 4seconds in duration). Work done by Jones and Monosmith (2007, 2008) in the Delta, showed that peak short period waves ranged from 0-0.5m in Grizzly Bay and 0-0.3m in Franks Tract. As the depths of water in Franks tract is similar to Liberty Island (although the fetch may be much different), we used the approach of Jones and Monosmith to measure short period waves. The SBE26 is not capable of measuring both large period waves (e.g. gravity waves 12-16 hours) and short period waves at the same time, due to the limitation of the fundamental sampling frequency of 4Hz. Using the following setup parameters: water depth (2m), Instrument height above bottom (0.7m), Spectral Estimates per band (5-10), Wave sample duration (0.25 seconds), and wave samples per burst (256; outlined below), we were able to measure a frequency span of 0.0938 to 0.8750 Hz (or 1.14 to 10.66 seconds) with a spectral bandwidth of 0.1563 Hz (or 6.40 seconds).

The raw data from the SBE26 was processed using SeatermW from SeaBird Electronics to compute surface wave statistics and time series of wave height, wave period and energy contained in the

surface waves. These data allow for the calculation of maximum shear stress (τ_w) at the bed exerted by the waves (Chung et al., 2009). Using the small amplitude wave theory τ_w can be calculated from the fluid density, wave orbital velocity, and the bottom friction factor, which is a function of the wave Reynolds number, this equation reduces to:

$$\tau_W = \rho \left(\frac{H_W \pi}{T_W \sinh\left(\frac{2\pi H}{L_W}\right)} \right) \sqrt{\frac{2\pi\mu}{\rho}} \tag{1}$$

where ϱ is the fluid density (which is a function of temperature, salinity and suspended solids), H_w is the wave height, T_W is the wave period, H is the water depth, L_W is the wavelength, and μ is the dynamic viscosity. This calculation allows us to differentiate between shear stress at the bed induced by currents or waves, and determine if increased suspended sediment is a result of wind induced sediment re-suspension.

Acoustic Velocimetry and Acoustic Backscatter Intensity

A Nortek Aquadopp 2Mhz acoustic Doppler current profiler (ADCP) from Nortek, AS, was used to measure vertical profiles of water currents, and relative suspended sediment concentration (SSC) using the acoustic backscatter intensity (ABS). For the Liberty Island summer deployment we used an Aquadopp with high resolution (HR) technology. This technology utilizes pulse coherent technology which allows for low noise measurements, which increasing accuracy of the measurement, and burst sampling, which allows for turbulence estimates (Rusello, 2009). This increased accuracy and burst sampling capability of the Aquadopp HR allows for estimation of turbulent kinetic energy (TKE) in the water column. The Aquadopp was successfully deployed for a portion of both Grizzly Bay deployments, and the Aquadopp HR was deployed for the duration of the Liberty Island summer

deployment. The Aquadopp was not deployed for the Liberty Island winter deployment because of logistical complications.

The Aquadopp was programmed to sample a vertical profile of water with 40 bins at 0.1 m increments for a total water profile of 4m. The sample period was 1 minute and a sampling frequency of 15 minutes. This allowed for velocity resolution of 1.3 cm s^{-1} in the vertical and 4.0 cm s^{-1} in the horizontal. The Aquadopp HR was programmed to sample a vertical profile of water with 28 bins at 0.03m increments for a total water profile of 0.84m. The sample period was 1.5 minutes at 2 Hz burst sampling, and a sampling frequency of 15 minutes.

The raw Aquadopp data is converted in the software Aquadopp (Nortek, AS) to convert binary data into ASCII data. These data sets are further analyzed in MATLAB to compute vertically averaged water current and ABS for each 15 minute time step. The residual water current data is computed using a Godin filter, which is a resultant of three moving averages, 24 hr (2) and 25 hr (1). This computation allows us to determine the net transport time scales of a parcel of fluid within the domain of the measurement location.

An ancillary data variable that is output from the Aquadopp is echo intensity (EI) or ABS, which is a measure of the amount of material that scatters sound in the water. The feasibility of relating this measurement to total SSC has been tested and compared with other instruments to determine overall accuracy of this method to measure SSC (Gartner, 2004; Gray and Gartner, 2009). In order to accurately determine the correlation between ABS and SSC corrections to account for losses due to (1) acoustic spreading (2) water absorption and (3) particle attenuation must be made (Lohrmann, 2001). The result of these corrections yields an ABS measurement that can be used to correlate to SSC:

$$ABS = EI * 0.43 + 20\ log_{10}(R) + 2\alpha_w * R \tag{2}$$

where *EI* is the variable output by the Aquadopp, *R* (m) is the range along the acoustic beam, and α_w (dB m^{-1}) is the water absorption coefficient, which is found to be constant value of 1 for a 2MHz system through a range of salinities (0-35 ppt). This measurement allows for examination of relative vertical profiles of SSC.

To generate vertical profiles of TKE, we used the inertial dissipation method (Gross and Nowell, 1985; Lorke, 2007). This parameter yields information about the turbulent energy contained in the water column. In the context of particle dynamics this information is pertinent because floc size is partially a function of the Kolmogorov length scale (the smallest energy containing eddy), and can help us better understand the PSD data generated from the LISST.

Meteorological data

Meteorological data was acquired from the California Irrigation Information System (CIMIS) network (*http://wwwcimis.water.ca.gov/cimis/welcome.jsp*). These data include wind speed and direction, precipitation, and solar radiation. For the Liberty Island data set we selected station Dixon # 121 located at 38°25.20 'N, 121°47.40'W, approximately 19 Km to the northwest from the measurement location. For the Grizzly Bay data set we selection station Concord #170 located at 38°0.74 'N, 122°0.80'W, approximately 10 km to the south of the measurement location. To properly analyze the wind speed and direction data as it relates to the surface wave data from the SBE26, the wind vector was rotated along the axis which is aligned with the maximum fetch. For the Liberty Island deployment this vector is in the north wind component, and for the Grizzly Bay deployment this is vector is the northeast wind component. The precipitation data allows us to examine the influence of rainfall runoff in the context of our in situ measurements, and the solar radiation data can be used to determine surface heat flux, as it can relate to diurnal nutrient cycling.

Discrete sample collection

Discrete field water samples for water quality and sediment analysis were collected throughout the deployments using USGS clean-sampling procedures including; (1) equipment constructed of noncontaminating materials cleaned rigorously before field work and between field sites; (2) handling equipment in a manner that minimizes the chance of altering ambient sample composition; (3) handling samples in a manner that prevents contamination; and (4) routinely collecting quality-control (QC) samples (U.S. Geological Survey 2006). Multiple vertical samples were collected throughout the water column in close proximity to the deployed instrumentation using a clean PVC pole and 2L PETG bottle. The 1.5L to 2L subsamples (approximately 4 to 7) were composited into a 13L fluorinated jerrican, double bagged, and placed in an ice-filled cooler until return to the lab for processing.

Water samples were analyzed for TOC, TN, %OC, %N, and C:N by the University of Oregon. All liquid samples were kept frozen and thawed as needed. The filtration system used was a home-made vacuum driven unit composed of: two dual head vacuum pumps (Barnant Air Cadet, 0.02 HP, P/N 420-2901), one 6 inch internal diameter PVC sewer pipe used as filtered-water holding tank (capacity of 9 liters) and a four filters manifold made of schedule-40 PVC parts and four 500 ml magnetic funnels/filters holders (Pall Life Science, P/N 28150-496). Prior to each sample filtration, funnels were washed with DI water and the filter holders fitted with 47mm GF/F filters (Whatman, P/N 1825-047). Filters had been previously combusted (450ºC, 3 hrs) in a furnace (Fisher Scientific, Isotemp Muffle Furnace), pre-weighed (Ohaus, Explorer Pro, Model EP64C) and individually stored in a labeled Petri dish.

The containers holding the liquid samples were generously shaken to ensure homogenization and partially poured into a 1liter graduated cylinder. After recording the volume, the liquid was filtered. This process was repeated as many times as needed until either the whole container was emptied or the

filter was mostly clogged (very slow filtration speed). Prior to removal, filters with samples were rinsed with DI water to remove salt. The total filtered volume was then determined and recorded. The filters were placed back into the labeled Petri dishes, and placed half-uncapped into an oven (VWR, model 1340) at 60ºC and left until dry (typically 24hrs). Each filter was then re-weighed to determine the "filter + sample" weight. Subtracting to this value the initial unloaded filter weight allowed the determination of the sample weight. Finally, TSS (mg L^{-1}) was obtained by dividing the sample weight by the volume of water filtered. Petri dishes were then closed and stored until needed for elemental analysis. Analysis proceeded as described above for the filtered sediments (Task 3).

3.6 Task 6: Partitioning and redox effects on metals cycling.

For this study sediment material from intertidal deposits and water samples were collected at two sites in the Sacramento-San Joaquin Delta in Northern California (Figure 1, Table 1), in the course of two field sessions: (1) Grizzly Bay, sampled in January/April 2008, and (2) Liberty Island, sampled in April 2008. In order to assess spatial and seasonal changes due to hydrodynamic processes, different sampling depths (0 - 2 and 2 - 4 cm) were investigated during the first field session. Based on results obtained from subsequent laboratory analyses, a sampling level of 0 - 2 cm was only studied in the second field session. All sediment samples were collected manually using a 7-cm-diameter clear polycarbonate (Lexan®) core tube tightened on to a 2 m polyvinyl chloride (PVC) driver head equipped with a check valve (Benthos Inc.). After retrieval of the core, the material was separated with an acid-cleaned plastic sheet, stored in clean glass jars with Teflon-lined lids, and shipped in coolers to the USGS in Boulder, CO. The temperature, pH, conductivity, dissolved oxygen and turbidity of the water were measured at Grizzly Bay and Liberty Island (0.61 m under water surface) using a YSI 6920 V2-0 Multi-Parameter Water Quality Sonde connected to an YSI-650 display data logger. Water samples

were collected at each site in 20 L high-density polyethylene (HDPE) carboys, which were shipped on ice over night to the USGS in Boulder, CO.

Sediment samples

Sediment samples from Grizzly Bay were freeze-dried for 3 days using a VirTis Unitop 600 L vacuum chamber and a VirTis Freezemobile 35ES. After Charm (1967), this method can be used for fine-grained, homogenous material without harming individual grains. Since samples from Liberty Island were poorly sorted, air-drying for 3 days at room temperature was chosen. After drying and disaggregation with mortar and pestle, composite samples were prepared for each investigation area as described in Table 2. This procedure allowed assessment of the general chemical character of the sediment for each study area and provided enough material for the subsequent analyses and experiments (Table 2).

To avoid an impact from coarse particles like shell fragments or brick on the results of the batch extractions experiments, composite samples from Grizzly Bay were sieved with a mesh size of 250 µm and Liberty Island samples with a mesh size of 1180 µm (using U.S. Standard Testing Sieves - A.S.T.M. E-11 Specifications). The different sieve mesh sizes were chosen for this separation step in order to maintain the general grain size distribution because the sediment samples from Liberty Island were notably coarser and less sorted than the samples from Grizzly Bay. Based on field observations and laboratory results (accounts only for the second field trip), additional composite samples were prepared from sediment samples of selected areas of the field site grid (Table 2). The two January composite samples from the sampling depth of 0 - 2 cm – GB1 and GB2 - were used for all mercury release experiments. All other composite samples were used for comparative experiments (Table 2).

Water samples

Collected water samples from Grizzly Bay and Liberty Island were filtered within 24 hours (Bird et al., 2003) using high capacity disposable filter capsules from Geotech with a pore size of 0.45 μm. Samples were stored at 4 °C in a refrigerator until analyses for cations, anions, and selected metals, as well as fractionation, quantification and characterization of the dissolved organic matter (DOM).

Particle size analysis

Particle size distribution was determined by dry-sieving according to the classification system of the United States Department of Agriculture (USDA) (Jackson, 2005). For each run 15 g of the composite sample was sieved through a set of stainless steel sieves (U.S. Standard Sieve Series, A.S.T.M. E-11 Specifications) with the following micron mesh sizes: 1180, 500, 250, 106, and 53 (Table 3).

Sieves were weighed out before (tare weight) and after sieving to calculate the net weight of each sediment fraction, and subsequently normalized to the initial sediment input. In addition to the classification of all composite samples (Table 3), sieving was also carried out to achieve material for analyzing mineralogy, total organic carbon (TOC) and total mercury (T-Hg) of each available sample fraction. Based on the relative percent difference (RPD) between the initial sediment input and the sum of all corresponding fraction net weights, a mean method error of 1.1 % was calculated.

Quantitative XRD analysis

The mineralogical composition of all composite solid samples and corresponding size fractions was ascertained by quantitative X-ray diffraction analysis (XRD) using a Siemens D-500 X-ray diffractometer with graphite monochromator. According to the instructions in Srodon et al. (2001), a sample amount of 1.0000 g was mixed with an internal standard (0.1111 g ZnO), and ground with 4 mL

of methanol in a McCrone micronizing mill for 5 minutes. The mixture was filled in a plastic beaker, and then dried for more than 10 hours at 85 °C in a lab oven. The dry material was disaggregated with mortar and pestle, sieved (500 μm), and side packed into an XRD holder against frosted glass. While filling material into the holder, tapping on a hard surface insured random distribution. Samples were X-rayed by Cu K-alpha radiation from 5 to 65 degrees, with a step size of 0.02 degrees two theta (Eberl, 2003). To calculate the mineral composition of the powdered sample in weight percent, measured X-ray patterns were entered in the computer program RockJock 5, aligned to stored XRD patterns of standards and pure minerals, integrated to intensities, and then compared to intensities of the internal standard (Eberl, 2003). The total mineral sum is 100 ± 5 % due to inaccuracies in sample preparation and inconsistencies in chemistry and microstructure of minerals. The minimum detection limit (MDL) for each mineral is 1 wt % (Eberl, 2008). Analyses were assisted by D. D. Eberl and A. E. Blum, both from the USGS Boulder, CO.

TOC analysis

For total organic carbon (TOC) analyses, 10 to 15 mg of sediment material was filled in pressed tin capsules and stored unfolded together with a beaker of concentrated trace metal grade hydrochloric acid (HCl, approximately 50 mL) for 12 hours in a desiccator to remove inorganic carbon (Bergamaschi, 2008). TOC concentrations were determined from all composite samples and particular size fractions in duplicate. The samples from the first field trip were analyzed using a PDZ Europa ANCA-GSL elemental analyzer interfaced to a PDZ Europa 20-20 isotope ratio mass spectrometer at the University of California (UC; Stable Isotope Facility) in Davis. TOC of the sediment samples from the second field trip were determined by the laboratory of the California Water Science Center (U.S. Geological Survey in Sacramento, CA) using a Perkin Elmer 2400 Series II CHNS/O Analyzer. Reproducibility was checked for all samples by the Huffman Analysis Laboratories in Golden, CO.

Total mercury analysis

Total mercury (T-Hg) concentrations of all composite samples and their particular size fractions were determined by atomic absorption spectrometry (AAS) using a Milestone Direct Mercury Analyzer (DMA-80) with a silicon UV photodetector. In the course of analyses, liquid and solid samples were first dried to prevent sample loss, and then decomposed according to a predefined temperature-time-program (Table 4). An oxygen stream passing through the drying and combustion furnace carried the released mercury vapor to a gold amalgamation trap where mercury was then subsequently desorbed for quantitative detection (Milestone SRL 2007).

A sequence of five standard solutions in the range of 0 - 30 ng Hg(II) was run at the beginning of each measurement to set up a low (0 - 20 ng) and a high (20 - 30 ng) calibration curve (Milestone SRL 2007). T-Hg concentrations of the sediment samples were determined as average from duplicate measurements of approximately 50 to 100 mg material, weighed out in nickel boats. Random accuracy checks were performed using WQB-1 (NWRI 1984) and TH-2 (NWRI 1992), as well as NIST® Standard Reference Material 1944: New York-New Jersey Waterway Sediment (NIST 1999). According to the manufacturer, the instrument detection limit is 0.005 ng of mercury (Milestone SRL 2007). Analyses were assisted by C. A. Gerbig, USGS Boulder, CO.

Quantification of selected mercury forms

To quantify mercury associated with organic matter, chelated in strong inorganic complexes, or as mercuric sulfide, selective extraction steps were performed (described in Table 5) according to the reported method in Bloom et al. (2003). The following composite solid samples and particular size fractions were chosen for extractions based on results from T-Hg and TOC analyses: GB1, GB2, and LI1, the size fraction 250-106 μm from GB1, GB2 and LI1, as well as < 53 μm from LI1. Samples were analyzed for total dissolved mercury as described above.

DOC analysis

Dissolved organic carbon (DOC) concentrations of unfiltered and filtered sample solutions were determined by persulfate wet oxidation with subsequent infrared detection using an O.I. Analytical Model 700 TOC analyzer. High concentrations of chloride (greater than 0.7 g Cl L^{-1}) in solutions interfere with DOC analyses by wet oxidation (Aiken, 1992), thus, samples from Liberty Island and Grizzly Bay (e.g. Table 6, no. 3C) were analyzed using the catalytic high-temperature combustion TOC analyzer from Shimadzu Scientific Instruments (Model: TOC-V CPH). The MDL for TOC according to the manufacturer is 4 μg C L^{-1} (Shimadzu, 2008). Carbon standards were run on both instruments in the range of 0.2 - 30.2 mg C L^{-1} every 10 samples. At the beginning of each run quality control standards containing caffeine or sodium benzoate were analyzed and checked for recovery.

UVA and SUVA

UV absorbance measurements were performed on a Hewlett-Packard photo array spectrometer (model 8543) at a wavelength of 254 nm, using a quartz cell with a path length of 1 cm and a detection range of 0.1 - 4 cm^{-1} according to the manufacturer. Samples were warmed up to room temperature before analyses, and ultrapure water (UPW) was measured as blank every 10 samples. Interferences with UV light are known for iron in concentrations greater than 0.5 mg Fe L^{-1}, and nitrate greater than 40 mg NO_3^- L^{-1} (Weishaar et al., 2003). Hence, the iron concentration of each sample solution was checked by ICP-MS analyses. Calcium- and magnesium-stock solutions which were used in some batch extractions experiments contained substantial amounts of nitrate; UV results from these experiments were corrected with a separate experiment blank. The specific UV absorbance (SUVA) can be used to estimate the aromatic carbon content of DOC (Weishaar et al., 2003). SUVA was calculated for each solution by normalizing the measured UVA [cm^{-1}] at a wavelength of 254 nm to the DOC concentration [mg L^{-1}]. UVA and SUVA data of experiments were used to determine changes in DOC characteristics.

Fractionation of DOC and fluorescence spectroscopy

DOC fractions from Grizzly Bay and Liberty Island water were acquired by adsorption on nonionic macroporous resins (XAD-8/XAD-4 resin method described e.g. in Aiken et al., 1992) by J. Riggs, USGS Boulder, CO. The DOC concentration of each fraction (hydrophobic organic acid fraction (HPOA), hydrophobic organic neutral fraction (HPON), hydrophilic fraction (HPI), transphilic organic acid fraction (TPIA) and transphilic organic neutral fraction (TPIN)) was normalized to the DOC measured for the whole Grizzly Bay and Liberty Island water. Fluorescence spectra were recorded at an excitation of 370 nm using a Jobin-Yvon FluoroMax-3® instrument. Data were processed by K. Butler, USGS Boulder, CO, and K. Cawley, University of Colorado in Boulder, CO. The fluorescence index (FI) is calculated from the ratio of the emission intensity at a wavelength of 470 nm to that of 500 nm, and reveals information of the source of aquatic fulvic acids (McKnight et al., 2001).

Mercury analysis

Mercury concentrations of unfiltered and filtered sample solutions were determined by cold vapor atomic fluorescence spectroscopy (CVAFS) using a PSA 10.025 Millenium Merlin mercury analyzer following the instructions of EPA method 1631 (Telliard and Gomez-Taylor, 2002). Immediately after sample collection the preservative bromium chloride (BrCl) was added to each solution to oxidize all mercury forms to total dissolved mercury Hg(II) which is stable in solution. After an oxidation time of at least 24 hours, each sample was reduced with hydroxylamine hydrochloride ($NH_2OH{\cdot}HCl$) to remove free halogens. Instrumental stannous chloride ($SnCl_2$) was added to convert Hg(II) to volatile, elemental mercury Hg(0) which then was purged out of the solution by high purity argon gas. During analyses a sequence of six calibration standards in the range of 0 to 100 ng Hg(II) L^{-1} was run every 10 samples. A MDL of 1.12 ng Hg(II) L^{-1} was calculated for the

instrument, based on the 3-σ-criterion which is the standard deviation (STD) above the average instrument response chosen for 1.5 ng Hg(II) L^{-1} standards (n = 71) multiplied by three.

Cation, anion and elemental analysis

Cation (sodium, potassium, ammonium, magnesium and calcium) and anion (chloride, sulfate and nitrate) analyses were performed for the batch extraction experiments, Grizzly Bay and Liberty Island water using a Dionex DX-120 Ion Chromatograph (IC). Since hydrogen carbonate (HCO_3^-) was not determined, quality controls in the form of electrical balance calculations were not conducted. Selected elements (aluminum, barium, calcium, copper, iron, magnesium, manganese, nickel, potassium, sodium, strontium and zinc) were analyzed for the batch extraction experiments, Grizzly Bay and Liberty Island water in the laboratories of the Center for Trace Analysis at the University of Southern Mississippi (Prof. A. M. Shiller) using a Thermo Finnigan Element 2 sector-field inductively coupled plasma mass spectrometer (ICP-MS), and an internal standard of 2 ppb of indium. All sample solutions were acidified with 1 % trace metal grade nitric acid (HNO_3) after filtration or centrifugation. MDL´s were calculated based on the 3-σ-criterion.

Contamination control

Membrane filter discs, syringe filters, and Nalgene® Oak Ridge centrifuge tubes were tested for contamination of mercury or organic matter (OM) on samples using UPW as test solution. New cleaning procedures were established based on the results of the equipment tests. For other laboratory equipment (e.g. glassware, HDPE bottles, Corning® centrifuge tubes), cleaning steps were adopted from previous studies (Süß 2006) combined with knowledge and experience of the USGS laboratory in Boulder, CO. These steps included rinsing with UPW followed by soaking in aqua regia (24 hours) with or without subsequent burning in an oven (6.5 hours, temperature: 450 °C).

Standards, stock solutions and chemicals

Chemicals used in experiments and analyses were all from Fisher Scientific, unless otherwise noted. Stock solutions and calibration standards of mercury analyses were prepared from NIST® Standard Reference Material 3133 (NIST 2007).

For the buffered batch extraction experiments a 1 M phosphate buffer for pH, and a 3 M sodium perchlorate ($NaClO_4$) stock for ionic strength. For DOM stock solutions used in batch experiments, a freeze-dried, fractionated fulvic acid isolate (F1-FA, Table 6) from a marshland in the Northern Everglades (Ravichandran et al., 1998; Haitzer et al., 2003) was used after dissolution in UPW. A 1 M calcium stock (as calcium nitrate $Ca(NO_3)_2 \cdot 4H_2O$), and a certified, 10,000 mg Mg L^{-1} magnesium solution (ChemScan AS, as magnesium nitrate $Mg(NO_3)_2 \cdot 6H_2O$) was employed in calcium and magnesium experiments.

Equipment tests

Equipment (e.g. filters and centrifuge tubes) was checked for experimental applicability before starting with the batch extraction experiments. All tests were performed in duplicate except the syringe filter tests.

Different test solutions, containing mercury, DOM, or sodium chloride (NaCl), were run stepwise (in 50 ml steps) through Pall® filter discs (diameter: 47 mm) and Acrodisc® syringe filters (diameter: 25 mm) with pore sizes of 0.45, 0.2 and 0.1 μm in order to identify possible contamination or adsorption effects of mercury or DOM. Filter media of all applied filters was hydrophilic polyethersulfone (Supor® membrane: low in protein binding and for single-use). All filtered samples, as well as initial, unfiltered solutions were analyzed for Hg(II), DOC, and UVA.

Centrifuge tubes (Nalgene® Oak ridge with polypropylene copolymer (PPCO) cylinders and polypropylene (PP) plug seal caps, 50mL) were exposed for 3 hours to test solutions according to the

time interval, subsamples of batch extraction experiments were usually stored in centrifuge tubes. Afterwards, unfiltered solutions were analyzed for Hg(II), DOC, and UVA, and compared to initial test solution results. Pipette tests (Fisherbrand® Finnpipette®) were performed by determining the STD between the defined volume which was set on the pipette and the average of ten actual pipette steps. The volume of UPW for each step was calculated from the measured weight and temperature.

Quality control of mercury analyses

To assure the quality of the method performance for mercury determination, and the accuracy and precision of duplicate samples, a quality control experiment according to the procedures of Telliard and Gomez-Taylor (2002) was performed. A 10 mL subsample from the solution of an unbuffered batch extraction experiment (without additional DOM) was spiked with a known amount of mercury (100 % of the initial mercury concentration), and compared to the background mercury concentration of the other, non-spiked 10 mL of the solution. The experiments were performed for each sediment sample in duplicate. The recovery of the spike (%R) was calculated as follows after Telliard and Gomez-Taylor (2002):

$$\%R = 100 \cdot \frac{(A - B)}{T} \tag{3}$$

where: *A* = measured concentration of Hg(II) in sample after spiking

B = measured concentration of Hg(II) in sample before spiking

T = calculated spike concentration The accuracy and precision of the measured duplicate samples were determined by calculating the RPD after Telliard and Gomez-Taylor (2002):

$$RPD = 200 \cdot \frac{(D1 - D2)}{(D1 + D2)} \tag{4}$$

where: *D1* = concentration of Hg(II) in spiked sample

D2 = concentration of Hg(II) in duplicate spiked sample

EPA method 1631 (Telliard and Gomez-Taylor 2002) requires the recovery of matrix spikes to be in the range of 71 – 125 %, and for the relative percent difference to be a maximum of 24 %.

Experimental conditions

Batch extraction experiments were conducted to investigate the effects of several key aspects on the mercury release from composite samples of Grizzly Bay and Liberty Island (GB1, GB2 and LI1): buffered and unbuffered extraction experiments in combination with OM (fulvic acid isolate F1-FA), the influence of divalent cations (calcium, magnesium), and the effect of water from Liberty Island. Two grams of the sample material was suspended in a total volume of 200 ml in glass jars with Teflon-lined lids (wrapped in aluminum foil to prevent photoreactions), and equilibrated for 24 hours (Süß 2006) in an end-over-end mixing apparatus (Figure 4) with 4.5 rotations per minute (rpm).

Additionally, two sediment samples MCL131B and MCL134B1 from McLaughlin Reserve (Coastal Range, CA, USA), investigated in detail in a previous study (Süß 2006) and described in Table 7, were used for verification of the results in these experiments (Table 8, no. 0A, 3C) with a soil to liquid ratio of 1 g 200 mL^{-1}. Batches were run in duplicate for each experiment, and supplemented by two blank replicates which were prepared in the exact same way but without the addition of sediment material. The average of the respective experimental blanks was used to correct the sample extraction results for DOC, UV, Hg(II), cations and anions. The amount of released mercury and OM specified based on the amount of sediment used in the batch experiment.

The pH value in the buffered release experiments (Table 8, no. 0A/B) was adjusted to 6.4 ± 0.1 (STD calculated from the pH of 60 experimental solutions) by adding a 1 M phosphate buffer. The ionic strength was set to 0.1 M in solution with NaClO4 (Ravichandran et al., 1999; Haitzer et al., 2003). To investigate the general release of mercury, OM, major anions and cations from the sediments

in the absence of buffers and additional reagents, experiments were conducted with UPW (Table 8, no. 1A).

For the DOM-batch extraction experiments which were carried out in unbuffered and buffered solutions, a DOC concentration of 5 mg C L^{-1} was achieved by the addition of the stock solution prepared from the F1-FA isolate. In further unbuffered batch extraction experiments, with and without addition of DOM (5 mg C L^{-1}), a sediment to liquid ratio of 20 g 200 mL^{-1} was employed to investigate in detail the impact of OM on the release of mercury (Table 8, no. 1B, 2C).

The effect of divalent cations was studied in the presence and absence of OM (5 mg C L^{-1}) in unbuffered batches. Calcium nitrate or magnesium nitrate was added to establish a concentration of 0.2 mM calcium or magnesium (Table 8, no. 3A/B, 4A/B). Furthermore, experiments with Liberty Island water (Table 8, no. 3C) were performed before and after the removal of divalent cations by cation exchange. To achieve cation exchange the water was run with a flow rate of approximately 0.07 mL s^{-1} through a Spectra/Gel® cation exchange resin with sulfonic acid as the active group to remove divalent cations like calcium against sodium.

Separation techniques and subsampling steps

After sample equilibration for 24 hours, solutions were filled in Corning® centrifuge tubes (PP cylinders with polyethylene (PE) plug seal caps) and centrifuged at 2700 rpm for 8 minutes (Fisher Scientific, accu Spin ™ 1/1R, round-bucket centrifuge). Centrifuge time was calculated to remove particles with a diameter of 0.45 μm using an integrated form of Stokes law (Jackson, 2005):

$$t_{min} = \frac{63{,}0 \cdot 10^8 \cdot \eta \cdot \log_{10} \cdot \frac{R}{S}}{(N_m)^2 \cdot (D_{\mu m})^2 \cdot (\Delta s)} \quad (5)$$

with: η = viscosity [P] = $\left[\frac{g}{cm \cdot s}\right]$ = 0.00894 (at 25°C)

R = radius of rotation of the top of the sediment in the centrifuge tube [cm] = 1

S = radius of the rotation of the surface of the suspension in the tube [cm] = 9

N_m = rotations per minute of the centrifuge [rpm] = 2700 rpm

$D_{\mu m}$= particle diameter [µm] = 0.45 µm

Δs = difference in specific gravity between solvated particles and solution [-] = 1.65

(density of water at 25°C = 0.997071 $\frac{g}{cm^3}$; particle density of quartz = 2.65 $\frac{g}{cm^3}$)

t_{min}= time for sedimentation [min]

After the first separation step, subsamples for analyses and further separations were obtained by filtration through a 0.45 µm membrane filter disc (Pall® Supor®, diameter: 47 mm, filter media: hydrophilic polyethersulfone), pre-cleaned with 150 ml UPW.

The first 50 mL of filtered sample solution was wasted for membrane rinsing and pH measurement (Beckman Instruments, pH-meter ϕ 210). The pH-meter was calibrated using buffer solutions of pH 4.00, 7.00 and 10.00. According to the manufacturer the accuracy is 0.01 pH-units. The remaining solution of 150 ml was filtered. Samples of 50 ml were taken for mercury (CVAFS), DOC, elemental (ICP-MS), cation and anion analyses (IC), as well as UV absorbance and fluorescence measurements (Figure 5). The remaining 100 ml were used for the second filtration step with the 0.1 µm membrane filter disc (including equilibrating with 50 ml solution) and the corresponding subsampling.

To investigate the distribution of the released mercury between various size fractions for the buffered batch experiment (Table 8, no. 0A/B), the supernatant of the first centrifugation step was subsequently separated by vacuum filtration (microns: 0.45 and 0.1), or spinning in a superspeed

centrifuge (SORVALL®, Superspeed RC2-B, angle-head centrifuge). Centrifugation was carried out for mercury in the fractions < 0.45, < 0.1 and < 0.025 μm according to the time and speed recommended by the manufacturer (Table 9). Nalgene® Oak Ridge centrifuge tubes (PPCO cylinders with PP plug seal caps) were used for centrifugation. Subsampling occurred in the same way as described previously.

3.7 Task 7: Modeling intertidal contributions to system turbidity and biotic contamination.

The model analysis focuses on development and evaluation of a one-dimensional (horizontal), time-dependent model of the particle size, concentration and optical and acoustical properties. The model reveals effects of sediment resuspension by bottom shear stresses produced by waves and currents, horizontal transport of suspended particles by turbulence, gravitational settling of particles, and particle aggregation and disaggregation.

4. Achieved Objectives, Findings, and Major Contributions

4.1 Findings and Major Contributions

Task 2: Physical, hydrodynamic, and meteorological field measurements.

Suspended sediments and weather data were collected during rain events in January 2011 at Liberty Island and February and March 2011 at Grizzly Bay, and fair-weather tidal cycle data collected in April. No rain events occurred at Liberty Island in January, but 5 occurred at Grizzly Bay in February and March (Figure 6). The average 15-minute rainfall intensity per event was 2 mm hr^{-1}, with an average total accumulation per event of 20.52 mm and average duration of 175 minutes. Average

rainfall kinetic energy per event was 134.09 W m^{-2}. Wind speed varied up to 14 m s^{-1} and averaged 2.88 m s^{-1}, while the wind direction was predominantly southwesterly.

Of the 5 rain events recorded in February, 2 occurred during low tide. The suspended sediment concentration during low-tide rain events was noticeably higher than the SSC observed during high-tide rainfall or during a fair-weather tidal cycle (Figure 7A). The average SSC during the tidal cycle was 94.03 mg L^{-1}, but the average SSC during the two low-tide rain events was 343.69 and 337.85 mg L^{-1}. Furthermore, the SSC varied by about 400 mg L^{-1} during the course of a low-tide rain event, but remained rather steady during the tidal cycle and high-tide rain events. The suspended sediment concentration in the 16 February event was higher than that observed during the 13 March event, as was the rainfall intensity and duration, so the 16 February event was chosen for closer analysis.

The rainfall on 16 February began just after low tide, and featured two pulses of heavier rain within lighter drizzle (Figure 8). The kinetic energy in the initial pulse reached a maximum of 689.5 W m^{-2}, and totaled 2794 W m^{-2}. SSC increased from 199 to 464 mg L^{-1} during this first pulse and continued to rise a little during the subsequent lighter rain. The second pulse of heavier rain began about 1 hour after the first ended, and featured lower maximum and total kinetic energy (329.8 and 1842 W m^{-2} respectively). SSC had begun to decrease before the second pulse, but increased again by another 184 mg L^{-1} during the second rainfall pulse. The rain event transported 2.47 kg L^{-1} of sediment during the 2 hour sampling window, for a rate of 343.69 mg L^{-1} s^{-1}.

Suspended sediments and weather data were collected during the summer windy season as well. Wind speed at Grizzly Bay in July 2011 varied up to 10 m s^{-1}, with an average value of 3.98 m s^{-1}, while the wind direction was predominantly southwesterly (Figure 9). No rain was observed. Suspended sediments were sampled during 4 wind events, with 30-minute average wind speeds of 6 m s^{-1}, 6 m s^{-1}, 7.5 m s^{-1}, and 8 m s^{-1}. Suspended sediment concentration tended to increase slightly during sampling or

remain steady (Figure 7B), with values between 60 and 163 mg L^{-1} for all but the 8 m s^{-1} wind event, which was about 100 mg L^{-1} higher. The suspended-sediment concentrations during the 8 m s^{-1} wind were the highest of all the wind events, so that set of samples was selected for further analysis.

The 13 July wind event at Grizzly Bay featured winds between 7 and 9 m s^{-1} from the west (Figure 10). The 30-minute running average wind speed exceeded the trigger value of 8 m s^{-1} for 11 minutes and stayed above 7.8 m s^{-1} for a further 23 minutes. SSC began at 663.33 mg L^{-1}, then dropped to 218.0 mg L^{-1} and increased steadily throughout the 2 hour sampling window to a value of 304.67 mg L^{-1}. The wind event transported 2.13 kg L^{-1} of sediment over the 2 hour window, for a rate of 295.64 mg L^{-1} s^{-1}.

Winds at Liberty Island during summer were weaker than those observed at Grizzly Bay, up to 7 m s^{-1}, while the predominant wind direction remained southwesterly (Figure 11). Only two wind events were sampled at Liberty Island due to problems with the equipment. In both cases SSC varied up to 120 mg L^{-1}, but SSC varied little during the 5 m s^{-1} event and increased in a stepwise fashion during the 6 m s^{-1} event.

During the tidal cycle sampling event on 30 March 2011, no rain was observed. Winds varied between 0 and 5 m s^{-1} from the south to southwest (Figure 12). SSC was steadily close to 100 mg L^{-1} throughout the first half of the sampling period, but increased to 167 mg L^{-1} just after low tide. This higher SSC was also preceded by an hour of stronger winds. SSC nevertheless remained below 170 mg L^{-1} throughout the tidal cycle event. During the tidal cycle, 0.69 kg L^{-1} of sediment was transported for a rate of 95.71 mg L- s^{-1}.

Task 3: Laboratory physical and chemical characterization of sediments.

Metals analysis

Metals analysis was run on three sets of samples from Grizzly Bay: the fair weather tidal cycle, the 2-16-11 rain event, and the 7-13-11 8 m s^{-1} wind event (referred to as tidal, rainy, and windy events hereafter). Forty-one elements were measured, 7 of which are known contaminants in the study area (Ag, Cd, Cr, Cu, Ni, Pb, and Zn) (e.g. Lu et al., 2005). Table 10 lists the measured elements along with the content per dry weight of sediment and the content normalized to values listed in the North American Shale Composite (EarthRef.org database version, accessed 27 October 2011) for the three events. Iron had the highest overall content, followed by Al and Mn. Normalized values were greater than 1 for 10 elements, indicating enrichment beyond average upper continental crust: ^{133}Cs, ^{167}Er, ^{208}Pb, ^{7}Li, ^{53}Cr, ^{55}Mn, ^{60}Ni, ^{63}Cu, ^{66}Zn, and ^{107}Ag. Of these elements, only Cs, Er, and Li are not reported in the literature as current or historical contaminants. Twelve metals were chosen for further analysis: ^{111}Cd, ^{133}Cs, ^{208}Pb, ^{53}Cr, ^{55}Mn, ^{57}Fe, ^{60}Ni, ^{63}Cu, ^{66}Zn, ^{107}Ag, ^{89}Y and ^{146}Nd. These elements are either known contaminants, elevated with respect to the NASC, or rare earth elements provided for contrast.

The total leachable metal content in suspended sediment samples was higher during the rainy event than the windy event for most of the 12 target metals (Figure 13). Only Fe, Cr, Cs, and Ag were similar in content for the first 60 minutes of both events. After 60 minutes, however, when the rain stopped, these four elements increased in content above the windy samples. The other 8 metals were consistently higher in rainy suspended sediments than windy, up to 2.8 times higher on an event-averaged basis and up to 6 times higher in individual samples. The wind event occurred within the 2 hours before low tide and the rain event in the two hours after. The average metal content for this 3.5 hour subsection of the tidal cycle was higher than both the wind and rain events for Fe, Pb, Cr, Cs, and Ag, and comparable to the rain event content for Mn. Only 5 metals had higher concentrations during

the rain event than during the tidal cycle: Cd, Cu, Ni, Zn, and Y. In all five cases the low tide average was comparable to the wind event metal concentrations.

The fraction of total leachable metal that was leachable by acetic acid indicates the fraction of metal that was weakly adsorbed to the sediment and therefore presumably labile or bioavailable. The acetic-leached fraction of the 12 target metals varied from close to zero up to 0.9, with the highest bioavailability in Cd and Mn, and the lowest in Cs and Ag (Figure 14). The acetic leachable fraction was very similar between the rainy event and the windy event for most metals, with a few exceptions. Cu and Cd had slightly lower bioavailability during rain than during wind, while Ni and Zn were slightly higher. The bioavailable fractions of Pb and Mn were very similar between the rainy and windy events until the rain stopped (at about 60 minutes into sampling). After this time the bioavailable fractions of both elements increased in the rainy samples relative to both the windy samples and the first half of the rainy samples. The highest acetic-leachable fraction was seen in Cd and Mn and the lowest in Ag and Cs.

The relationship between total leachable metal content and SSC was highly variable between metals and between types of event. Most of the metals had no apparent trend in the relationship during the rainy event, but there were a few with distinct trends (Figure 15). Fe, Zn, Cr, Pb, and Cs decreased with increasing SSC. Mn, and Cu, however, increased with increasing SSC. Furthermore, several metals were present in concentrations noticeably different from the range of concentrations during the tidal cycle. Cs, Pb, Ag, Cr, and Fe were all lower during the rain than during the tidal cycle, while Cu and Cd were higher during the rain. During the windy event only Pb, Nd, and Zn displayed a noticeable trend with respect to SSC, in this case decreasing (Figure 16). During the tidal cycle sample, the only metal with a relationship to SSC was Cu, which increased with increasing SSC (Figure 17).

Nutrients analysis

Nutrients analysis was run on the same sets of samples as the metals analysis. Particulate organic carbon (POC), particulate nitrogen (PN), percent organic carbon (%OC), and percent nitrogen (%N), and the carbon-nitrogen ratio (C:N) were all higher during the 2-16-11 rain event than during either the 7-13-11 wind event or the tidal cycle sampling (Figure 18). The range of each of these parameters was also much greater during the rain event. POC varied between 25.96 and 165.03 mg g^{-1} dry sediment during the rain event, but was between 15.98 and 45.98 mg g^{-1} during the wind event and 24.23 to 46.23 mg g^{-1} during the tidal cycle. PN varied from 2.72 to 10.27 mg g^{-1} during the rain event, 1.57 to 4.08 mg g^{-1} during the wind event, and 2.73 to 4.59 mg g^{-1} during the tidal cycle. Organic carbon percent ranged from 2.6 to 16.5% during the rain event, but was 4.6% and lower for the wind and tidal cycle. Percent nitrogen varied between 0.27 and 1.03% during the rain, 0.27 and 0.46% during the wind, and 0.16 and 0.41 during the tidal cycle. Values of C:N were the closest of the measured parameters, varying from 10.1 to 18.7 during the rain event, 7.7 to 15.6 during the wind event, and 10.6 to 15.9 during the tidal cycle. Means and ranges of variability were similar between the tidal cycle and the wind event, indicating that the major differences seen in the rainy event are due to rainfall runoff from marsh and levee sediments that are not exposed to wave and tidal resuspension.

During the rain event, C:N increased gradually until the rain stopped, after which values decreased steadily (Figure 19). Other measured parameters were more stable throughout the sampling period, increasing slightly during rainfall and decreasing slightly after it stopped. All parameters increased briefly following pulses of increased rainfall kinetic energy, with the greatest increases seen at minute 50, about 10 minutes into a burst of concentrated rainfall.

Both values and timeseries of measured parameters were quite different during the wind event and the tidal cycle (Figure 20). All mean values were lower for the wind event than during the rain

event, and the ranges of variation were much smaller. The timeseries of the measured parameters remained relatively steady during the wind event, varying within a much smaller range and exhibiting neither an increasing nor decreasing trend. During the tidal cycle, ranges of variability were smaller than both the wind and ran events (Figure 21). Means of C:N, PN, and POC were lower than both events, but %OC and %N were intermediate between the values generated by the rain and wind events, albeit closer to the wind event values.

Task 4: Laboratory physical and chemical characterization of mobilized particles and dissolved constituents.

Mercury relationships

Mercury speciation (THg and MeHg) and partitioning (particulate and dissolved) are intimately linked with organic matter in the environment potentially allowing the use of in situ optical measurements as proxies for tracking Hg cycling and transport in dynamic systems (Bergamaschi et al., 2011; Dittman et al., 2010). The underlying hypothesis of the study was to identify whether enhanced organic signature of both resuspended particulates and dissolved constituents in the pore water liberated during resuspension events would relate to enhanced contaminant transport. Therefore, the identification of the relationships between the different Hg species and their distribution is essential to understanding whether the same processes that mobilize particulate organic matter (POM) and dissolved organic matter (DOM) do in fact also mobilize mercury such that pelagic biota are more exposed to this contaminant. Because other toxic metals, pesticides and organic contaminants share the strong association with OM, the relationships between Hg and OM serve as a general indicator of this process

on contaminant mobilization in the greater Delta ecosystem. Please see Task 5 below for physical and optical data.

Particulate total mercury (pTHg)

Relationships between pTHg and in situ optical proxies for particle concentration differed between sites. Despite the difference between sites, the in situ relationships were relatively strong within each site, such as for turbidity (Figure 22A). Similar but weaker site-specific relationships were observed for particle absorption and particle attenuation (not shown). The difference between sites was in spite of the strong relationship between pTHg and TSS across both sites and seasons (Figure 22B), suggesting that the difference between sites was a result of optically different particles rather than a mere difference in particle concentration. The Grizzly Bay site showed strong relationships between particle scattering and TSS suggesting difference in particle character, such as reflectivity, may have affected the optical relationships (not shown). At the Liberty Island site, TSS was more closely related to optical absorbance and fluorescence than scattering, suggesting the light field of the water may affect the relationship.

Overall, there was a relatively consistent Hg concentration on the particles averaging 190 ng g^{-1} and a full range of 150 to 250 ng g^{-1} across all discrete samples collected (Figure 22B). These concentrations were lower than expected based on previous published values of 300 ng g^{-1} in background suspended sediment for the San Francisco Bay and Delta (Wood et al., 2010; Bouse et al., 2010).

Particulate monomethyl mercury (pMeHg)

The relationship between TSS and particulate MeHg showed a seasonal effect with summer MeHg concentrations higher than winter and a weak relationship across sites within season (Figure 23A). The MeHg content of the particulates was highly variable across seasons with low values

occurring in winter (0.6 to 1.8 ng g^{-1}) and higher values occurring in summer (1.6 to 4.2 ng g^{-1}). The difference between seasons was not explained by organic content or carbon:nitrogen ratios which varied little across sites or season (data not shown). The only explanatory variable for the seasonal difference was the median particle size (D50) measured by the LISST (Figure 23B). Although there are limited data for in situ particle size, the observed trend covers each site during a different season which adds confidence to the explanatory power of the relationship. Alternatively, algal activity could also play a role in the site specific relationship because Chl-a fluorescence was also strongly related to pMeHg concentration in Grizzly Bay (Figure 23C).

The ratio pMeHg to pTHg normalizes the relative MeHg content from general particle concentration effects and can be used as an indicator of comparing net MeHg production in the particle source environment (Mitchell and Gilmour, 2008). The absorption slope, an indicator of DOM character, shows a different relationship within each site as relative pMeHg content increases with slope (Figure 24A). The relationship is not as apparent in the visible part of the spectrum measured in the lab or in situ (Figure 24B-D) which, may reflect the influence of Fe on absorption slopes in the ultraviolet range (Weishaar et al., 2003; Pullin et al., 2007). Alternatively, an increase in A_{500}-A_{650} in summer may be responsible for the relative decrease in S_{ag} and S_{cp} compared to the ultraviolet slope range. This could be attributed to the effect of algal activity.

Filter-passing (dissolved) total mercury (fTHg)

The filter passing (dissolved) fraction of THg was strongly related to in situ optical measurements, particularly FDOM (Figure 25A) and ag440 (Figure 25B). The relationship appears to differ at Grizzly Bay in the winter, showing a steeper slope when isolated. The relationships with the laboratory measurements were similar to the in situ relationships (Figure 25C and D), although

absorbance measurements in near ultraviolet (350 to 370 nm) collected in the lab improved the overall relationship across sites and seasons (Figure 25D).

Filter-passing (dissolved) monomethyl mercury (fMeHg)

Similar to fTHg, the filter passing (dissolved) fraction of MeHg was strongly related to in situ optical measurements, particularly FDOM (Figure 26A) and ag440 (Figure 26B); however, the relationship was stronger for ag440 compared to FDOM due to better discrimination in the highest samples from Liberty Island. Also unlike fTHg, there did not appear to be a different relationship for the winter Grizzly Bay samples, instead it appeared there was no relationship in the summer samples from Grizzly Bay. The relationships with the laboratory measurements were similar to the in situ relationships (Figure 26C and D), although absorbance measurements in the ultraviolet (280 nm) collected in the lab improved the overall relationship across sites and seasons, especially the Grizzly Bay summer samples, compared to the visible wavelengths measured in situ (Figure 26D).

Task 5: Physical, chemical, and optical characterization of mobilized particles and dissolved constituents in the field.

Liberty Island

In situ measurements revealed a dynamic suspended sediment field at Liberty Island closely related to physical and meteorological measurements (Figure 27). Major turbidity, particle absorption and particle attenuation peaks were observed in association with high wave energies (>40 J m^{-2}) associated with winds exceeding 8 m s^{-1}. In both the winter (12/29/10) and summer (6/5/11) deployments high wind events produced elevated particulates in the water column at low tides (Figure 7A and E). A large wind event was observed in the summer deployment (6/19) but a higher tide stage

appeared to depress the particulate response in the water column (Figure 27). Smaller wave energies (10 J m^{-2}) and moderate winds (4-6 m s^{-1}) also produced indications of elevated particulate concentrations in the water column but the effect was not consistent depending on wind direction and water depth. Moderately elevated signals were also observed during tidal shear.

Particle character also appeared to change following wind events but to a very small degree. Particle size (S_{cp}) decreased following the large wind events (12/29 and 6/5) but the opposite effect was observed on 6/19. The opposing effects appear to be related to the turbulent field; higher turbulence may be responsible for disaggregation of flocs and organic particles, while more moderate turbulence may have resuspended larger aggregates or encourage floc formation. The algal fraction of the particles, measured as chlorophyll-A fluorescence, also responded both tidally and to wind events (Figure 27D, 27H) and showed a strong negative correspondence with NO_3 over the semi-diurnal tidal record suggesting uptake or growth dynamics. No marked difference in the change in particle character was observed between storms with wind and rain and those with just wind.

In situ measurements of dissolved constituents showed less response to local physical or meteorological events than particulate measurements (Figures 27 and 28). Dissolved species do not appear to respond to wind events but respond strongly to regional water levels (watershed-scale runoff signal) and tidal stage (non-local exchange response). The increases in FDOM and ag440 correspond with increases in stage at the nearby Lisbon Weir on 12/24/10 and 1/2/11 which reflect a watershed scale response to widespread rainfall events. A smaller variation in FDOM and ag440 was related to tidal exchange with increases associated with lower tides.

Grizzly Bay

Turbidity peaks occurred primarily with wind events ion 2/25/11 and 3/7/11 when winds exceeded 8 m s^{-1}, the same threshold observed in Liberty Island (Figure 29). There were no wind events

greater than 4 m s^{-1} measured at the CIMIS station in the summer deployment (Figure 29G). Despite the low summer winds, moderate to high wave energies were observed on 6/28, 7/10, 7/12, 7/13, 7/14 (Figure 29F). The cause of these high wave energy events is unclear but may be related to a localized wind pattern not seen at the CIMIS station.

Small changes in particle character were also observed following wind events, at a scale similar to Liberty Island. The algal fraction measured by chlorophyll-A fluorescence responded to resuspension on only one occasion in the winter (Figure 29D). Chlorophyll-A also increased on two occasions in the summer deployment (Figure 29H).

In situ measurements of dissolved constituents were less affected by wind events at Grizzly Bay (Figures 29 and 30). Dissolved species do not appear to respond to wind events but respond strongly to regional rainfall signal and tidal signal (non-local response). During the winter deployment, both FDOM and ag440 increased with decreasing specific conductance (Figures 30A, B, D) but did not show any short-term increase due to local rainfall events (Figure 30C). At Grizzly Bay, the regional rainfall runoff signal is best seen in the specific conductance at the deployment site (Figure 30D) rather than stage because the stage in this part of the estuary is controlled more by tide stage than upstream river stage. In the summer, FDOM and ag440 decreased with decreasing specific conductance and then increased as the range in specific conductance varied more tidally (Figures 30E, F, H). In this case, the conductance was less related to upstream river flows of freshwater changing the conductance within Grizzly Bay than a change in the tidal exchange between Grizzly Bay and the more river dominated channel of Suisun Bay measured at the deployment site. The low conductance, low FDOM period was likely a representation of river water dominating the deployment site when Grizzly Bay was isolated from the instrument location during above normal flows caused by large dam releases of snow melt in

early summer 2011. The ensuing increase in both conductance concentration and range suggests that Grizzly Bay became reconnected to the deployment site.

Task 6: Partitioning and redox effects on metals cycling.

Preliminary experiments

Equipment tests

Equipment deployed in this study was tested in preliminary experiments in order to identify possible contamination effects of mercury or DOM from experimental equipment, or loss of both by sorption on experimental equipment. Test solutions were designed to investigate both cases. All samples of the batch experiments had to be filtered prior to analyses. Therefore, it was necessary to check on interactions of mercury or DOM with the filter membrane and their influences on experimental results. Two filtration techniques were tested for their applicability; vacuum filtration using filter discs (tests performed in duplicate) and filtration with Acrodisc® syringe filters both from Pall® with Supor® membrane and pore sizes of 0.45, 0.2 and 0.1 μm.

The data in Figure 31 indicate a loss of Hg(II) in the range of 16 % (0.45 μm) to 25 % (0.1 μm) for the syringe filters, and 25 % (0.45 μm) to 62 % (0.2 μm) for the membrane filter discs in the first filtration step (0-50 ml) for the test solutions B1 (90 ng Hg(II) L^{-1}) and B2 (90 ng Hg(II) L^{-1} and 10 mg L^{-1} from the fulvic acid isolate F1-FA). For the subsequent 50 mL filtration step syringe filters showed recoveries in the range of 91 % (0.45 μm) to 71 % (0.1 μm), and achieved from the beginning of filtration more steady mercury recoveries than the membrane filter discs (Figure 31).

Test solutions (B1 and B2) were spiked with 90 ng Hg(II) L^{-1}, and with or without additional DOM (10 mg F1-FA L^{-1}). Recoveries as vertical bar charts in % are normalized to the concentrations in unfiltered solutions. Tested filter pore sizes: 0.45, 0.2 and 0.1 μm.

A notable increase in comparison to the first filtration step was observed for the Hg(II) recoveries of the membrane filter discs that ranged for the second filtration step between 92 % for the 0.45 µm filter and 48 % for the 0.2 µm filter. However, the mercury loss through the 0.2 µm membrane filter disc was in all experiments inexplicably higher ranging between 31 to 62 % compared to the suitable results of all other filter types and pore sizes (Figure 31). Regarding the results for the DOC containing test solution (B2), a loss of 19 % DOC through sorption on the membrane filter discs was observed for the first filtration step. The second filtration step revealed a DOC loss in the range of 2% (0.45 and 0.1 µm) and 7 % (0.2 µm). DOC recoveries for syringe filters were in all filtration steps 2 % (0.1 µm) to 6 % (0.45 µm) above the initial concentration of the test solution. Except for the unsuitable 0.2 µm membrane filter disc, the 0.45 and 0.1 µm membrane filter discs showed after equilibration with 50 mL test solution in general enhanced recoveries in Hg (II) and DOC than the syringe filters.

Test filtrations with UPW were carried out to estimate the amount of UPW necessary for pre-rinsing and pre-cleaning the filters to avoid contaminations from the filter membrane. Mercury and DOC concentrations in the filtered solutions decreased from the first 50 ml step with maximum concentrations of 3.7 ng Hg L^{-1} and 0.6 mg C L^{-1} for the membrane filter discs, and 0.0 ng Hg L^{-1} and 0.4 mg C L^{-1} for the syringe filters to a minimum level underneath the detection limits in the subsequent filtration steps.

Since in all experiments, the whole batch solution was filtered through a 0.45 µm membrane filter disc first (Table 8), a test was run to investigate the clogging influences from suspended sediment material on the experimental results. Therefore, batches were prepared in duplicate with Grizzly Bay composite samples GB1 and GB2 (Table 2), and after 24 hours equilibration, run stepwise (in 30 ml steps) through the membrane filter disc. Results in Figure 32 show, except for the first Hg(II) and DOC concentration (equilibration of the filter membrane), even concentrations for mercury and DOC with 0.8

± 0.0 ng Hg(II) L^{-1} and 0.2 ± 0.0 mg C L^{-1} for GB1, and 0.6 ± 0.0 ng Hg(II) L^{-1} and 0.2 ± 0.0 mg C L^{-1} for GB2.

Centrifuge tubes

Nalgene® Oak Ridge centrifuge tubes were used to investigate the distribution of mercury release between various size fractions by spinning in a SORVALL® RC2-B superspeed centrifuge. Before starting the batch extraction experiments, ultrapure water was stored for 3 hours in centrifuge tubes to assess the potential release of mercury and OM from the tube walls. Based on the background concentration of mercury in UPW, 0.5 ± 0.2 ng Hg(II) L^{-1} was released from the tube walls (Table 11) which is below the MDL of the mercury analyzer.

DOC concentrations were unaffected from the storage in the centrifuge tubes (Table 11). The loss of Hg(II) and DOC from solution by sorption on the tube walls was determined by using test solutions spiked with 90 ng Hg(II) L^{-1} and with or without additional DOM (10 mg F1-FA L^{-1}). Results for mercury indicate a loss of mercury in the range of 9 % for the test solution without additional DOM and 31 % with additional DOM. DOC loss for the test solution with additional DOM was 2 % (Table 11).

Quality control of mercury analyses

Interferences of the solution matrix, as well as precision and accuracy of Hg(II) analyses by CVAFS were studied on GB1 and GB2 extractions from unbuffered batch experiments (without additional DOM) according to the procedures of Telliard and Gomez-Taylor (2002). Measured Hg(II) concentration of solutions before and after spiking, and the calculated spike recovery, as well as RPD were performed. The RPD which is a measure of the precision and accuracy was calculated for all spiked duplicate samples in this control experiment and did not exceed with a maximum RPD of 15 % the defined EPA quality control acceptance criteria of 24 % (Telliard and Gomez-Taylor, 2002). Effects

of the solution matrix were assessed by determining the recovery of the spike that was added to each sample solutions. Calculated spike recoveries were with 77 to 101 % in the range of the recommended quality control acceptance criteria of the EPA Method 1631 with a range of 71 – 125 % (Telliard and Gomez-Taylor, 2002).

Characterization of sediment samples

Particle size distribution

A major task in the characterization of the sediment samples was the determination of the particle size distribution by sieving. The classification of the size fractions (Table 3) was accomplished according to the system of the USDA outlined in Jackson (2005) but limited by the lack of available sieves in standardized mesh sizes. However, the differences in the particle size ranges between the set of sieves used in this study and the USDA classification system were very small, except for the size fractions "very coarse sand" and "coarse sand" (Table 3) which, thus, were summarized as one group "coarse sands" in this study.

Grizzly Bay sediment samples were dominated by clay and silt in the range of 66 to 72 %, followed by very fine sand (except for GB5) with a range of 19 to 31 % (Figure 33). All other size fractions were present as minor constituents in amounts of 8 to less than 1 %. Hence, sediments at Grizzly Bay can be characterized as well-sorted clayey silt.

Small variations in particular size fractions between the composite samples (Table 2) reflect the spatial changes in the sediment composition of the site as a coarsening trend from the margin into the estuarine basin. GB1 represents the general particle size distribution of the sediments in Grizzly Bay in 0 - 2 cm sampling depth and GB3 for 2 - 4 cm, whereas GB2 and GB4 show the conditions close to Grizzly Island in January and April 2008, and GB5 from the farthest sampled section at Grizzly Bay in April 2008 (Figure 33). Due to the initial size distribution of the sediments, the sieving of composite

samples through the 250 µm sieve did not change the bulk composition of sediment samples that were used in batch experiments.

Liberty Island sediments (LI1) were poorly sorted and dominated by medium sand with 32 % (Figure 33). Compared to unproblematic sample preparation of Grizzly Bay samples for sieving, Liberty Island samples were difficult to handle because air-drying caused the generation of aggregates that were not possible to grind entirely by mortar and pestle. Hence, underestimation of fine material was not avoidable. Other methods, such as wet-sieving, would have caused a change of the sediment chemistry.

Since the very coarse sand fraction of the sediments (4 %) contained only debris of brick stone, the sieving of composite samples through the 1180 µm sieve did not affect the initial composition of sediment samples that were used in batch experiments.

Mineral composition

The mineral composition was determined for each composite sediment sample, as well as corresponding size fractions by XRD analyses. At the Grizzly Island site, sediments were dominated by non-clay minerals, especially quartz, which ranged from 27 to 45 %, and feldspar (plagioclase and kalifeldspar) with approximately 26 % (Table 12). Clay minerals such as illite, chlorite and serpentine were present in lower quantities (25 to 41 %, Table 12). A general increase in the clay mineral content from January (25 %) to April (32 to 41 %) with the concurrent decrease of the non-clay mineral quartz (from 40 to 27 %) was particularly investigated for the corresponding sampling sites GB2 (January) and GB4 (April) at Grizzly Bay, and for GB5 (April) in comparison to GB4. Besides this overall seasonal and spatial shift in the mineral distribution, a further change (all minerals > 1 wt % MDL) was noticed in the composition of the minor constituents of the non-clays. Unlike the samples from January, the ones from April contained the iron oxide maghemite in amounts of 2.5 to 2.8 % (Table 12). The

analyzed size fractions of the corresponding composite samples showed notable quantitative differences in the mineral composition especially for the 106 - 53 and 106 - 250 µm fractions. The 106 - 53 µm fractions were characterized by higher amounts of quartz ranging between 47 and 55 %, and lower quantities of clay minerals (20 to 25 %), the 106 - 250 µm fractions contained more clay minerals (34 to 49 %), and less amounts of quartz and feldspar.

In contrast to the sediments from Grizzly Bay, the composite sediment sample from Liberty Island was dominated by clay minerals (68 %) such as illite, smectite, and chlorite. The non-clay minerals quartz and feldspar were present in equal amounts of approximately 16 % (Table 12). The size fraction < 53 µm differed from the general mineral composition, containing more feldspar (19 %) and quartz (19 %), and less clay minerals (59 %). With increasing particle size fraction, the ratio of all three changed gradually to the mineral distribution of the composite sample. Due to the adherence of phyllosilicates to other particles, uncertainties within the different size fractions exist. However, a preferred accumulation of minerals in a certain particle size fraction was not investigated and, thus, a correlation between grain size and mineral composition like clay minerals was not achievable (R^2= 0.43 Spearman rank correlation, significance level $\alpha = 0.05$).

TOC and total mercury concentration

Total organic carbon concentration in composite sediment samples ranged from 4.1 to 7.5 mg C g^{-1}, and total mercury concentration from 0.12 to 0.18 mg Hg kg^{-1} (Table 13). GB1 and GB3, representing the same investigation area at Grizzly Bay, in different depths, showed in all analyzed size fractions (Table 13) higher TOC and T-Hg values for the 2 - 4 cm sample (GB3) than for the 0 - 2 cm sample (GB1). For the TOC and T-Hg content in the sediment samples and corresponding size fractions two trends, were observed which are, however, according to the Wilcoxon signed rank test not significant; (1) a seasonal increase from January to April from GB2 to GB4 (p-value of 0.07 for TOC,

for T-Hg not possible to determine), and (2) an increase from the margin into the estuarine basin from GB4 to GB5 (p-value of 0.1 for TOC, for T-Hg not possible to determine). Particle size fraction related TOC and T-Hg determinations showed the highest concentrations of T-Hg (0.24 to 0.33 mg Hg kg^{-1}) and TOC (6.5 to 14.9 mg C g^{-1}) in the 250 - 106 µm fraction for all sediment samples (Table 13), which also contained the highest amount of clay minerals.

However, a significant correlation was determined between T-Hg and TOC concentration (R^2 = 0.75 for January, R^2= 0.89 for April), and between T-Hg concentration and clay mineral content (R^2 = 0.78 for January, R^2= 0.85 for April) for all size fractions and samples (Spearman rank correlation, α = 0.05). The correlation between T-Hg and TOC concentration for all Grizzly Bay sediment samples and size fractions are displayed in Figure 34.

The composite from Liberty Island showed a higher TOC content (19.4 mg C g^{-1} sediment) compared to the Grizzly Bay sediments, whereas T-Hg concentrations (0.17 mg Hg kg^{-1} sediment) were similar (Table 13). As was the case for the Grizzly Bay sediment samples, the correlation between T-Hg and TOC concentration was significant (R^2 = 0.68, Spearman rank correlation, α = 0.05). An inverse correlation was revealed between the T-Hg concentration and the content of clay minerals of all size fractions (R^2 = -0.67, Spearman rank correlation, α = 0.05) which could be the result of inadequate sample preparation and dry sieving steps for Liberty Island samples.

Quantification of selected mercury forms

In the conducted selective extraction steps for GB1 and GB2, the majority of mercury (56 to 72 %) was found to be associated with organic matter (Table 13), thus, supporting the correlation between TOC and T-Hg concentration, described in the previous section. Mercuric sulfide (fraction 5) seemed to be a minor form of mercury in the sediments (Table 13). The sum of extracted mercury was consistent with the data achieved from T-Hg analyses for the respective sediment samples. Uncertainties may

occur for fraction 3 (organic-chelated mercury) because not all extraction steps (fraction1, 2) were performed (Bloom et al., 2003).

Mercury in Liberty Island samples was also predominantly associated with OM ranging from 55 to 70 % (Table 13). In contrast to sediments from Grizzly Bay, mercury in Liberty Island samples occurred chelated in strong inorganic complexes, and as mercuric sulfide in equal amounts (Table 13).

Water chemistry

Water temperature in Grizzly Bay increased from January to April from 6.9 to 14.3 °C (Figure 35), while pH remained at 7.9. Results of water analyses showed higher cation and anion concentrations in spring than in winter (Figure 36). Simultaneously, the conductivity increased from 6.5 in January to 8.2 mS cm^{-1} in April (Figure 35), and the salinity rose from 4.7 to 5.0 ppt.

The amount of dissolved oxygen in water was higher in January (11.3 mg L^{-1}) than April (9.9 mg L^{-1}), while the saturation increased from 95 to 104 % (Figure 35), caused by the seasonal changes in water temperature and salinity. Differences in the turbidity between January and April (Figure 35) reflected mainly the conditions at Grizzly Bay for the day of field session, instead of representing the general seasonal situation.

Results for DOC, SUVA and fluorescence analyses (Table 14) revealed no significant differences in Grizzly Bay water between seasons (Wilcoxon signed rank test, p-value of 0.3). Investigations of the respective OM fractions of the water showed that the majority (43 to 45 %) is in the hydrophobic organic acid fraction (Figure 37) which is mainly composed of fulvic acid (Aiken et al., 1992), followed by the hydrophilic fraction with 24 to 30 %. The calculated fluorescence index (FI) of 1.4 (Table 14) indicates that the DOC is predominately composed of terrestrially derived fulvic acid (McKnight et al., 2001). Microbially derived fulvic acid would typically have a FI value of 1.9 (McKnight et al., 2001).

The water temperature at Liberty Island was lower with 11.5 °C and the pH higher (8.3) than the respective field parameters measured at Grizzly Bay (Figure 35). The gradual change of salinity in the estuary due to different mixing behavior between freshwater and marine water is shown in the results for cation and anion analyses (Figure 36), as well as the measured conductivity for Grizzly Bay and Liberty Island (Figure 35). Conductivity (0.5 mS cm^{-1}) and salinity (0.06 ppt), as well as the amount of dissolved oxygen in water (9.7 mg O_2 L^{-1} and 89 % saturation), were lower for Liberty Island than for Grizzly Bay in April (Figure 35). Except for a slightly higher concentration in DOC (Table 14), no significant difference (Wilcoxon signed rank test, p-value of 0.3) was determined for the OM present in Liberty Island water in comparison to Grizzly Bay.

Batch extraction experiments

Batch extraction experiments were conducted to investigate the influence of OM (fulvic acid isolate F1-FA) and divalent cations (calcium and magnesium) on the mercury release from Grizzly Bay sediment samples GB1 and GB2, both collected in January in a depth of 0 – 2 cm at different areas of the field site (Table 2). In the course of the experiments, different separation techniques (e.g. centrifugation, filtration through different filter pore sizes) were tested to investigate the distribution of released mercury from sediments between various size fractions, i.e. dissolved and colloidal mercury fractions. Main results of this sub-study are summarized in the last section of this section. Results presented in all other sections of this section are related to the results of the 0.45 µm filtration step. In contrast to the sediment samples from Grizzly Bay, samples from Liberty Island (LI1) and McLaughlin Reserve (MCL131B and MCL134B1, Süß 2006) were mainly used for comparative studies (Table 2, Table 8) and are reviewed in the respective sections of this section.

Experiments in the presence and absence of buffers

Batch extraction experiments without the addition of buffers to adjust pH and ionic strength (Table 8, no. 1A) were conducted to investigate the unaffected release of mercury, OM, cations and anions (e.g. Na^{+}, Ca^{2+}, Mg^{2+}, Cl^{-}) from the solid. Results summarized in Table 14 show a release of 2.3 to 1.8 ng Hg(II) g^{-1} sediment for the extractions corresponding to 1.6 to 1.5 % of T-Hg for GB1 and GB2. In contrast to Grizzly Bay sediment samples, only 0.5 ng Hg(II) g^{-1} sediment (0.3 % of T-Hg) was released from Liberty Island sediment samples (LI1).

A relative standard deviation (RSD) of 8.5 % for all duplicate measurements was calculated. The released OM from the sediments of the batch was higher for LI1 (0.3 mg C g^{-1} sediment) than for GB1 and GB2 (0.2 mg C g^{-1} sediment), due to general higher TOC concentrations (Table 13) in the sediments from Liberty Island (19.4 mg C g^{-1} sediment) than from Grizzly Bay (4.1 to 5.2 mg C g^{-1} sediment). In contrast, SUVA (Table 15) was slightly lower for LI1 (3.5 $L \cdot mgC^{-1} \cdot m^{-1}$) than for GB1 (3.8 $L \cdot mgC^{-1} \cdot m^{-1}$) and GB2 (3.7 $L \cdot mgC^{-1} \cdot m^{-1}$). Further differences, were noticed comparing the concentrations of cations (Na^{+}, Ca^{2+}, Mg^{2+}) and anions (Cl^{-}) released from sediments during experiments. Particularly, higher concentrations of sodium and chloride were determined in batch experiments with Grizzly Bay sediments (Table 15). In addition, the pH in the batch solutions from Grizzly Bay was slightly higher with 7.7 than the one measured for Liberty Island (7.0).

In contrast to the unbuffered extractions, mercury release decreased for the Grizzly Bay sediments in the buffered experiments (Figure 38) where a phosphate buffer was added to adjust the pH to 6.4 ± 0.1 and the ionic strength was set to 0.1 M with $NaClO_4$ (Table 8, no. 0B). For instance GB1 decreased about 1.4 ng Hg(II) g^{-1} sediment from 2.3 to 0.9 ng Hg(II) g^{-1} sediment (Figure 38). Contrary, mercury release from the Liberty Island sample increased about 0.6 ng Hg(II) g^{-1} sediment from 0.5 to 1.1 ng Hg(II) g^{-1} sediment (Figure 38).

Furthermore, a slight increase of OM release for GB1 from 0.20 to 0.22 mg C g^{-1} sediment and a notably higher one for LI1 from 0.30 to 0.49 mg C g^{-1} sediment was noted (Figure 38). More calcium and magnesium (Figure 39), as well as iron, potassium, strontium and manganese, were released in the buffered batch solutions for all three composite samples than in the unbuffered.

Values for SUVA increased for GB1 from 3.8 to 4.3 $L \cdot mgC^{-1} \cdot m^{-1}$, for GB2 from 3.7 to 4.4 $L \cdot mgC^{-1} \cdot m^{-1}$and for LI1 from 3.5 to 3.6 $L \cdot mgC^{-1} \cdot m^{-1}$, which could be probably caused by interferences due to slightly elevated amounts of iron in the solutions of the buffered batch extraction experiments (Weishaar et al., 2003).

Effect of DOM

The addition of 5 mg C L^{-1} OM in the form of fulvic acid from the F1 site in the Everglades (Table 6) to the solution caused a decrease in mercury release from GB1 about 0.6 ng Hg(II) g^{-1} sediment from 2.3 to 1.7 ng Hg(II) g^{-1} sediment and from GB2 about 0.8 ng Hg(II) g^{-1} sediment from 1.8 to 1.0 ng Hg(II) g^{-1} sediment in the unbuffered experiments (Figure 40). Contrary, a slight increase was noticed in the buffered experiments in presence of 5 mg C L^{-1} OM (Figure 40). With regard to the T-Hg concentration of Grizzly Bay sediments (Table 13), approximately 0.7 % of mercury was released from GB1, and 0.5 % from GB2 in the buffered experiments. The cation and anion concentration in solution slightly increased in the presence of DOM in both experiments (Table 8, no. 2A,/B), while the general pattern regarding the difference in release between unbuffered and buffered (Figure 39) experiments maintained.

SUVA increased with addition of F1-FA to a general value of 4.4 $L \cdot mgC^{-1} \cdot m^{-1}$ in all buffered and unbuffered experiments, probably indicating the dominance of the isolate F1-FA in solution over the released OM from the sediments. In the course of these experiments; further information to the isolate F1-FA (Table 6) were obtained (summarized in Table 16).

Since the release of mercury from Grizzly Bay sediments was significantly lower in unbuffered experiments with additional DOM than without (Figure 40), the possibility of OM loss through sorption to sediment particles was considered. In theory, DOC concentrations in unbuffered experiments in the presence of DOM (e.g. 5 mg C L^{-1}) should represent the sum of the background OM release from the sediments (measured in the unbuffered extractions) and the added OM from the F1-FA isolate. Receiving a lower DOC concentration for this solution could indicate that interactions with the sediment particles and the additional DOM occurred. However, the amount of released OM from Grizzly Bay sediments was in general very low (Table 15), thus, it was difficult to ascertain if small-scale differences in the presence of additional OM occurred or not. Therefore, in a separate experiment with and without additional DOM (achieved concentration: 4.5 mg C L^{-1} in solution), a higher sediment to liquid ratio of 20 g 200 mL^{-1} was chosen to achieve a higher release of OM from the sediments and to prove the validity of the assumption. DOC results (Figure 41) show that a certain amount of OM is lost because the measured DOC concentrations in the experiment with additional DOM were lower with 13.2 mg C L^{-1} for GB1 and 12.1 mg C L^{-1} for GB2 than it was expected with 16.7 mg C L^{-1} for GB1 and 15.4 mg C L^{-1} for GB2 (Figure 41). The expected DOC concentrations were calculated from the DOC concentrations which were released from the sediments themselves (unbuffered experiment), plus the DOC concentration of the F1-FA isolate (4.5 mg C L^{-1}) which was added to the batch solution. Furthermore, the expected (based on the sum of the UVA from the unbuffered background solution and the added isolate) and the actual SUVA calculation showed that the actual SUVA value was with 5.1 to 5.6 $L \cdot mgC^{-1} \cdot m^{-1}$ greater than the expected SUVA with 4 to 4.4 $L \cdot mgC^{-1} \cdot m^{-1}$ for GB1 and GB2.

Effect of divalent cations

The outlined results of the previous studies indicated a potential connection between mercury release from the estuarine sediments GB1 and GB2 (Figure 38), and calcium and magnesium

concentration (Figure 39) in the batch solutions. To confirm this assumption, unbuffered experiments with additional 0.2 mM calcium or magnesium in the absence and presence of DOM (F1-FA, 5 mg C L^{-1}) were conducted (Table 8, no. 3A/B, 4A/B, Figure 42).

Calcium – unbuffered extraction experiments in the absence and presence of DOM

The amount of calcium which was added in form of calcium nitrate ($Ca(NO_3)_2 \cdot 4H_2O$) to the unbuffered batches, was aligned to the mean calcium concentration, measured in the solutions of the buffered extraction experiments (Figure 39). The aim was to ascertain if the released calcium in these buffered experiments was responsible for the inhibited mercury release.

The presence of 0.2 mM calcium in the unbuffered batch solutions (without additional DOM) caused the inhibition of mercury release. Only 0.2 % of the respective T-Hg concentration from GB1 and GB2 was released (Figure 42), which is even lower than the observed mercury release (0.4 to 0.6 % of the respective T-Hg) from sediments in the buffered experiments (Figure 40). The addition of fulvic acid to this series of batches caused a slight increase in the mercury release (Figure 42) from 0.2 - 0.3 ng Hg(II) g^{-1} sediment (without DOM) to 0.4 - 0.7 ng Hg(II) g^{-1} sediment (with DOM).

The release of OM from the sediments in the absence of additional DOM decreased in this study from 0.2 mg C g^{-1} sediment (without calcium) to 0.1 mg C g^{-1} sediment (with calcium) accompanied by a depression in SUVA from 3.8 $L \cdot mgC^{-1} \cdot m^{-1}$ (Table 15) to 2.7 $L \cdot mgC^{-1} \cdot m^{-1}$. In the presence of additional F1-FA, OM release from sediments was only in the range of 0.04 to 0.07 mg C g^{-1} sediment (Figure 42).

Further evidence that interactions between the added calcium and the sediments are taking place, can be derived from calcium concentrations in the batches of GB1 and GB2. A decrease of about 66 - 76 % compared to the initially added calcium concentration of approximately 6.0 mg Ca^{2+} L^{-1} was noted (Figure 42). In return, magnesium release from the sediments increased about 1.2 - 1.7 mg Mg^{2+} L^{-1} (Figure 42). Furthermore, potassium, manganese, and strontium slightly increased in both series of

batches whereas aluminum increased in comparison to the unbuffered experiments without additional calcium.

Magnesium – unbuffered extraction experiments in the absence and presence of DOM

Like the previous experiments with calcium, the addition of 0.2 mM magnesium in the form of magnesium nitrate ($Mg(NO_3)_2 \cdot 6H_2O$) to the batches in the absence of additional DOM caused a decrease in mercury release. Mercury decreased around 1.1 to 1.9 ng Hg(II) g^{-1} sediment (Figure 42) from 2.3 - 1.8 ng Hg(II) g^{-1} sediment (without magnesium) to 0.4 - 0.7 ng Hg(II) g^{-1} sediment (with magnesium). Hence, the impact of magnesium on the system seemed to be less than the one of calcium. Especially in the presence of F1-FA, an elevated mercury release for GB2 was perceived in the range of 1.5 ng Hg(II) g^{-1} sediment (Figure 42).

The pattern of OM release from sediments was similar to the one observed in the calcium experiments (Figure 42). SUVA in experiments without additional DOM was around 3.1 $L \cdot mgC^{-1} \cdot m^{-1}$ which is higher than the SUVA obtained in the calcium experiments. The determined SUVA value in experiments with F1-FA and in the presence of calcium or magnesium was slightly decreased (4.1 $L \cdot mgC^{-1} \cdot m^{-1}$) in comparison to the SUVA without additional divalent cations.

Based on the initially added magnesium concentration of approximately 5.6 mg Mg^{2+} L^{-1}, a decrease of 56 to 66% was also observed for the added magnesium concentration in GB1 and GB2 batches. In return, calcium release from the sediments increased about 0.9 mg Ca^{2+} L^{-1} (Figure 42). As already noted in the calcium experiments; potassium, manganese and strontium slightly increased in both series of batches, whereas aluminum increased in comparison to the unbuffered experiments without additional magnesium.

Experiments with Liberty Island water

To approach more realistic environmental conditions, batch extraction experiments with freshwater sediments from the Coastal Range in Northern California (MCL 131B and MCL134B1, Table 7) and saline water from Liberty Island were conducted. Especially, the impact of magnesium and calcium was of particular interest. Therefore, one experiment with untreated Liberty Island water (28.0 mg Ca^{2+} L^{-1}, 23.2 mg Mg^{2+} L^{-1}) and one, where divalent cations were removed against sodium by cation exchange (0.0 mg Ca^{2+} L^{-1}, 0.0 mg Mg^{2+} L^{-1}) were accomplished (Table 17).

The removal of divalent cations resulted in the increase of mercury release (Figure 43) by a factor of four (MCL 131B: from 2.9 to 12.0 ng Hg(II) g^{-1} sediment) to six (MCL134B1: from 2.7 to 15.6 ng Hg(II) g^{-1} sediment), as well as slight increase in the amount of released OM from the sediments from 2.8 to 3.0 mg C g^{-1} sediment. Taking the total mercury concentration of the sediments into account (Table 7), 0.03 to 0.008 % T-Hg were released in untreated Liberty Island water whereas 0.18 to 0.03 % of T-Hg was released in treated water. Values for SUVA also slightly increased from 2.8 in the untreated to 3.1 $L \cdot mgC^{-1} \cdot m^{-1}$ in the treated Liberty Island water experiment.

Mercury distribution between various size fractions

The distribution of mercury between various size fractions in solution was investigated for the buffered batch extraction experiment by filtration through membrane filters with pore sizes of 0.45 and 0.1 µm, or spinning in a superspeed centrifuge for mercury in the fractions < 0.45, < 0.1 and < 0.025 µm (Table 9). In general, the non-parametric Wilcoxon signed rank test indicated with a p-value of 0.18 no significant difference between the separation steps of filtration and centrifugation (Figure 44). However, the results from centrifugation and filtration of the same sediment sample differed in a range of 0.2 to 1.9 ng Hg (II) L^{-1} in the first separation step (Figure 44, Table 13). The separation between the 0.45 and 0.1 µm size fraction by centrifugation was more stable with regard to the standard deviations

than filtration (Figure 44). Filtration was more practicable in this study, however, because the preparation time was shorter (prevention of mercury loss) and the sample amount of each separation step was not limited by a definite volume like it is when using centrifuge tubes. A significant difference in mercury concentration between the 0.1 and 0.025 µm separation step, which was only possible to perform by centrifugation, was not observed (Wilcoxon signed rank test, p-value of 0.07). Based on the largest difference in mercury concentration between 0.45 and 0.025 µm observed in the experiment for MCL134B1 (Figure 44), 86 % of mercury in solution is present in dissolved form. A significant difference in the amount of DOC, as well as metals like aluminum, barium, iron and manganese between the size fractions was not observed (Wilcoxon signed rank test, all p-values > 0.07).

In the further course of this study, solutions of all performed batch extraction experiments (Table 8) were nevertheless separated by vacuum filtration with pore sizes of 0.45 and 0.1 µm (Figure 45) in order to maintain the possibility to investigate even small variations in mercury sizes in solution under different conditions. According to the Wilcoxon signed rank test, no significant difference (p-value of 0.07) was observed between the mercury concentrations of the 0.45 and 0.1 µm filtration step, which corroborates with the respective standard deviations (Figure 45). However, approximately 10% more mercury in the size fraction greater than 0.1 µm was released in experiments which had less divalent cations in solution such as the batch extraction experiments in the absence of buffers or with treated Liberty Island water (Figure 45). Differences in mercury amounts between the 0.45 and 0.1 µm size fraction ranged for instance in experiments without buffers between 2.3 ± 0.2 and 1.9 ± 0.0 ng Hg(II) g^{-1} sediment for GB1 and with treated Liberty Island water between 15.6 ± 0.5 and 13.1 ± 0.1 ng Hg(II) g^{-1} sediment for MCL134B1, whereas for the same sediment sample with untreated Liberty Island water, no variations in the mercury concentration (both 2.7 ng Hg(II) g^{-1} sediment) were achieved (Figure 45). The DOC amount (p-value of 0.01), as well as the concentrations of aluminum (p-value of 0.03), copper

(p-value of 0.01), iron (p-value of 0.04), and zinc (p-value of 0.04) significantly differed between the 0.45 and 0.1 μm size fraction according to the Wilcoxon signed rank test and based on all conducted experiments.

Task 7: Modeling intertidal contributions to system turbidity and biotic contamination.

Multivariate model proxy development

Bergamaschi et al., (2011) showed that the use of a multivariate PLS model could vastly improve the prediction of MeHg dynamics and transport over a single variable proxy. However, this approach did not provide any substantial improvement for this dataset (Table 18). Because the multivariate relationships were not significantly better than single variable relationships, single proxies were used for evaluating Hg dynamics.

Hydrodynamic Data

Data was collected at Liberty Island for 26 days in the winter from Dec. 17, 2010 – Jan. 12, 2011 (LIW) and for 17 days in the summer from June 3 – June 20, 2011 (LIS). Data was collected at Grizzly Bay in the winter for 27 days from Feb. 17 – March 16, 2011 (GBW) and in the summer for 28 days from June 24 – July 15, 2011 (GBS). One of the leading hypothesis of this study was that sustained wind events produce surface waves containing sufficient energy to increase near bed shear stress and thereby resuspend sediment, the resuspension of which has the potential to alter contaminant loading in the water column. The hydrodynamic data collected for this study permits assessment of the linkage between surface wave energy and re-suspension, and provides insights into the various other forcing mechanisms causing sediment resuspention, allowing an assessment of whether wind-wave resuspension is the dominant mechanism of increases in suspended sediment during these measurement periods. This study uses turbidity as a surrogate for suspended sediment concentration (SSC). There

were good calibrations of turbidity to SSC, with modest spread, for both Liberty Island (r^2=0.732) and Grizzly Bay (r^2=0.790), but the range of the turbidity signal was not covered (Figure 46). We note that the baseline turbidity signal for both locations was is well represented in the data, but SSC data is not available for the larger events because samples were not collected during these events.

Liberty Island

The hydrodynamics that characterize the physical forcing for the LIW data set are as follows: (1) frequent rain events until Jan. 3, 2011 after which there was no rain; (2) increased flows on the Sacramento River at Fremont Weir, with a crest from Dec. 20 – Dec. 25 and from Dec. 30 – Jan. 2, 2011 (*http://cdec.water.ca.gov/*) over the weir height that flooded the Yolo Bypass and potentially increased runoff into Liberty Island; (3) two significant wind events (> 6 m s^{-1}) on Dec. 18 and Dec. 29, 2010 that resulted in elavated energy from surface waves, and (4) semi-dinural gravity currents that resulted from tidal variations. Figure 47, shows the time series for data that best represent these forcing mechanisms. In Figure 47A, the water stage is taken at Yolo at Lisbon, approximately 23 km to the north/northwest of the measurement location. Yolo Bypass is inudated when the water stage is above 8.5 ft.

In the absence of (1-3), then tidal forcings act to maintain a baseline turbidity signal that peaks in phase with the low-low tide, on a dinurnal basis. This is most likely the result of sediment settling out of suspension. At the start of the ebb tide (see Figure 47A, time 1) and for the duration of the ebb tide the turbidity does not appreciably increase until the end of the ebb tide (time 2). We postulate that the baseline shift in the turbidity signal (which started on Dec. 28, 2010, see Figure 48C) is the result of increased runoff after the the Yolo Bypass started to flood on Dec. 20, 2010, as indicated by the water level at Yolo at Lisbon (Figure 47A). After this hydrologic influence there is a sufficient upstream sediment supply to increase the turbidity signal by a factor of two. Turbidity also peaks on a semi-

diurnal basis as sediment is advected from the upstream of the measurement location for the duration of each ebb tide, and the peak signal is out of phase with the low tide. Figure 48B indicates that more sediment is being carried through on the ebb tide (time 3), and the concentration peaks at maximum velocity (time 4), when more sediment can be maintained in suspension.

An increase in the turbidity signal in phase with the energy generated from surface wind waves is and indication there was localized resuspension of sediment. Surface waves that occur at low stage heights have the highest potential for resuspension as the shear stress at the bed increases proportionally to the depth of water (see Equation 2). There does appear to be a corresponcence between wind waves with sufficient energy and increases in turbidity. Two significant events with elevated surface wave energy were identified in the time series (see Figure 49). Primary and secondary turbidity peaks corresponding with low tide and with the beginning of the rise in the energy peaks can be seen in the time series where indicated by the black and red arrows, indicating surface wave energy energy is the likely cause of resuspension, but in a stepwise fashion. The maximum in turbidity during this period (black arrows) does not correspond to peaks in energy (blue arrows) from surface waves, while the secondary turbidity peaks (red arrows) corresponds to the energy peak. The reason for this double peak is related to the interaction between water height and resuspension. Resuspension occurred at the northern end of Liberty Island, away from the instruments, where the water level was lower. Subsequently, this sediment was transported with the receeding ebb tide waters to the measurement location, causing the initial spike in turbidity. When the ebb tide lowered the water height in the vacinity of the instruments sufficiently to permit surface wave energy to propogate to the bed, localized resuspension occurred, causing a secondary turbidity spike.

The turbidity event (highest recorded for the LIW data set) at the end of the day on Dec. 28, 2010 resulted from several forcing mechanisms acting in concert to produce and maintain an elevated

turbidity signal. The runoff from the Yolo Bypass and resuspension of sediment upstream, was advected to the measurement location. As the tide is turning a large wind event produces large enough surface waves (approximately 0.3m) to create the largest recorded energy, and create a secondary spike in turbidity on the flood tide. On the next ebb tide the lower turbidity signal, is due to less runoff because velocity magnitude is most likely less because the strength of the tide is less and the absence of sufficient energy to create increased resuspension.

The hydrodynamics that characterize the physical forcing for the LIS data set are as follows: (1) small amount of rain on June 4 – 5, 2011 (2) a possible small amount of runoff from residual water in the Yolo Bypass (3) one significant wind event (>6 m s^{-1}) on June 19, 2011 and two minor events (also > 6 m s^{-1}) on June 4 and June 11, 2011 (4) semi-diurnal gravity currents as a result of tidal variations. Figure 50 shows the time series that best represent these forcing mechanisms. The water stage at Yolo at Lisbon never reached the threshold of 8.5 for this measurement period, so this influence is thought to be minimal or nonexistent for this measurement period.

As was discussed with the LIW data set, the same tidal variations would be expected in absence of the other forcing mechanisms. We do not see any baseline shift or sustained values turbidity signal above 40 NTU, as we saw in the LIW data set. We will then focus on the three higher energy events that have been indicated in Figure 50, in order to test our hypothesis that sustained wind events cause surface waves that contain enough energy to induce localized re-suspension of sediment. The first two events show a clear correlation between the energy contained in the surface wave and an increase in the turbidity signal (Figure 51). The third event indicates a lag in the energy and turbidity signal. Examination of Figure 50C shows that the wind event on June 19, 2011 occurred during a maximum in stage indicating that the water depth was too deep to cause localized re-suspension. The increase in the turbidity signal was probably a result of re-suspension in the shallows upstream of the measurement

location, and sediment was advected during the subsequent ebb tide. What should also be noted is that the turbidity on June 4, 2011 was increased by a factor of over two from the turbidity on June 19, 2011, even though the energy on June 19, 2011 is increased by almost a factor of three. This would indicate that timing of the wind events is a driver of sediment re-suspension since the likelihood increases with a decrease in water depth. During event one the water level was a minimum, and during event three the water level was at a maximum.

The LIS data set contains data from the Aquadopp and LISST, these measurements help to better describe the particle dynamics and the mechanisms for increased turbidity and fluctuations in median grain size (D50). The D50 is a measure of particle size and amount of flocs in the water column. Flocs are important component in estuary particle dynamics because they can increase the potential to transport primary particles because their effective density relative to water is becomes lower. Figure 52 shows the time frame for the first energy event, as indicated by the peak in the turbidity (blue arrow). The two components of velocity (horizontal and vertical) are also represented to indicate the relative shear or turbulence present in the water column. For the first wind event the vertical velocity component is negative indicating the orbital velocities created by the surface wave are propagating through the water column. It is not clear that the near bed up velocity is increasing as a result of this energy partitioning. The up velocity near the bed is at a maximum during the flood tide, and these values do not differ during the wind event, relative to the background values (see Figure 52B, black arrows). The peak periods in the D50 (green arrows) correspond to the flood tide, indicating that flocs are either being advected in to the measurement location or that flocculation is occurring during the flood tide.

The third wind event (June 19, 2011) and the water column dynamics is represented in Figure 53, the timing of the max energy is shown by the blue arrow (see Figure 53A). This event occurs at the

beginning of the ebb tide when the water depth is near a maximum. As this is a high energy event, factor of 3 higher than the first, there are clear disturbances in the water column, indicated by the black arrow showing the oscillations and high magnitudes of upward velocity component for the duration of the ebb tide. For the duration of the ebb tide the turbidity signal increases, reaching a local maxima at low tide, suggesting that sediment is advected in from upstream and settles at low tide. The fluctuations in the upward velocity suggest that the water is more turbulent and this increased turbulence corresponds to the sharp decrease in the D50 indicating that flocs are breaking up. The green arrows in the Figure 52 show the local maxima for D50, which also corresponds to the flood phase of the tide, which shows the same pattern as was described in Figure 51.

Grizzly Bay Hydrodynamics

The hydrodynamic forcing to characterize the GBW is as follows (1) frequent rains throughout the measurement period (2) no noticeable runoff from surrounding watershed (3) three significant wind events (<4 m s^{-1}) on February 18 and 25, 2011 and March 7, 2011, and (4) semi-diurnal gravity currents as a result of tidal forcing. Figure 54 shows the time series that best represent these forcing mechanisms. The water stage (see Figure 54A) represents the potential runoff from Suisun March, the variations in stage only appear to tidal therefore we conclude that there is no influence of runoff from the local watershed.

We will focus our discussion then to the three wind events that have been identified in Figure 54 to determine whether increases in turbidity occur from local re-suspension or advection of sediment, and the sources of sediment. For the first two events (see Figure 55, A, B) the peaks in turbidity (black arrows) are out of phase with the peaks in energy (blue arrows), however there are peaks in the turbidity that seem to correspond to lesser peaks in the turbidity (red arrows). The peaks in turbidity preceding the first event correspond to high tide at the end of the flood, after the energy increase (see Figure 56,

time 1) the turbidity signal then peaks at low tide, and then reaches a maximum at the next high tide (time 2). The timing of these events suggests that more sediment is being carried in on the flood tide, and the energy from the waves is strong enough to re-suspend sediment upstream of the measurement location and it is advected in during the ebb tide. The second event shows that there is some local re-suspension of material at the peak of the energy (time 3), which occurs on the ebb tide. Just prior to low tide (time 4) there is another increase in turbidity most likely as sediment is settling out of suspension. On the next ebb tide there is a local maximum of turbidity (time 5) as more sediment that had been re-suspended continues to be transported out of the shallows. The third event (see Figure 55C) indicates that the turbidity peak and energy peak are in phase. The turbidity signal increased by almost an order of magnitude for two consecutive ebb tides during this event. The first peak in turbidity (see Figure 56, time 6) occurs during the ebb tide. The second peak (time 7) also occurs during the ebb tide, and is of the same magnitude as the first. These events suggest that the bulk of sediment is being advected in from upstream and that higher energy waves are creating re-suspension of material in shallower waters.

Velocity profile and PSD measurements were taken from March 3, 2011 until the end of the deployment, for that reason we will only focus on the third wind event in relation to these measurements. Figure 57 shows this time period in more detail, with the blue arrow indicating the turbidity response to the peak energy. We do not see a response in the water column due to the surface waves as was seen in the LIS data set, this is most likely due to technological limitation of the Aquadopp that was used for this deployment. In fact it is difficult to determine the degree of turbulence in the water column that would aid in determining likely re-suspension events and breakup and aggregation of flocs. The D50 data shows no obvious trends, except for the dips at beginning of the ebb tide (green arrows) preceding the turbidity spikes. The D50 increases before the two spikes in turbidity and then decreases (red arrows) as the turbidity signal continues to increase. This could be the result of

more fine material being introduced as a result of re-suspension or the breaking up of microflocs due to turbulence. The D50 then increases to a local maximum after the turbidity signal decreases, possibly due to the availability of more primary particles as a result of re-suspension mechanisms.

The velocity vectors rotate counterclockwise on both the ebb and flood tides, complicating this system, because the source of sediment can come from a variety of directions. Figure 58 illustrates this point, on the ebb tide the velocity direction due east at the start of the tide and the direction rotates over the course of the tide. This variation is due to the fact that there are two inputs into Grizzly Bay, Montezuma Slough to the north and the Sacramento River to the east, and the momentum balance is therefore shifted during the ebb tide. During the flood tide, the velocity is more unidirectional from the west, except during the end of the tide when the direction switches 120° to a more easterly direction. The predominant forcing of the flood tide is from Carquinez Strait, but as the tide begins to reverse this balance is overcome by the Sacramento River as shown by the easterly direction.

These complexities in the velocity vectors can help to explain the turbidity signals to some degree. For the first wind event (see Figure 56A) there are increases in turbidity at the end of the flood tide, which as we can now see correspond to input from the Sacramento River. The velocity vectors of the ebb tide indicate that most of the sediment seen during this tide is from Grizzly Bay proper, with some input from Montezuma Slough. Therefore we can reasonably conclude that increases in turbidity on the ebb tide that correlate with energy increases is most likely the result of wind wave re-suspension in the near shore of Grizzly Bay, and that sediment is advected into the measurement location. There appears to be minimal localized re-suspension at the measurement location for the GBW data set.

The hydrodynamic forcing to characterize the GBs is as follows (1) one period of rain on June 28, 2011 (2) no noticeable runoff from surrounding watershed (3) two significant wind events (~3 m s^{-1}) on July 9 and 12, 2011 with sustained wind throughout the measurement period and (4) semi-diurnal

gravity currents as a result of tidal forcing. Figure 59 shows the time series that best represent these forcing mechanisms. The water stage (see Figure 59A) once again appears to only have tidal variation therefore no influence of localized runoff is assumed. Diurnal winds are between 2-3.5 m/s and maintain surface waves throughout the measurement period, these baseline waves do not appear to effect the baseline turbidity, as the mean turbidity is 30 NTU as opposed to 35 NTU during the GBW data set.

The two significant wind events identified in Figure 59 show a similar pattern to what has been seen in the previous measurement periods. The first event occurs at a low-low tide and a response in the turbidity signal is seen by a factor of three (Figure 60A). The subsequent ebb tide shows an increase in turbidity of the same magnitude that peaks in the middle of the tide, suggesting there has been enough re-suspension in the near shore shallows to maintain higher turbidities. The increase in turbidity for this time period is a combination of localized re-suspension and advection. The second event (Figure 60B) shows three energy peaks (blue arrows), two in phase with a turbidity peak and one out of phase with the local turbidity maxima (black arrow). The first two peaks (time 1 and time 2) correspond with low tide, and the third happens at high tide. This event does not have as high of a magnitude as the first therefore the signal is decreased on the subsequent ebb tide, suggesting that there was not a large amount of sediment re-suspended in the near shore.

As with the GBW data set we see increases in the turbidity signal at the end of the flood tide suggests input from the Sacramento River. The velocity vectors (Figure 61) show a similar pattern to the GBW data, but the directions are slightly rotated, with the ebb tide showing more predominance from slightly west of north, with some southeasterly component. The flood tide shows predominance just north of west, with some southeasterly component. These patterns suggest dominant inputs from the Sacramento River to the southeast and Montezuma Slough to the northeast, but the directional

components on the ebb tide still aligns with Grizzly Bay. The hydrodynamic complexities of this system make the turbidity signal hard to interpret but velocity information aids in the interpretation.

4.2 Achieved Objectives

All project objectives were achieved through the findings and contributions described above.

1. Quantify the relationship between wind and rain intensity and the elevated concentration of aggregated sediments.

Results associated with Task 2 fulfilled this objective. Suspended sediment concentration was elevated above the tidal cycle background range for all rain events that occurred during or near low tide at both Liberty Island and Grizzly Bay. Low tide rainfall at Grizzly Bay produced SSC values that were between 2 and 5 times higher than SSC during the fair weather tidal cycle and the rain events occurring during high tide. Peak and event total rainfall kinetic energy were less important to SSC than the timing of rainfall with respect to the tidal cycle. Wind events at Grizzly Bay generated SSC's that were very similar to the tidal cycle values and to each other for all wind speeds up to 7.5 m s^{-1}. SSC during the 8 m s^{-1} event, however, was over twice as high, indicating a resuspension threshold between 7.5 and 8 m s^{-1}. At Liberty Island there appears to be a resuspension threshold for wind events exceeding 5 m s^{-1}.

2. Investigate the extent to which dissolved contaminant concentrations are influenced by resuspension of sediment aggregates containing elevated contaminant concentrations.

Results associated with Tasks 2, 3, 4, and 5 achieved this objective. At both field sites, the character of dissolved material was more strongly affected by rainfall runoff than by wind resuspension. Similarly, SSC and metals content both increased more during rain events than wind events and fair-weather tides. There is greater resuspension of benthic sediments during wind events and a larger overall effect in Grizzly Bay and Liberty Island, but rainfall is a much greater contributor to metals contamination due to the mobilization of contaminated marsh sediments, at least in close proximity to the marshes. It is possible, therefore, that the sediments in suspension in the larger shallow waterways during rain events have a higher percentage of marsh-derived particles, and therefore a higher metals content, than sediments that are resuspended from the bay bottoms during winds and tides.

3. Characterize properties of particle and dissolved constituents that govern elevated contaminant load released through the mobilization process

a. Source of particles (benthic polymers, algal, mineral, detrital, etc)

b. Particle character (OM content, nutrients, grain and aggregate size)

c. Partitioning

Results associated with Tasks 3, 4, and 5 fulfilled this objective. Suspended sediments during rain events are elevated in leachable metals, organic carbon, and organic nitrogen relative to values measured during the tidal cycle survey. Five metals in particular, Cd, Cr, Cu, Ni, and Y, are

present in concentrations greater than both wind events and the tidal cycle. Given that rainfall events can erode subaerially exposed sediments that are unavailable to in-water resuspension processes, the higher concentrations of metals and organic matter likely come from marsh sediment or soil exposed on the levee tops. Suspended particles during wind events, however, have higher proportions of algal material than background and rain-derived sediments. Changes in suspended particle character were minor throughout the study period, with low and inconsistent responses of the algal fraction of suspended particles, and moderate responses of median grain size, to rain and wind events. Dissolved constituents measured by optical instruments responded more strongly to the regional rainfall signal than to wind events, or even to individual rainfall events.

4. Estimate contribution of this mobilization process on biotic contaminant burden relative to the system background.

Results from Task 7 fulfilled this objective. Simple 1-D model suggests that resuspension of intertidal particles by wind in the Bay-Delta occurs frequently. Rainfall has a more distinct effect on particulate character and dissolved transport but the signal is swamped by the regional response. However, the particulates measured in the subtidal habitats adjacent to the intertidal mudflats did not appear to be elevated in contaminants or organics suggesting that the effect on biotic uptake is small relative to baseline conditions on a regional scale.

Inundation models using moderate levels of future sea-level rise indicate up to 80,000 hectares of land surrounding San Francisco will be below mean sea level (Knowles and Cayan, 2002) suggesting future climate change will increase intertidal habitat considerably. Coupled with increased intensity of ENSO type rainfall events these may have a large effect – but still dependent on frequency of wind resuspension in this region such that sediment character is disturbed too

frequently to be altered in a way that enhances the biotic exposure of contaminants relative to the baseline condition.

5. Improve our ability to monitor for contaminant transport in restoration and regional settings by developing *in situ* methods for determination of contamination exposure potential using optical characterization of particulate and dissolved constituents.

Results from Tasks 4 and 5 achieved this objective. Demonstration of the use of optical instrumentation to track biogeochemistry in dynamic systems expands prior work done in the Delta by Downing et al. (2009) and Bergamaschi et al. (2011). Although the large suite of hyperspectral optical parameters were not necessary to track the variability of mercury dynamics in this study, nevertheless the frequency of the in situ measurements and the wide range of biogeochemical variables measured by the optical sensors greatly improved our ability to interpret and understand the dynamics of the complex system in which the study was conducted.

5. Management Implications of Project Findings

Rainfall mobilization of metals and organics

The data examined in this study support the hypothesis that low-tide rainfall can liberate more leachable metals from historically contaminated intertidal areas than can be generated by wind and tide resuspension. The amounts of total leachable metals on suspended sediments were consistently higher during rainfall events than during wind events for every metal examined, and higher than the low tide

average as well in some cases. These results are consistent with a Regional Monitoring Program study which found greatest sediment toxicity throughout San Francisco Bay, including Grizzly Bay, during the winter rainy season, attributing it to stormwater runoff (SFEI, 2003). Metal transport by rainfall has been observed in other environments, such as dredge spoil piles (Singh et al., 2000). In this case, simulated rainfall of 40 mm hr^{-1} and a surface slope of 19% resulted in high metal fluxes that were directly proportional to the metal content of the bulk sediment (Singh et al., 2000).

The metals with the largest difference between the rain event, the wind event, and the tidal cycle are Cd, Cu, Ni, and Zn, which are all known to be problematic in Suisun Bay. Phillips et al. (2003) found Grizzly Bay sediment to be highly toxic to bivalve embryos, and cationic metals, especially copper, to be the leading factor. The Sacramento River is a major source of dissolved and colloidal Cu, Zn, and Cd. The source of these metals is predominantly from acid mine drainage from historic copper and zinc sulfide mines in the mountains surrounding the river valley, with additional metals coming from agricultural and urban runoff (Alpers et al., 2000b). Copper contamination in the study area also comes from its use as an algicide in the rice fields on the Sacramento River (Alpers et al. 2000b).

The data indicate that rain events mobilize sediments from a source that is different from the usual sediment available for resuspension by tides or wind events. The total leachable metal content of the suspended sediment during the rain event was higher than the leachable metal content of sediments during the wind event for most metals. Some of the most problematic metals in Grizzly Bay (Cd, Cu, Ni, and Zn) are also elevated in the rain event samples with respect to the low tide average. Furthermore, some of the metals (Fe, Cu, Pb, Cs, and Cd) have very different ranges of concentrations during the rain event than during the tidal cycle, with concentrations at the beginning of the rain being the most similar to tidal cycle values. If metals concentrations were a function of the degree of resuspension of sediments available to fair weather tides, then one would expect the concentrations of

all metals to fall in the same range during all three events, and for the relationship between SSC and metal concentration to also be similar between events. Instead, the concentrations of these 5 metals are dramatically different during the rain, and relate to SSC as if the concentrations are governed by mixing.

The other source of sediment that is added to the background sediment suspended by tides and wind is relatively high in Cu and Cd, and low in Pb, Cr, Cs, and Fe. Most likely the source of background suspended sediments is the continuously subaqueous benthic sediment in Grizzly Bay and the sampled tidal creek. Field work activity revealed the creek bed to be quite soft up to about 0.5 m deep, almost to the point of being fluid mud, and the bay bottom firmer but still easily resuspendable. The SSC data reveal a resuspension threshold between wind speeds of 7.5 and 8 m s^{-1}, so the bay bottom sediments can easily be resuspended by typical summertime wind speeds. During rain events, however, sediments from the marsh surface and the top of the levee surrounding the bay can be eroded into the creek, providing different sediment than usual, likely with different concentrations of adsorbed metals.

The total leachable content of some of the metals do meet toxicity criteria (Table 19). Mean concentrations of Cr and Cu exceed the Effects Range Low determined by Long et al. (1995) during rain, wind, and tidal cycle events, and mean Ni concentration exceeds the Effects Range Median during all three events. Furthermore, the rain event and tidal cycle contain datapoints exceeding the ERL for Zn although the mean values are below the ERL. Cr, Cu, Ni, and Zn clearly remain problematic in Grizzly Bay suspended sediments.

To investigate the importance of rainfall-induced metals transport to the overall metals budget of Grizzly Bay, the total amount of leachable metal transported by each event was calculated by integrating:

$$[ME_{total}] = \sum_{i=1}^{24} SSC_i [ME_i] \Delta t, \quad (6)$$

where i is the sample number, SSC is the suspended sediment concentration, ME is the metal content, and Δt is the time between samples. Metal transport rates for the elements of interest spanned several orders of magnitude, with the lowest rate for Cd and the highest for Fe (Table 20). The total amount of metal transported per event was highest during the tidal cycle for all target metals but Cu and Mn. This is due to the longer total sampling time of the tidal cycle. The transport rate, however, was consistently between 1.8 and 9.4 times higher during the rain event than during either the wind event or the tidal cycle. Consequently, this rain event contributed disproportionately to the total metal load in Grizzly Bay. A similar event once per week for the approximately 4-month-long rainy season could conceivably add 4.68 g L^{-1} of Cu to Grizzly Bay, 5.4 g L^{-1} of Zn, and 4.5 g L^{-1} of Ni from just the sampled tidal creek.

Mercury release and partitioning

Grizzly Bay – key aspects of water chemistry and sediments

Sediments

Sediment samples collected in January and April 2008 from Grizzly Bay, in the western part of the Sacramento-San Joaquin Delta, were dominated by clay and silt (< 50 μm). Slight seasonal changes in the < 50 μm fraction from winter to spring (72 to 66 %) were the result of higher fluvial discharge of the Sacramento-San Joaquin river system in winter associated with the transport and the initial settlement of silt and clay minerals from the Great Central Valley drainage into the upper bays (Krone, 1977). Since deposition rates for Grizzly Bay have not been available till now (Cappiella et al., 1999), it is not possible to know how long the sediments from the first 2 to 4 cm that were analyzed in this study have been stored in the bay. In general, bathymetric surveys from the 1850s to the 1990s (Krone, 1977; Jaffe et al., 1998) compared to historical trends of metal contamination in sediment cores (Hornberger et

al., 1999) indicated that after the large-scale accumulation of sediments during the period of hydraulic mining (1853-1884), a hiatus followed due to predominant erosion in the Sacramento-San Joaquin Delta between 1888 and 1951. Presently, depositional rates for San Pablo Bay, which is adjacent to Grizzly Bay, are estimated to be in the range of 4.0 to 4.1 cm year^{-1} (Fuller et al., 1999; Hornberger et al., 1999), whereas Suisun Bay southward of Grizzly Bay has remained erosional, removing 1.2 cm sediment per year (Cappiella et al., 1999). The physical and biological reworking of the upper sediment column which could cause the persistence of contaminates in the surface sediments is noted to be less for San Pablo Bay (Fuller et al., 1999). Hornberger et al. (1999), however, measured the highest enrichment factor for mercury concentration in subsurface sediments in the whole Bay area with 0.95 μg g^{-1}, as well as the highest deposition rate of mercury with 1.49 μg cm^{-2} year, in a sediment core from Grizzly Bay collected in 1990. The data from this core material (Figure 62) showed higher amounts of mercury in the first centimeters in comparison to data revealed in the present study (0.12 to 0.18 mg Hg kg^{-1} sediment). A more similar data set is provided by Conaway et al. (2003), although the concentrations presented therein are still slightly higher (0.24 to 0.28 mg Hg kg^{-1} sediment). Possible reasons for different T-Hg concentrations obtained in these studies are the long time intervals between these three studies, different sampling locations within the bay, sampling at different times of the year at different depths and using different sampling techniques, and analytical methods.

In general, surface sediment concentrations for T-Hg in the present study are above the worldwide average crustal abundance (0.067 μg Hg g^{-1} sediment; Cox, 1989) and the level predicted to cause adverse biological effects in benthic fauna (Long et al., 1995). However, T-Hg concentrations do not exceed the geometric mean for U.S. coastal sediments of 0.22 μg Hg g^{-1} sediment (Daskalakis and O'Connor, 1995).

The mineral composition of Grizzly Bay sediment samples was dominated by quartz (27.4 to 45.2 %) and feldspar (26 %), with lesser amounts of clay minerals such as illite, chlorite and serpentine (Table 12). A representative analysis of the mineral spectrum including bulk samples from the entire study area has not been conducted. Hence, reliable conclusions regarding the provenance of the Grizzly Bay sediments mainly received by the Sacramento-San Joaquin river system are not possible. The composition of the clay mineral fraction (e.g. chlorite, mica), however, suggests the presence of metamorphic rocks in the catchment area.

The increase of clay mineral content from January to April (25 to 41 %) in the entire sample, as well as in each corresponding size fraction, was accompanied by an increase of TOC (4.1 to 7.5 mg g^{-1} sediment) and T-Hg concentration (0.12 to 0.18 mg kg^{-1} sediment, Table 13). The highest concentrations for all three parameters were measured each time in the fine sand fraction (250-106 μm; Table 13). The positive correlation between T-Hg and TOC concentration ($R^2 = 0.75$ for January, $R^2 = 0.89$ for April), and between T-Hg concentration and clay mineral content ($R^2 = 0.78$ for January, $R^2 = 0.85$ for April) determined for this area in the present study (Spearman rank correlation, $\alpha = 0.05$), was also observed by Conaway et al. (2003). In the Conaway et al. (2003) study, the correlation was related to the flocculating organic particulate matter that scavenges the dissolved mercury in the water column. A process like this is reasonable, since mercury has a high affinity for the active binding sites of the OM, such as thiols and other sulfur-containing groups (Ravichandran, 2004). Conaway et al. (2003) further suggested that the strong correlation between TOC and T-Hg amount could be due to a dominant single source of OM, the Sacramento-San Joaquin river system. The correlation between TOC concentration and clay mineral content can be explained by the affinity of OM to associate with fine-grained inorganic particles like clays (Schuster, 1991; Macalady and Ranville, 1998). Similar relationships were investigated in other estuaries (Benoit et al., 1998; Mikac et al., 1999; Stoicheva et

al., 2004). Based on these investigations, the observed spatial trend of T-Hg concentration in the sediments from Grizzly Bay from the margin into the estuarine basin is most likely controlled by the same factors that control the distribution of OM and fine-grained material in this tidal-influenced system (e.g. resuspension, Conaway et al. 2003) rather than pointing out a historic source of mercury contamination (Hornberger et al., 1999). The seasonal variability in the sediments could be explained by the higher input of reactive OM during spring runoff, but certainly there are more biogeochemical processes involved. However, reduced conditions in the surface sediments which may cause an additional accumulation and precipitation of metallic sulphides like metacinnabar as it is proposed for the Adour estuary in France by Stoicheva (2004) can be generally excluded since increased concentrations of iron oxides (e.g. maghemite, hematite) were noticed in collected sediment samples from April. The predominance of organic-chelated mercury in Grizzly Bay sediments is also supported by the results from selective extractions where 56 to 72 % of total mercury was extracted in fraction 3 (Table 13). In studies conducted by Bloom et al. (2003) with biologically active marine sediments, it was noted that the extracted inorganic mercury in fraction F3 was most strongly correlated with the methylation potential in sediments. However, it has to be taken into consideration that the bioavailability of mercury depends on the mercury-DOC complex itself. Mercury bound to long chain DOC molecules is supposed to limit the microbial driven methylation because the organic molecules are too large to cross the cell membrane (Gabriel and Williamson, 2004; Ravichandran, 2004). Mercuric sulfide and strongly complexed or elemental mercury forms were less present in Grizzly Bay sediments.

Release of mercury from Grizzly Bay sediments in the batch extraction experiments in the absence of buffers ranged between 1.5 and 1.6 % based on the total mercury concentrations (Table 15). These results indicated that only a small amount of T-Hg was dissolved.

Water chemistry

Water samples collected in January and April 2008 at Grizzly Bay, differed notably in salinity (4.7 versus 5.0 ppt), conductivity (6.5 versus 8.2 mS cm^{-1}) and in cation and anion concentrations (higher in spring than in winter, Figure 36) while pH remained at 7.9, a typical pH-level in the Sacramento-San Joaquin Delta (Domagalski et al., 2000). Most of the annual precipitation in the Sacramento River Basin (average: 91.4 cm) falls during the months of November through March in the form of rain or snow resulting in an average freshwater inflow of over 650 m^3 s^{-1} to the estuary system (Domagalski 2001). Freshwater inflow during the summer months is typically greatly reduced, to less than 500 m^3 $s-^{1}$ (Conaway et al., 2003). Thus, the observed increase in salinity, conductivity, cation and anion concentrations in April is mostly due to the seasonal change in the freshwater input into the Delta system which causes a change in the length and location of the mixing zone between freshwater and marine water. Salinity levels at Grizzly Bay in this study were related to oligohaline conditions (0.5 – 5 ppt) which are typical in estuarine systems (Mitsch and Gosselink, 1986). Freshwater from rivers has a salinity of less than 0.5 ppt and marine waters of more than 30 ppt (Mitsch and Gosselink, 1986). Earlier studies from 1999, 2000 and 2001 in Grizzly Bay (Choe et al., 2003; Conaway et al., 2003) also indicated lower salinities in winter than in summer. However, the differences in salinity between both seasons were significantly higher (Conaway et al., 2003) than in this study.

Results for DOC (3.6 mg C L^{-1}), SUVA (2.8 L·mg C^{-1}·m^{-1}), fluorescence analyses (Table 14) and investigations of the respective fractions of OM in Grizzly Bay water (Figure 37) revealed no significant seasonal changes (Wilcoxon signed rank test, p-value of 0.3). DOC data were in general slightly higher than the DOC concentrations received from water quality assessments (maximum observed DOC: 2.9 mg C L^{-1}) in the upper parts of the Sacramento River (Domagalski et al., 2000). Investigations of the respective OM fractions of the water showed that the majority (43 to 45 %) was in the hydrophobic

organic acid fraction (Figure 37) which is mainly composed of fulvic acid (Aiken et al., 1992), followed by the hydrophilic fraction with 24 to 30 %. The calculated fluorescence index (FI) of 1.4 (Table 14) indicates that the DOC is predominately composed of terrestrially derived fulvic acid (McKnight et al., 2001). Microbially derived fulvic acid would typically have a FI value of 1.9 (McKnight et al., 2001). In this context, mass balance calculations for OM in the Sacramento-San Joaquin Delta by Sobczak et al. (2002) indicated that external river inputs account for 69 % of the OM supply in the Delta, whereas internal primary producers like phytoplankton only account for 15 %. Since the Sacramento River provides 84 % of the freshwater input to the Delta (Sobczak et al. 2002), it is, as already assumed in the previous section, the dominant source of OM input to the northern reach.

Liberty Island – a comparative study

Sediments

Sediment material from the second field site in this study, Liberty Island in the northern part of the Sacramento-San Joaquin Delta, differed significantly from the sediments collected at Grizzly Bay. Since this area was in agricultural use until 1998 when levees breached during high flows, sediments collected in April 2008 were not sorted and contained brick debris (Figure 63).

A further difference between the sites was the periodic drying of areas at Liberty Island during low tide, whereas sediments at Grizzly Bay remained covered by water. Sediments from Liberty Island were dominated by clay minerals (68 %; Table 12) such as illite, chlorite and smectite, but a significant correlation with the TOC content with respect to the size fractions was not observed as it was for the sediments from Grizzly Bay. However, the TOC concentration was in general higher at this site (19.4 mg g^{-1} sediment), whereas the T-Hg concentration (0.17 mg kg^{-1} sediment) was not significantly different from the Grizzly Bay sediment samples (Table 13). Thus, it is possible that other forms of

mercury besides the organic-chelated forms could be important for Liberty Island samples. This assumption is supported by the results for selective extractions, indicating that 17.2 % of total mercury occurred in the form of mercuric sulfide (fraction 5; Table 13).

Unbuffered batch extraction experiments with Liberty Island samples also only showed a mercury release of about 0.3 % based on the total mercury concentration of the sediments (Table 15).

Water chemistry

In comparison to Grizzly Bay water from April, Liberty Island water was much lower in salinity (0.06 ppt), conductivity (0.5 mS cm^{-1}), amount of oxygen (9.7 mg O_2 L^{-1} and 89 % saturation), cation and anion concentration (Figure 36) while pH was slightly higher (8.3). Measured salinity was in the typical range of freshwater (Mitsch and Gosselink, 1986) indicating the stronger influence of the Sacramento River. Except for a slightly higher concentration in DOC (4.0 mg C L^{-1}), no significant difference (Wilcoxon signed rank test, p-value of 0.3) was noted for the OM (concentration, respective fractions, fluorescence index) present in Liberty Island water which probably reflects the dominance of the Sacramento River as a single source of OM input for both field sites (Conaway et al., 2003).

Influence of divalent cations on mercury release with respect to the estuarine environment

The mercury release from estuarine sediments was studied in batch extraction experiments using sediment samples collected from Grizzly Bay, California. The release of mercury from these sediments generally ranged from 0.23 to 2.30 ng Hg(II) g^{-1} sediment depending on the composition of the batch solution (Figure 64). Maximum mercury release was determined in experiments with UPW without buffers (Table 8, no. 1A), whereas the minimum was detected in experiments containing an additional 0.2 mM calcium (Table 8, no. 3A).

As outlined in previous sections, OM has the ability to enhance mercury solubility (Ravichandran et al., 1998; Ravichandran et al., 1999; Haitzer et al., 2002; Waples et al., 2005; Süß, 2006). Thus, experiments with additional DOM in form of isolated fulvic acid (F1-FA) were conducted in the presence and absence of buffers (Table 8, no. 2A-C). However, the addition of DOM (5 mg C L^{-1}) resulted in either no change or a slight increase in the concentration of mercury released from sediments (Figure 64). Corresponding laboratory results showed that a certain amount of added DOM was lost because the measured DOC concentrations in the experiments with additional DOM were lower than expected (Figure 41). But taking into account that the actual calculated SUVA values were greater (5.1 to 5.6 $L \cdot mgC^{-1} \cdot m^{-1}$) than expected (4 to 4.4 $L \cdot mgC^{-1} \cdot m^{-1}$), it is more likely that the difference in actual and expected DOC concentration was caused by an inhibited release of OM from the sediments, which presumably also resulted in an inhibition of (organic-chelated) mercury release, than by sorption of additional DOM on the sediments. However, it also has to be taken into consideration that nitrate and iron concentrations which are known for interferences with UV light (Weishaar et al., 2003) were not checked in this experiment. Thus, it is not possible to exclude sorption of additional DOM on the sediments completely.

In contrast to DOM, calcium and magnesium (0.2 mM) in solution significantly reduced the mercury release from sediments even in the presence of additional DOM (5 mg C L^{-1}) (Figure 64) which is of particular interest considering the water chemistry in estuarine environments. Extraction experiments in this study yielded a mercury release from sediments in the range of 0.2-0.3 ng Hg(II) g^{-1} sediment (without DOM) to 0.4 - 0.7 ng Hg(II) g^{-1} sediment (with DOM) in the presence of calcium, and 0.4 - 0.7 ng Hg(II) g^{-1} sediment (without DOM) to 1.5 ng Hg(II) g^{-1} sediment (with DOM) in the presence of magnesium, whereas in the absence of divalent cations 1.8 - 2.3 ng Hg(II) g^{-1} sediment was released (Figure 64). Similar effects were observed in other studies (Ravichandran et al., 1998;

Ravichandran et al., 1999; Melamed et al., 2000; Süß, 2006). In experiments with DOM, and added calcium or magnesium, the inhibition of mercury release from sediments might be due to the complexation of calcium and magnesium by carboxyl groups in OM that change the charge density and, thus, the ability of DOM to enhance the mercury release (Davis, 1982; Morel and Hering, 1993; Ravichandran et al., 1999). Especially in marine systems, it is generally noted that organic complexation of calcium and magnesium is more dominant than the complexation of trace metals (Davis, 1982; Morel and Hering, 1993). In freshwater systems, where the concentrations of calcium and magnesium are one to three orders of magnitude lower than in seawater, organic complexation of trace metals is more important (Davis, 1982; Morel and Hering, 1993).

With regard to the present results of the batch experiments and filtration studies, and the fact that the majority of mercury in sediments was found to be associated with OM (presumably sorbed on clay minerals), another process is more likely to be responsible for the inhibition of mercury release. Divalent cations like calcium or magnesium in solution can sorb on to colloidal surfaces, like clay minerals or aggregated organic matter, changing the surface charge and blocking the active surface sites against other dissolution agents (Davis, 1982; Ravichandran et al., 1999). In addition, the sorption of divalent cations can generally influence the mobilization of colloids by reducing the repulsive electrostatic forces between the colloids due to a better balance of the surface charges, and thus, favoring aggregation and inhibiting mercury release (Ryan and Elimelech, 1996; Ravichandran et al., 1999). The outlined mechanisms would explain why a loss of 66 to 76% of the added calcium (Table 8, no. 3A/B), as well as 56 to 66% of the added magnesium (Table 8, no. 4A/B) was observed in the calcium and magnesium addition experiments in the presence and absence of DOM. The batch extraction experiments with untreated and treated Liberty Island water (Table 8, no. 3C) particularly demonstrated the impact of calcium and magnesium on the mercury release from sediments (Figure 43,

Figure 45). The high concentration of calcium and magnesium in untreated Liberty Island water caused, the inhibition of mercury release (Figure 43) which might be attributed to colloid stabilization (Ryan and Elimelech, 1996; Ravichandran et al., 1999). The change in the solution chemistry of Liberty Island water by removal of the divalent cations could have forced the mobilization of colloids and thus, the observed release of mercury due to changes in the double layer potential energy that caused the increase of the repulsive forces between colloids (Figure 45). However to induce the mobilization of colloids, repulsive forces have to exceed the attractive forces between colloid surfaces based on the balance of the surface charges and the thickness of the double layer (Ryan and Elimelech, 1996). Results obtained from filtration studies (0.45 and 0.1 μm) would support this idea since more mercury (10 %) was released in the fraction greater than 0.1 μm in experiments which had lower divalent cation concentrations.

The release of OM from the sediments was also affected by the presence of divalent cations in solution (Figure 64). Organic matter release decreased in calcium and magnesium addition experiments in comparison to the unbuffered and buffered experiments without addition of divalent cations from 0.2 to 0.1 mg C g^{-1} sediment (Figure 64) accompanied by a depression in SUVA from 4.4 $L \cdot mgC^{-1} \cdot m^{-1}$ (Table 15) to 2.7 $L \cdot mgC^{-1} \cdot m^{-1}$. Since a strong correlation between molar absorptivity and molecular weights of humic substances exists (Chin et al., 1994), the reason in the decrease in OM release accompanied by the depression of SUVA can be found in the suppression of the solubility of higher molecular weight humic substances in the presence of divalent cations (Aiken and Malcolm, 1987). The decrease of solubility is due to the fact that calcium and magnesium are the predominant cations neutralizing the charges on humic substances (Hayes and Swift, 1978). Furthermore, potassium, manganese, and strontium slightly increased in calcium and magnesium addition experiments whereas aluminum increased in comparison to the experiments without addition of divalent cations. With

respect to these investigations and the observed seasonal changes in the water chemistry at the field sites, a key question to address is what magnitude of changes in divalent cation concentration in the estuarine environment would be sufficient to enhance or inhibit mercury release from sediments. In a study in the northern reach of the San Francisco Bay estuary, mercury was preferentially associated with suspended particulate matter (> 0.45 μm) during the low flow period in summer (high salinity) whereas colloidal material (1kDa – 0.45 μm) was more important during the high flow, lower salinity conditions in winter (Choe et al., 2003). During the high flow conditions, higher mercury concentrations were measured in solution (Choe et al., 2003), which would support the results obtained in this study. However, it also has to be taken into consideration that 67 % of the mercury input from the Sacramento River is already associated with colloidal material (Choe et al., 2003). Coquery et al. (1997) and Bilinski et al. (2000) also noted seasonal changes in mercury concentration and variable contribution of colloidal material based on changes in salinity in the Seine and Loire estuaries in France and the Krka river estuary in Croatia.

Besides these environmental conditions that could play a role in the estuarine system of the Sacramento-San Joaquin Delta, laboratory results from experiments in the presence of sodium containing pH and ionic strength buffers showed an inhibition in mercury release in comparison to experiments without buffers (Figure 64). The suppression was caused by high concentrations of sodium in the batch solutions (0.07 M) that caused, in turn, the release of calcium (0.1 mM) and magnesium (0.3 mM) from the estuarine sediments by ion-exchange. Besides the release of calcium and magnesium, OM which probably was sorbed to the sediment by bridging cations like calcium also showed an increased release in comparison to the unbuffered experiments where no calcium and magnesium was released from the sediments (Figure 64).

Ultimately, it is difficult to estimate the influence of divalent cations on mercury release from sediments in an estuarine environment like the Sacramento-San Joaquin Delta since it is an open system where a broad range of factors interact (e.g. seasonal changes in freshwater input and OM, tidal influence and wind with regard to resuspension of sediments, etc.). However, the present study showed that the presence of calcium in solution inhibits the mercury release from sediments which could be important for environments where calcium naturally occurs. It could be furthermore a tool for resource managers in the San Francisco Bay Delta, for instance, in restored wetlands where calcium could be added to decrease the amount of dissolved mercury.

Although, extensive mercury and gold mining in Northern California caused an estimated loss of 5.8 million kilograms of mercury in the watersheds of the Sacramento-San Joaquin river and the Delta between the 1850s to 1960s (Alpers et al., 2005; CALFED, 2005), mercury concentrations of surface sediments (0-2 and 2-4 cm) collected from Grizzly Bay and Liberty Island in the Delta in January and April 2008 did not exceed the geometric mean for U.S. coastal sediments of 0.22 μg Hg g^{-1} (Daskalakis and O'Connor, 1995). However, mercury contaminated sediments still comprise an internal source to the Sacramento-San Joaquin Delta, providing the potential of mercury release into the aquatic system and, thus, the availability for mercury methylation. Even low amounts of released mercury, as received for the estuarine sediments in this study (maximum 2.3 ng Hg(II) g^{-1} sediment), could be harmful with regard to bioaccumulation and magnification. Batch extraction experiments and filtration studies showed that the presence of calcium or magnesium in solution (0.2 mM) affects colloid mobilization and DOM in solution and, thus, the mercury release from sediments. The addition of calcium or magnesium caused a significant decrease in mercury release regardless of whether additional DOM (5 mg C L^{-1}), which typically increases the release by forming complexes with mercury, was also present in the solution or not. Additionally, filtration studies revealed that approximately 10% more mercury in

the size fraction greater than 0.1 μm was released in experiments which had lower concentration of divalent cations in solution. The water chemistry in the San Francisco Bay Delta seems to be highly dependent on the freshwater inflow by fluvial discharge and precipitation, influencing the length and location of the mixing zone between sea- and freshwater. The related changes in the water chemistry, especially salinity, could have, with respect to the results of the present study, a significant impact on mercury by increasing or inhibiting the release. With regard to the management and restoration of wetlands in the Bay-Delta ecosystem (Wiener et al., 2003), the presence of elevated amounts of calcium in the system could prevent or at least decrease mercury release. Even the small-scale insertion and application of calcium-rich minerals like calcium carbonate in wetlands could be a promising alternative. Further investigations are necessary to understand the physical and chemical processes and interactions controlling the mercury cycling in the Sacramento-San Joaquin Delta.

Local sediment resuspension

Intertidal habitats in the San Francisco Bay-Delta are highly dynamic systems with many modes of variability. The threshold wind speed was a surprisingly consistently 8 m s^{-1} for large sediment resuspension events at both Liberty Island and Grizzly Bay with suspended sediment concentrations increasing greatest during wind events that occurred at low tide and in the direction of greatest fetch. There was a smaller but still meaningful resuspension event observed with properly aligned winds at a mere 4 to 6 m s^{-1} and under spring tide excursions. The conditions for resuspension events therefore occur rather frequently from daily to weekly depending on season and tide phase. This frequency may explain the lack of marked changes in sediment character observed during resuspension events in this study.

Although rainfall driven mobilization of particulates and related porewater dissolved constituents occurs in the marshes and tidal creeks, there was no marked signal of the adjacent shallow

subtidal region at the deployment sites despite confirmation of the linkage between the deployment site and intertidal mudflats where the precipitation gage and runoff autosampler were located.

Large variability was observed in the dissolved measurements but at a less frequent and flashy nature than particulate resuspension suggesting that the effect was not localized in nature but rather due more to tidal and regional effects. This is particularly clear in the winter season when concentrations increased markedly over the deployment period as rainfall accumulated over the entire watershed. The largest variation was observed in Liberty Island as flows down the Sacramento River and Yolo Bypass increased rather than being related to localized wind and rain events.

Regional effect

Simple 1-D model suggests that resuspension of intertidal particles by wind in the Bay-Delta occurs frequently. Rainfall has a more distinct effect on particulate character and dissolved transport but the signal is swamped by the regional response. However, the particulates measured in the subtidal habitats adjacent to the intertidal mudflats did not appear to be elevated in contaminants or organics suggesting that the effect on biotic uptake is small relative to baseline conditions on a regional scale.

Inundation models using moderate levels of future sea-level rise indicate up to 80,000 hectares of land surrounding San Francisco will be below mean sea level (Knowles and Cayan, 2002) suggesting future climate change will increase intertidal habitat considerably. Coupled with increased intensity of ENSO type rainfall events these may have a large effect – but still dependent on frequency of wind resuspension in this region such that sediment character is disturbed too frequently to be altered in a way that enhances the biotic exposure of contaminants relative to the baseline condition.

Summary and Conclusions

This study investigated the extent to which mobilization of sediments by wind and rainfall affect concentrations of suspended sediment, organic matter, and metals in Grizzly Bay and Liberty Island in central California. Suspended sediment concentrations were higher after low-tide rain events than both wind events and fair-weather background measurements. Concentrations of selected leachable metals (^{111}Cd, ^{133}Cs, ^{208}Pb, ^{53}Cr, ^{55}Mn, ^{57}Fe, ^{60}Ni, ^{63}Cu, ^{66}Zn, ^{107}Ag, ^{89}Y and ^{146}Nd) were higher during the rain event than during the wind event. Concentrations during both events were higher than concentrations during the tidal cycle only for Cd, Cu, Ni, Zn, and Y. The relationship between metal content and suspended sediment concentration varied widely between different metals, but indicated that rainfall mobilizes sediments from a different source than is available to wind and tidal resuspension. Particulate organic carbon, particulate nitrogen, percent organic carbon, percent nitrogen, and the carbon to nitrogen ratio were all much higher during the rain event than during both the wind event and the tidal cycle. All organic parameters increased during pulses of rainfall, and decreased steadily after rainfall ended. By contrast, the parameters varied little during the wind and tidal cycle events.

Total mercury concentrations in the sediments from Grizzly Bay and Liberty Island ranged between 0.12 and 0.18 mg Hg kg^{-1} sediment, and were particularly associated with organic matter (56 to 72 %). In the presence of calcium or magnesium (0.2 mM), mercury release was significantly inhibited regardless of whether additional dissolved organic matter (5 mg C L^{-1}), which typically increase the release by forming complexes with mercury, was also present in the solution or not. Changes in the water chemistry in an estuarine system with regard to divalent cations and salinity could therefore have a significant impact on mercury release; the presence of elevated amounts of calcium in the system could prevent or at least decrease the mercury release and, thus, the potential of methylation and bioaccumulation of mercury.

Filter-passing mercury concentrations were strongly related to optical measurements and ranged from 0.5 to 3.5 ng L^{-1}, while filtered methyl mercury ranged from 0.02 to 0.2 ng L^{-1}. Mercury concentration on particles ranged from 150 to 250 ng g^{-1} and were well correlated with suspended sediment concentrations ($r^2 \sim 0.75$- 0.96). Methyl mercury on particles were measured lower in winter (0.6 to 1.8 ng g^{-1}) and higher in summer (1.6 to 4.2 ng g^{-1}), possibly related to higher median particle size and algal activity found in the summer. A 1-D model of resuspension processes suggests that resuspension of intertidal sediment by wind occurs frequently.

Although rain falling during low tide does mobilize marsh sediments, with associated organic matter and metals, into the adjacent tidal creek, the effect on the nearby larger shallow waters is relatively minor. Winds, while of minor importance in the tidal creek, are a more important driver of benthic sediment resuspension in the large shallow bays but of low importance to the mobilization of contaminant metals. The overall importance of metals input to Grizzly Bay and Liberty Island by rainfall mobilization seems to be minor, but further research into the place of rainfall mobilization in local metals budgets would help to clarify the situation.

6. Project Deliverables

- **List here any presentations given at the Bay-Delta Science Conference and at other events**
- **List here and provide hardcopies and electronic files of all materials and published papers resulting from this grant**

6.1 Accomplished deliverables

Papers:

Moskalski, S. and Torres, R., *in press*. Influences of tides, weather, and discharge on suspended sediment concentration. Continental Shelf Research. Attached.

Presentations:

Moskalski, S., and Torres, R., 2011. Variability of suspended sediment concentration in Suisun Bay, California, and the relative influences of tides, meteorology, and river discharge (oral presentation). Coastal and Estuarine Research Federation Conference, 2011. Attached.

6.2 Pending deliverables

Papers:

Moskalski, S., Torres, R., Rothenberg, S., and Bizimis, M., *in preparation*. Mobilization of metals in intertidal sediment by rainfall.

Figures

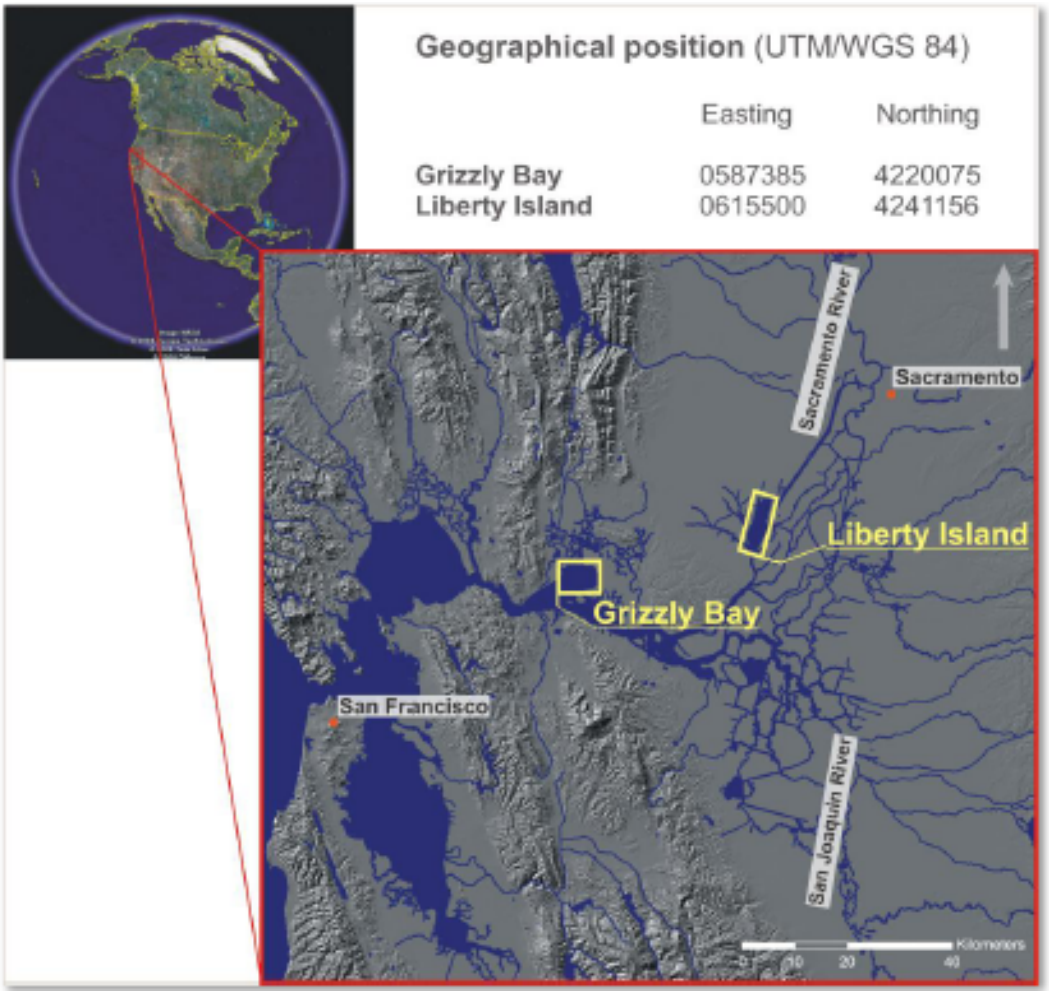

Figure 1. Field sites in the Sacramento-San Joaquin Delta/CA - Geographical information for both locations are based on the Universal Transverse Mercator (UTM) coordinate system (zone: 10S, reference-ellipsoid: WGS84). The left image is taken from Google Earth (2007).

A

6831 ft
© 2012 Google
Imagery Date: 9/23/2009
38°06'48.50" N 122°01'21.38" W elev 0 ft
Google earth
Eye alt 29528 ft

B

8219 ft
© 2012 Google
Imagery Date: 10/30/2011
38°16'53.20" N 121°40'17.56" W elev 6 ft
Google earth
Eye alt 35536 ft

Figure 2. (*A*) Grizzly Bay and (*B*) Liberty Island study areas, showing locations of sensor packages. Yellow stars mark the locations of the marsh sampling stations, and red starts mark the in-water instrument packages.

Figure 3. Example of moored instrumentation package consisting of underwater photometers, fluorometers, particle size analyzer, nitrate analyzer, YSI sonde, wave gauge, pumps and filtration system, and batteries. Acoustic Doppler moored in a separate system, but co located with the main moored optical system.

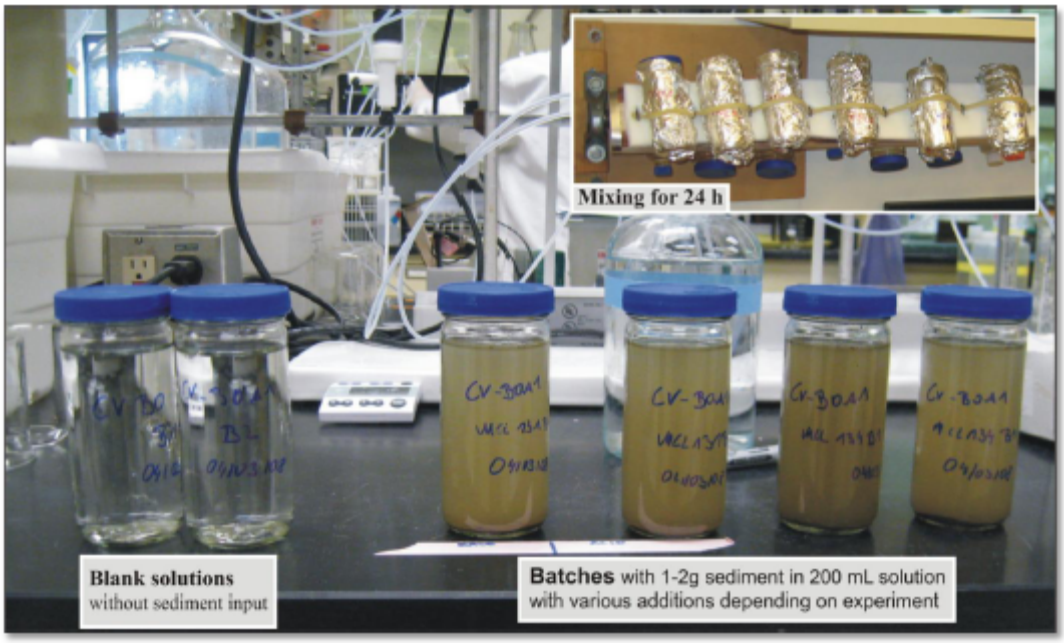

Figure 4. Experimental set-up of batch extraction experiments.

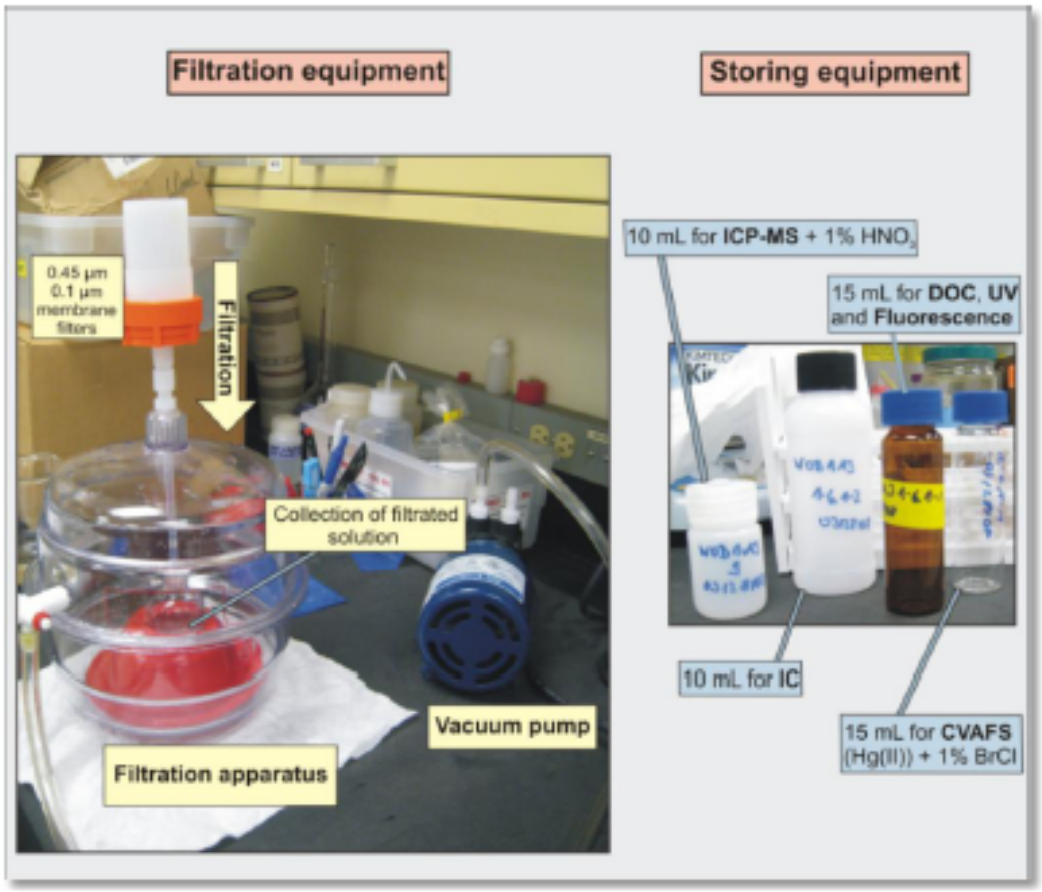

Figure 5. Vacuum filtration and subsampling for analyses (Vacuum pump: Barnant Company, Air Cadet®, single-head pump).

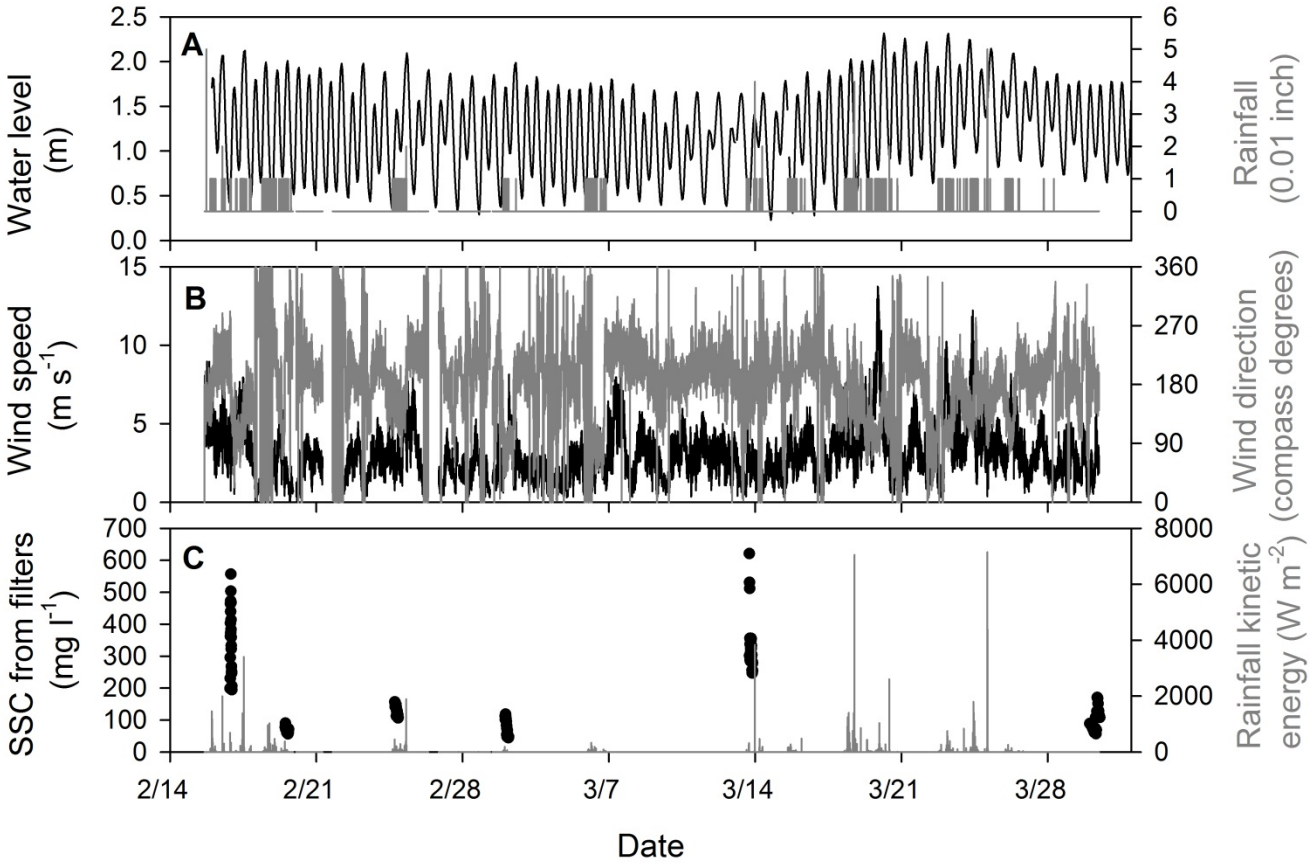

Figure 6. Weather and SSC summary for Grizzly Bay winter deployment. (*A*) Water level and rainfall, (*B*) wind speed and direction, (*C*) SSC and rainfall kinetic energy.

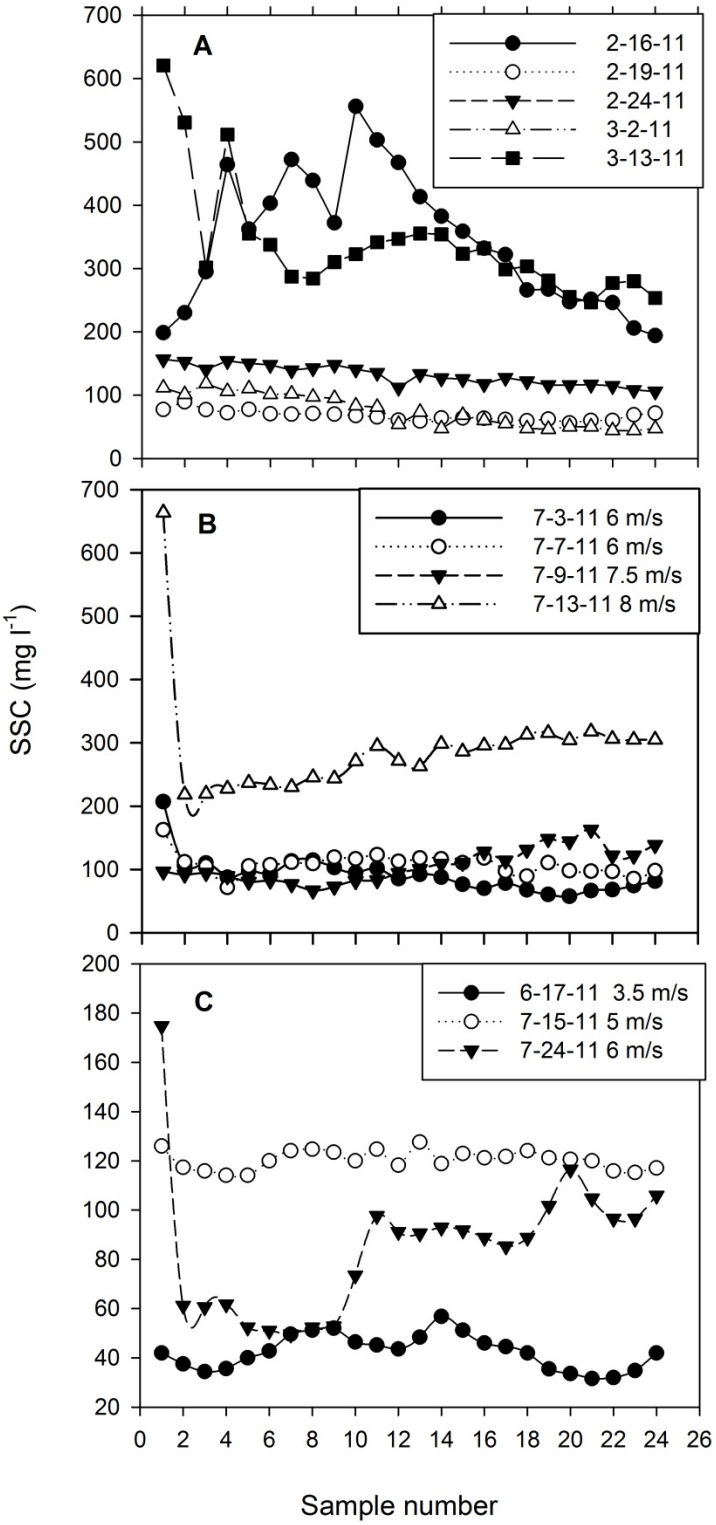

Figure 7. Comparison of SSC timeseries generated by (*A*) rain events, and (*B*) wind events at Grizzly Bay, and (*C*) wind events at Liberty Island.

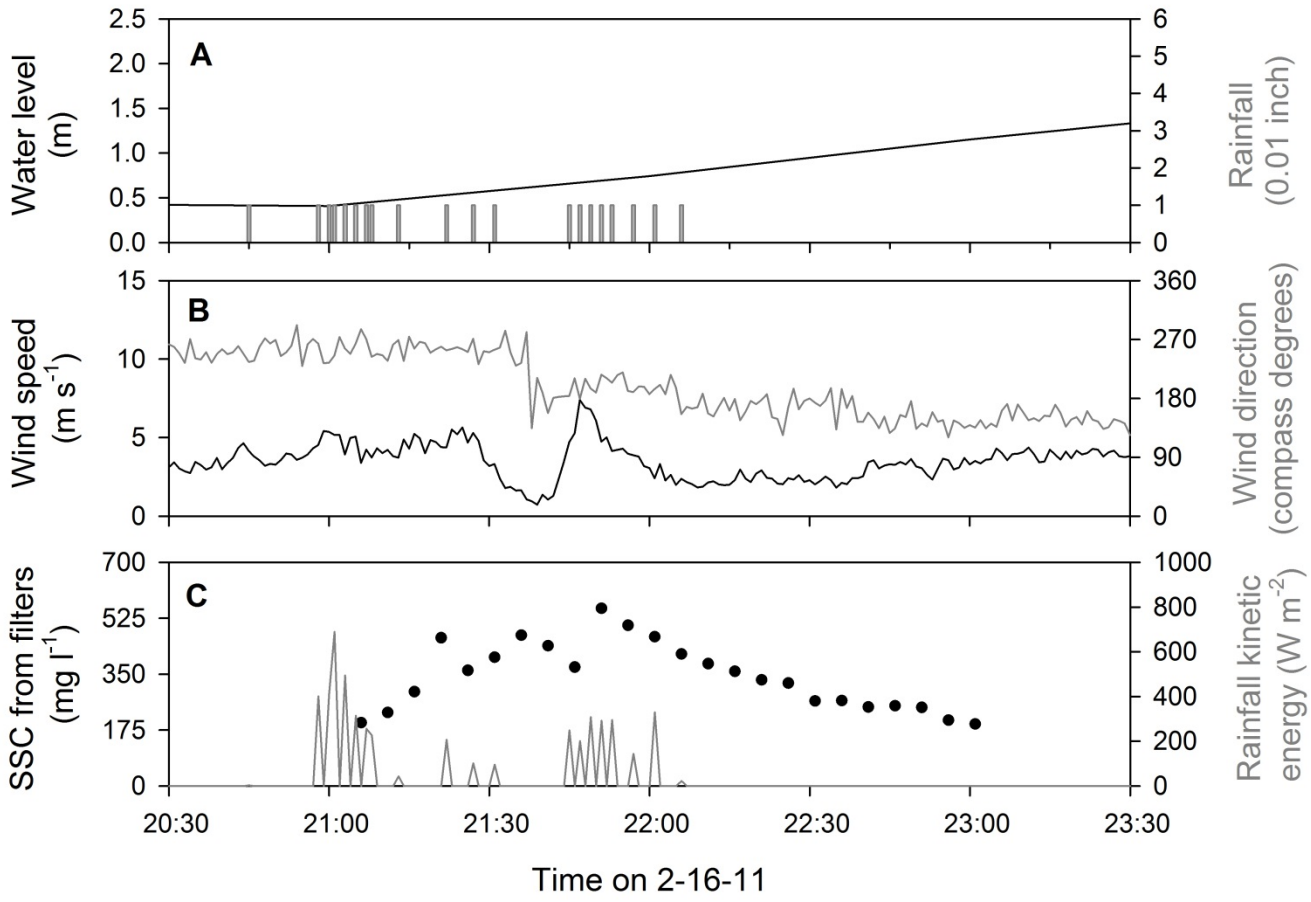

Figure 8. Weather and SSC data for the 16 February 2011 rain event at Grizzly Bay. (*A*) Water level and rainfall, (*B*) wind speed and direction, (*C*) SSC and rainfall kinetic energy.

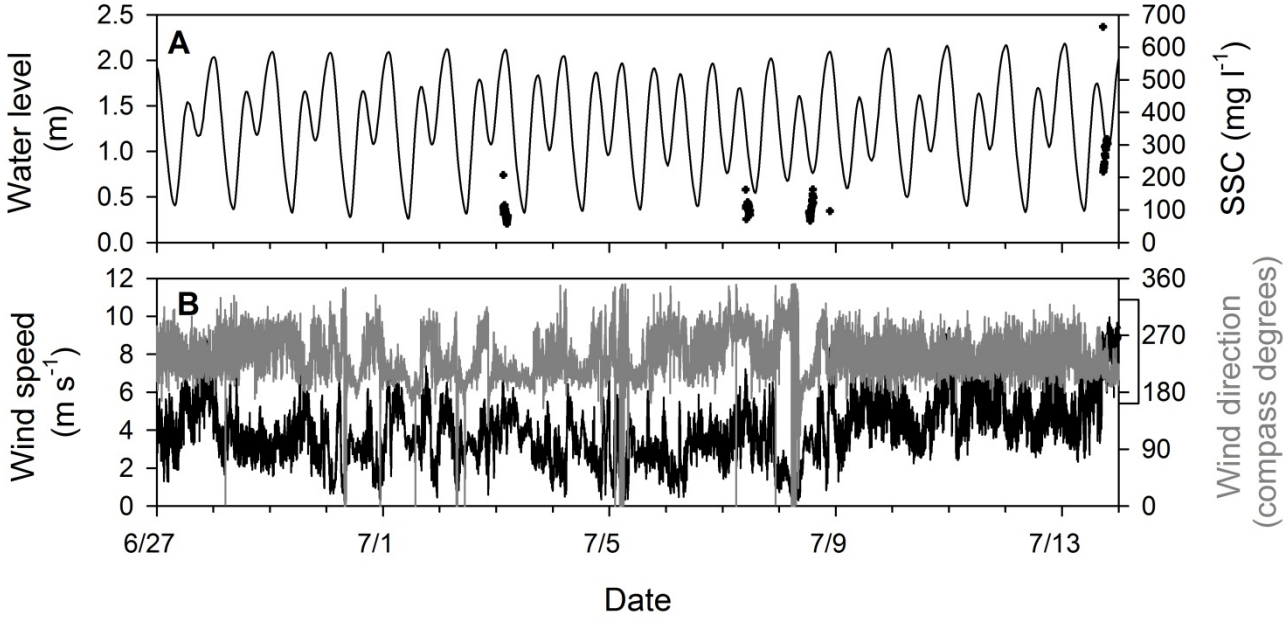

Figure 9. Weather and SSC summary for the Grizzly Bay summer deployment. (*A*) Water level and SSC, (*B*) wind speed and direction.

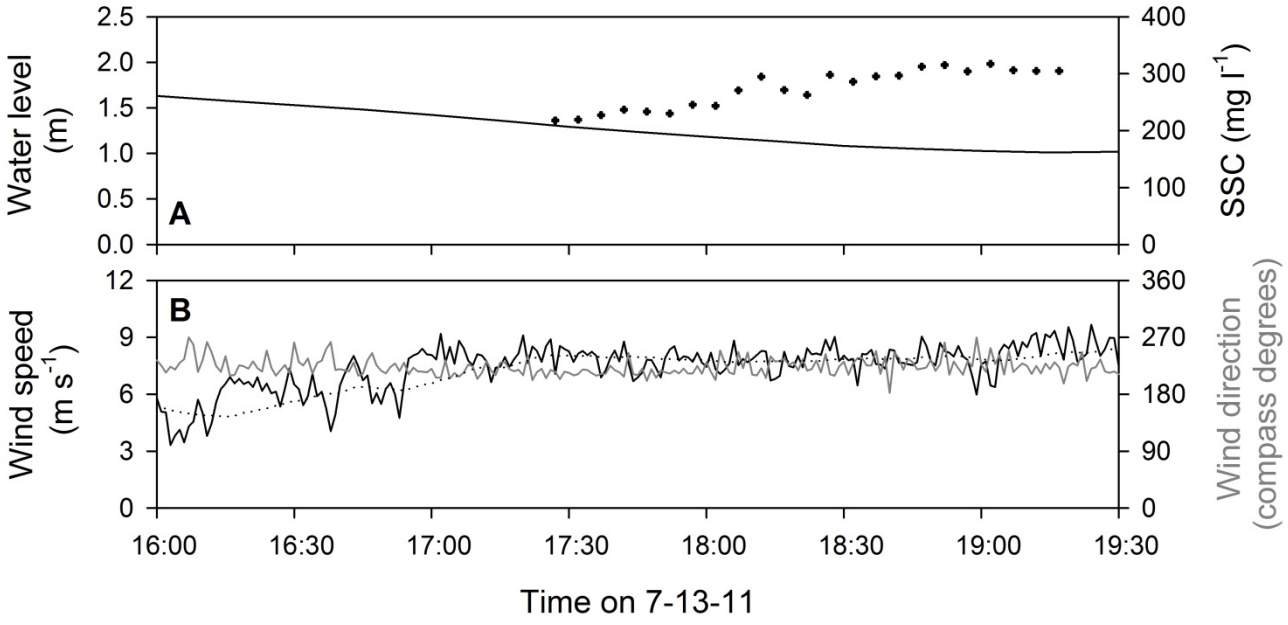

Figure 10. Weather and SSC data for the 13 July 2011 Grizzly Bay wind event.

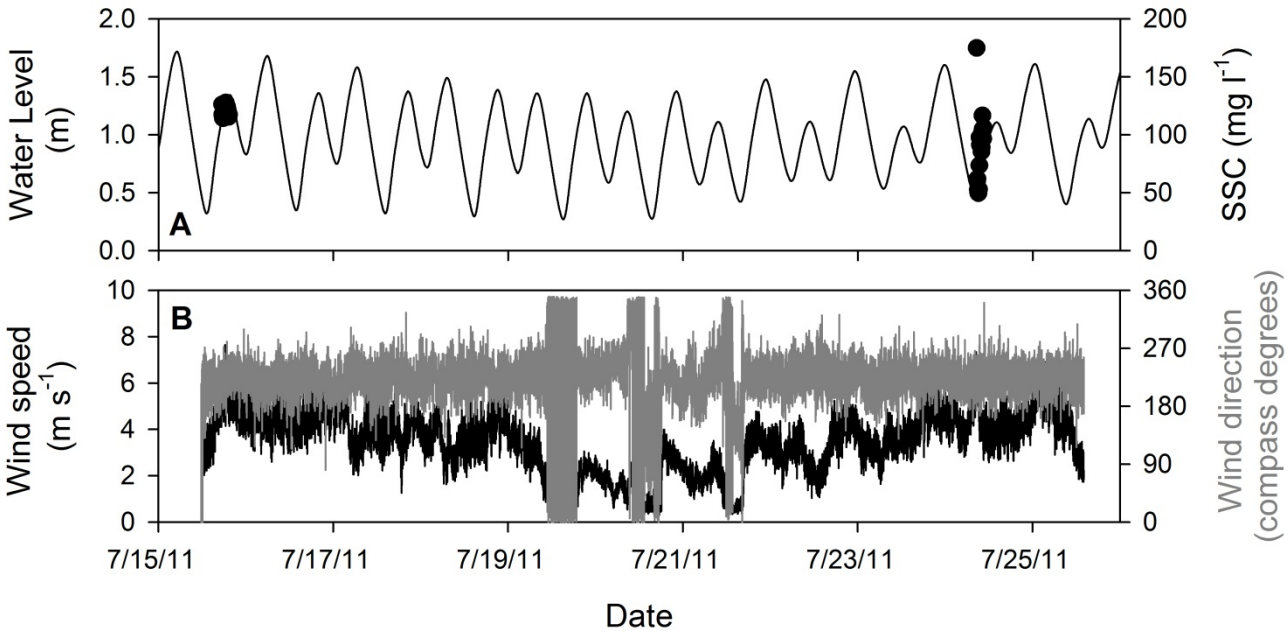

Figure 11. Weather and SSC summary for the Liberty Island summer deployment.

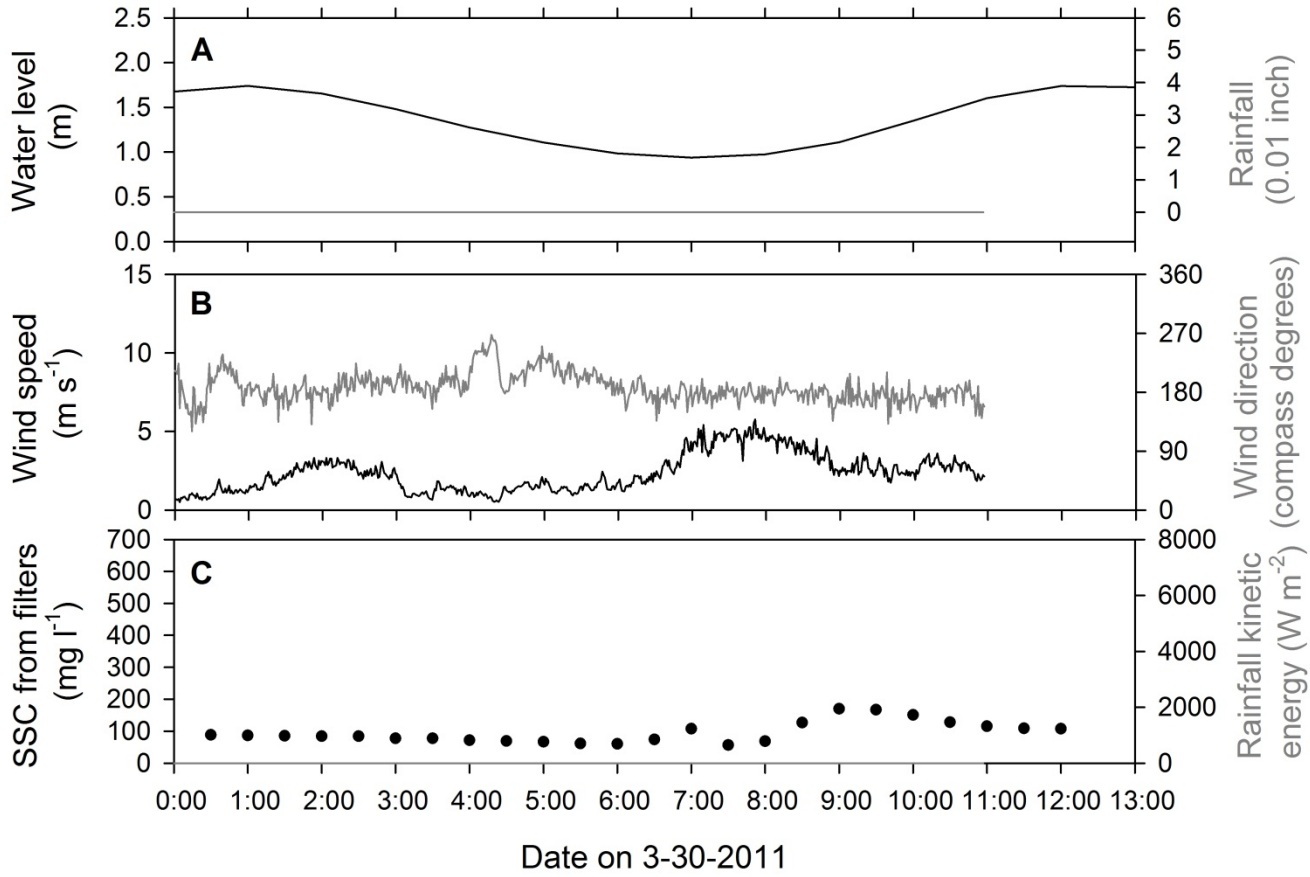

Figure 12. Weather and SSC data for the fair weather tidal cycle collected at Grizzly Bay. (*A*) Water level and rainfall, (*B*) wind speed and direction, (*C*) SSC and rainfall kinetic energy.

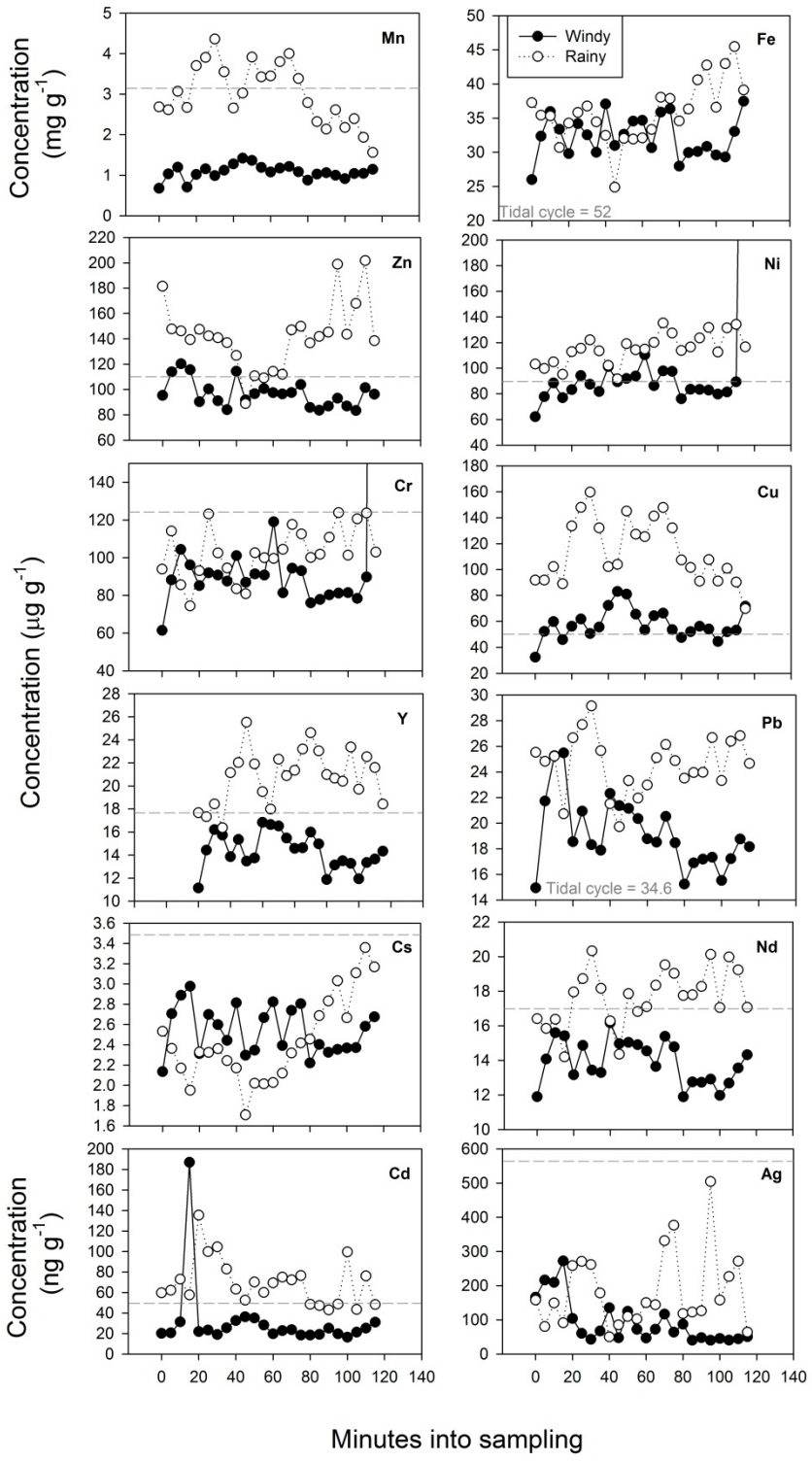
Concentration (mg g-1)
Concentration (µg g-1)
Concentration (ng g-1)
Mn
Fe
Zn
Ni
Cr
Cu
Y
Pb
Cs
Nd
Cd
Ag
Windy
Rainy
Tidal cycle = 52
Tidal cycle = 34.6
Minutes into sampling

Figure 13. Total concentration of metals in suspended sediment per gram of dry weight for selected metals. Open circles are the rain event and closed circles are the wind event. The gray dashed lines indicate the mean concentration for the two hours before and after low tide during the tidal cycle, except for the two metals where the low tide mean is outside the range of the plot. Note that the units on the y-axes change by several orders of magnitude.

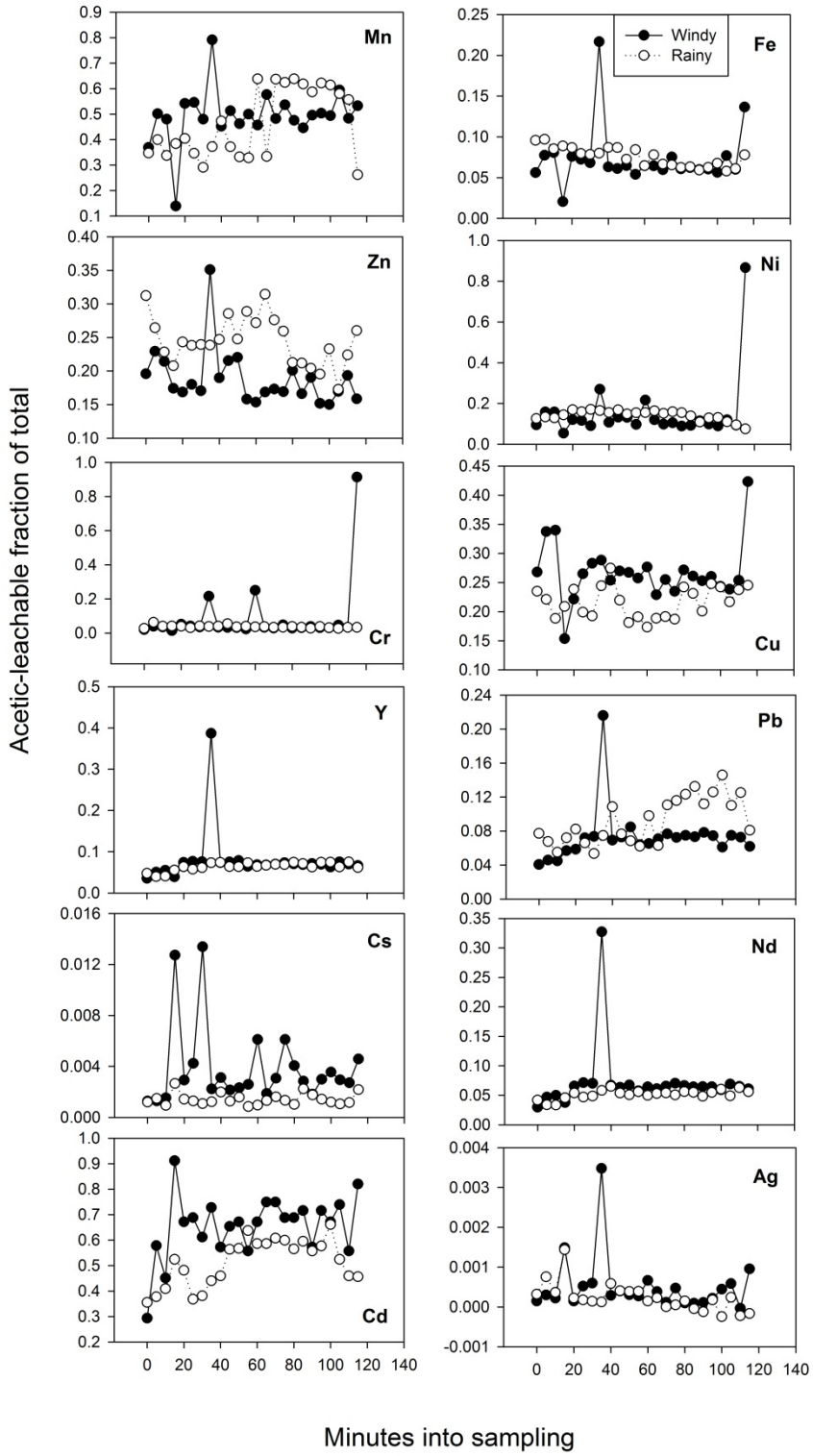

Figure 14. Acetic-acid-leachable fraction of total leachable metals. Open circles are the rain event and closed circles are the wind event.

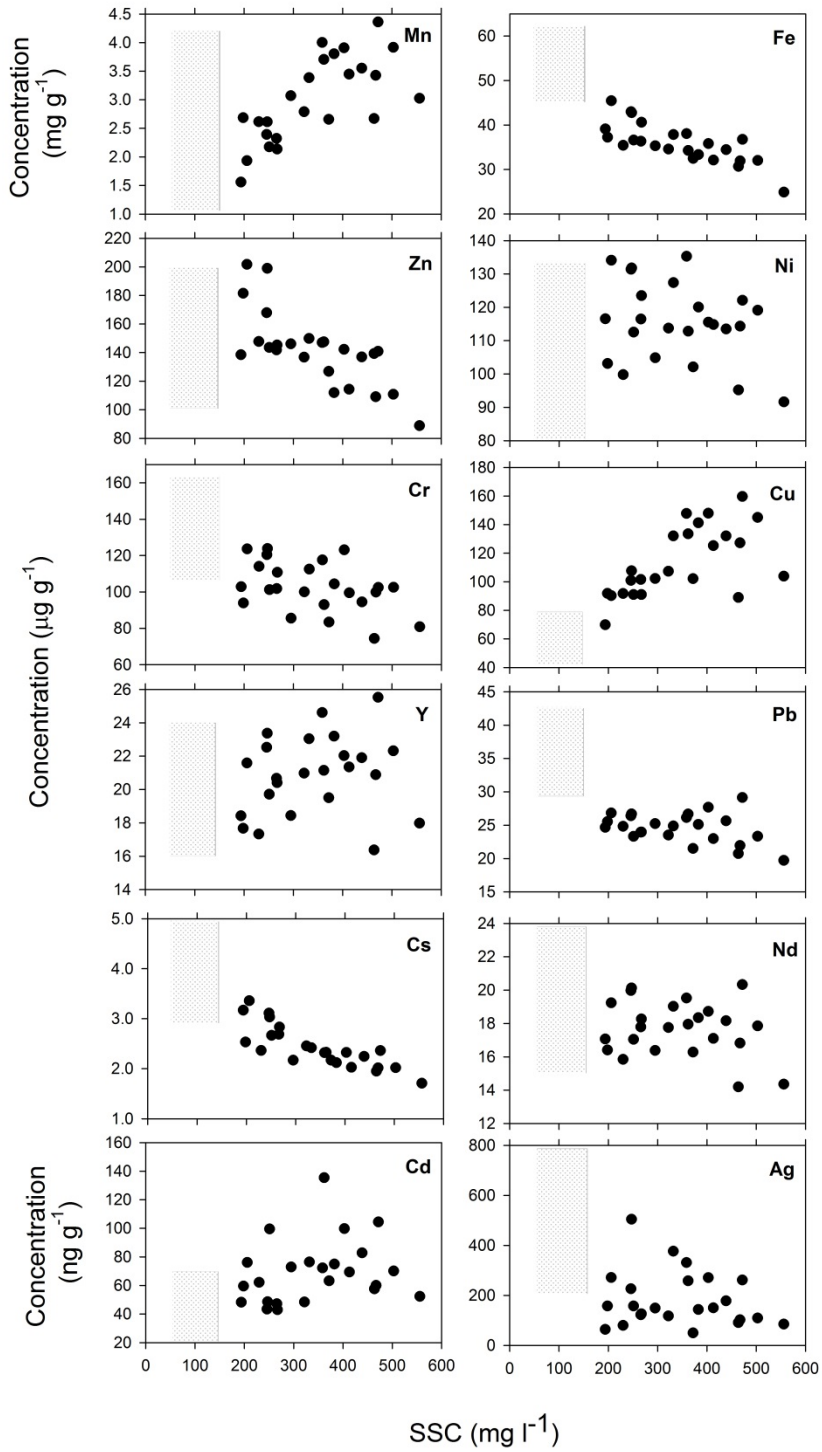

Figure 15. Total metal content versus SSC for the rainy event on 2-16-11. Note that the units on the y-axes change by several orders of magnitude. The stippled areas indicate the ranges of the values during 2 hours before and after low tide in the tidal cycle event.

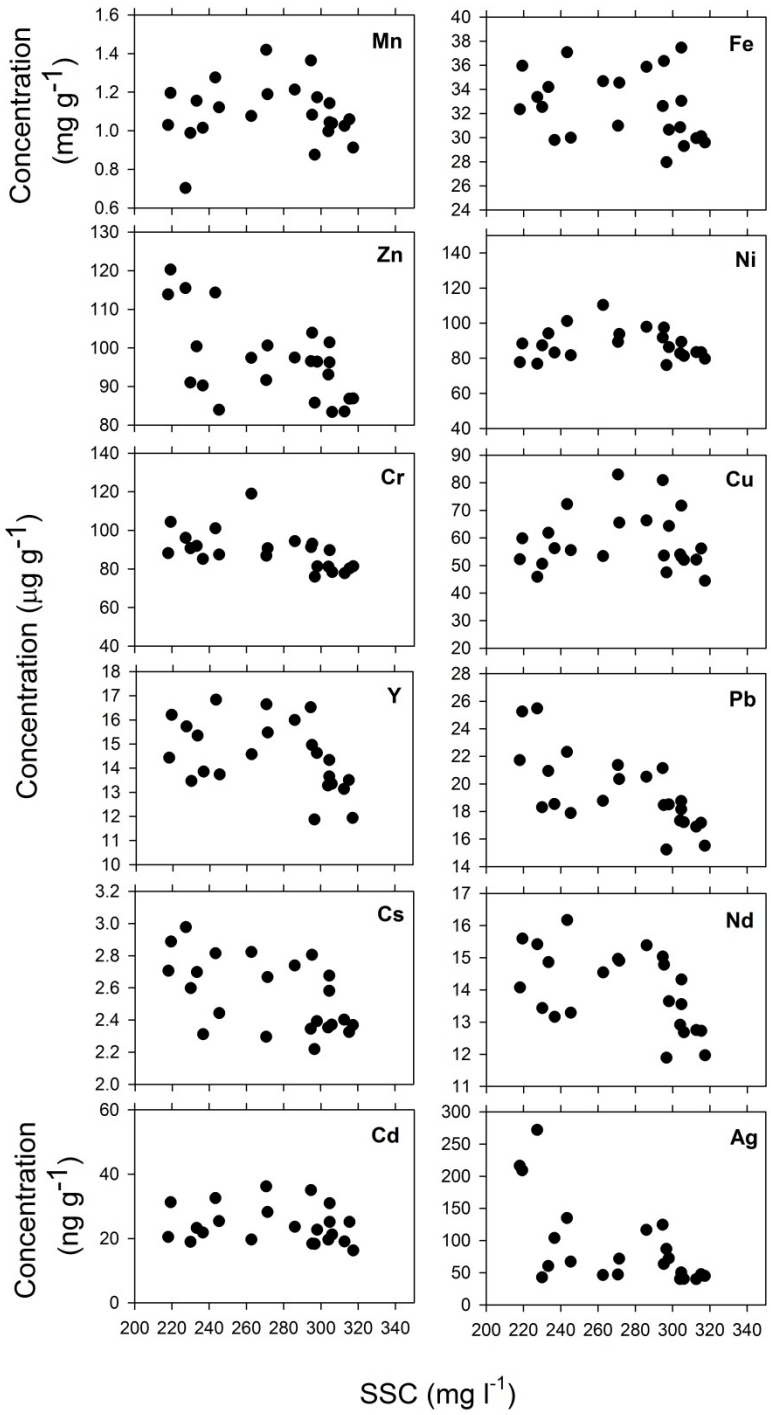

Figure 16. Total metal content versus SSC for the windy event on 7-13-11. Note that the units on the y-axes change by several orders of magnitude, and that two outliers were excluded.

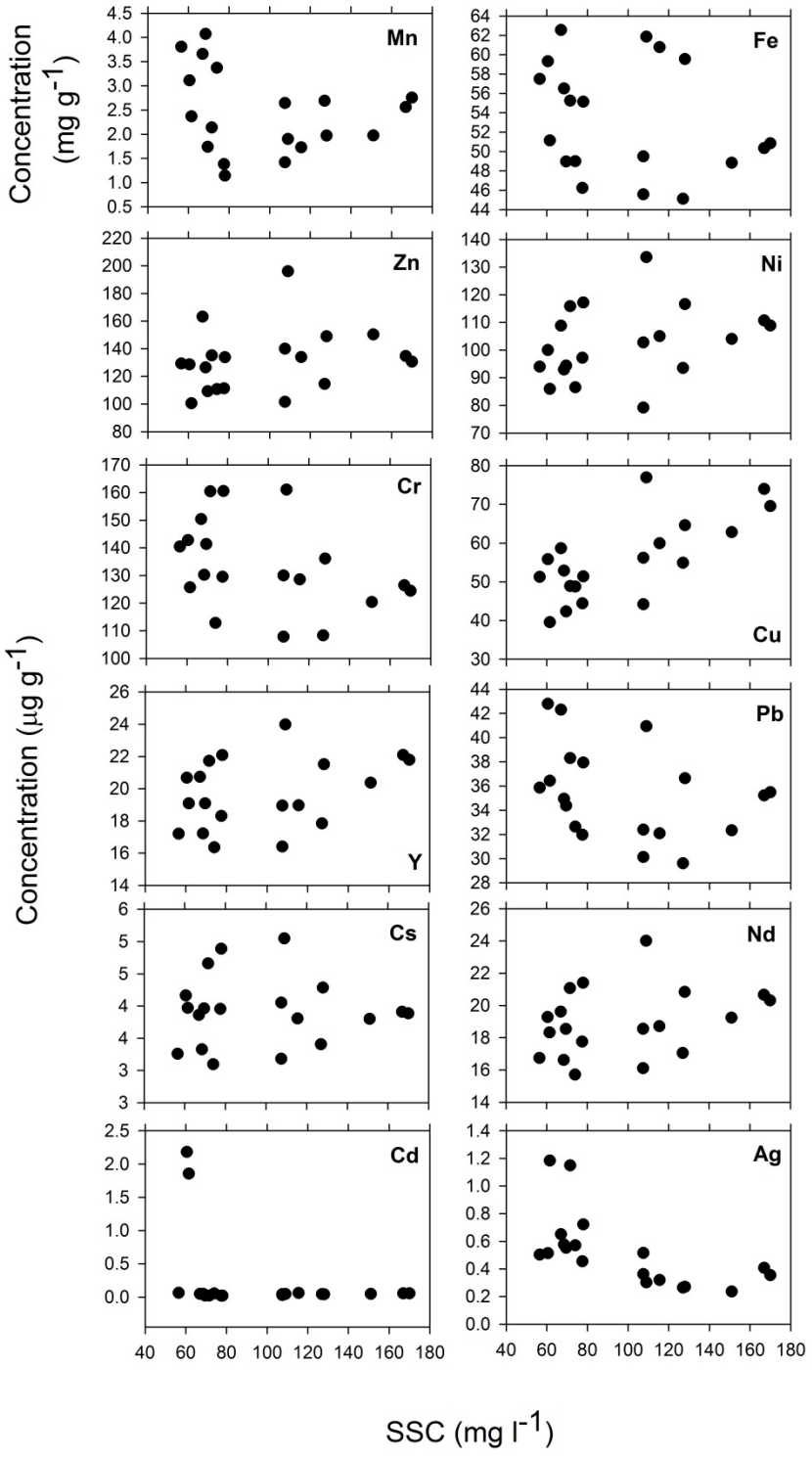

Figure 17. Total leachable metal concentration versus SSC for the tidal cycle survey on 3-30-11. Note that the units on the y-axes change by several orders of magnitude.

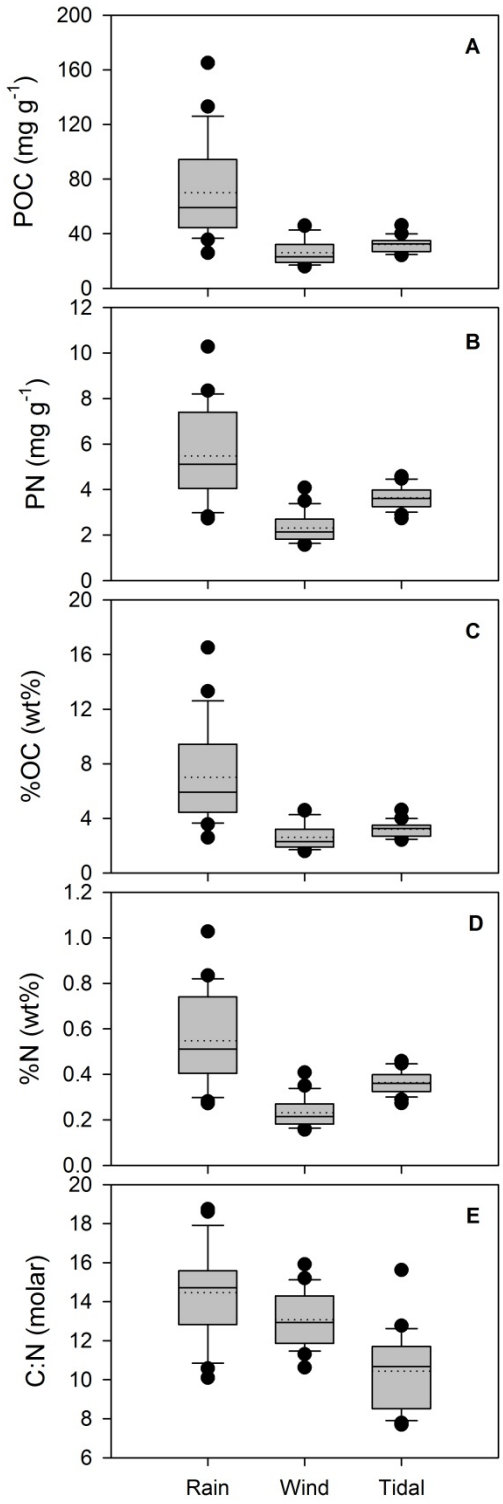

Figure 18. Summary plots of measured organic parameters. (A) POC (B) PN (C) %OC (D) %N (E) C:N. Solid line inside box is the median and dashed line is the mean.

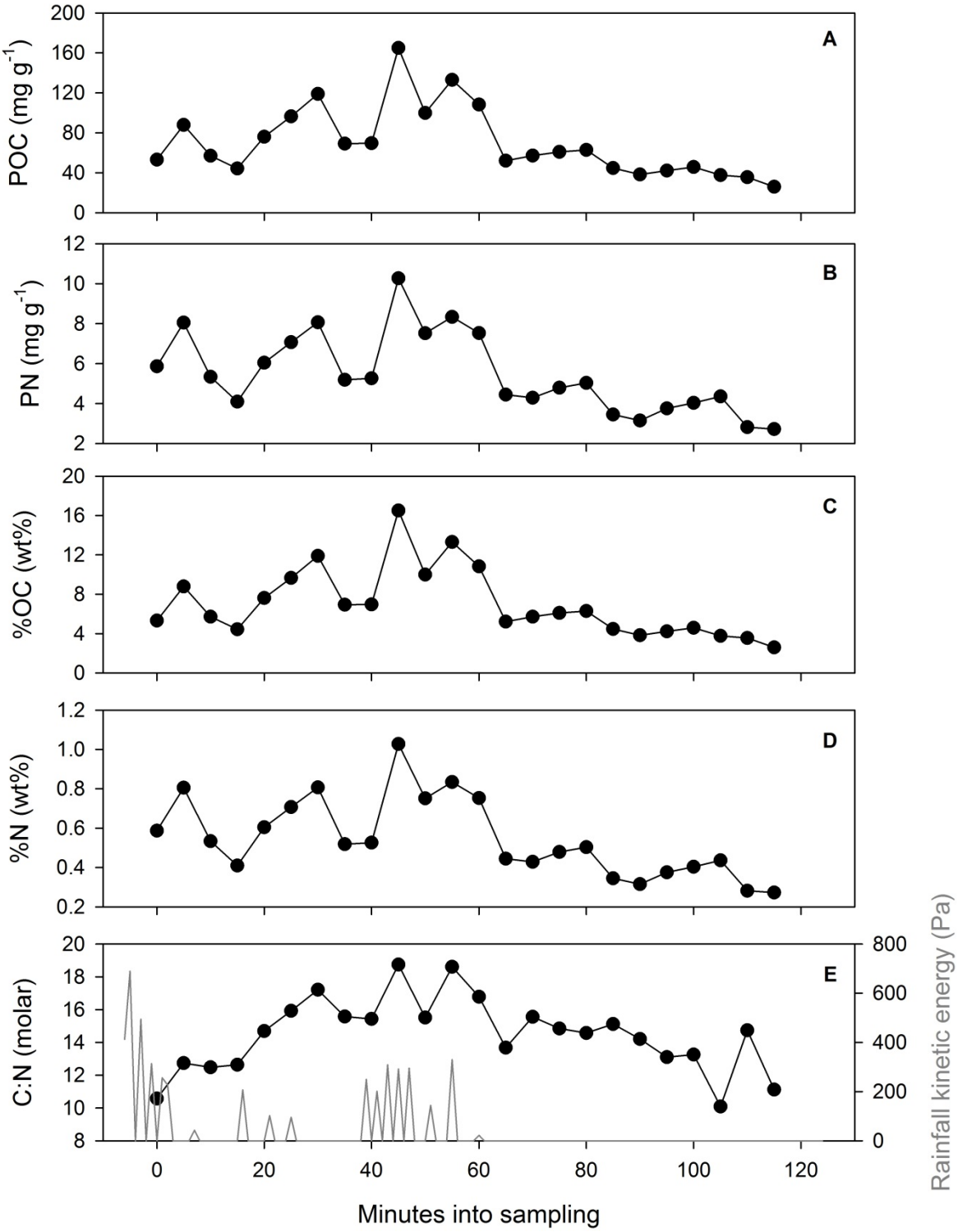

Figure 19. Organic nutrient data from the 2-16-11 rain event. (A) POC, (B) PN, (C) %OC, (D) %N, and (E) C:N and rainfall kinetic energy.

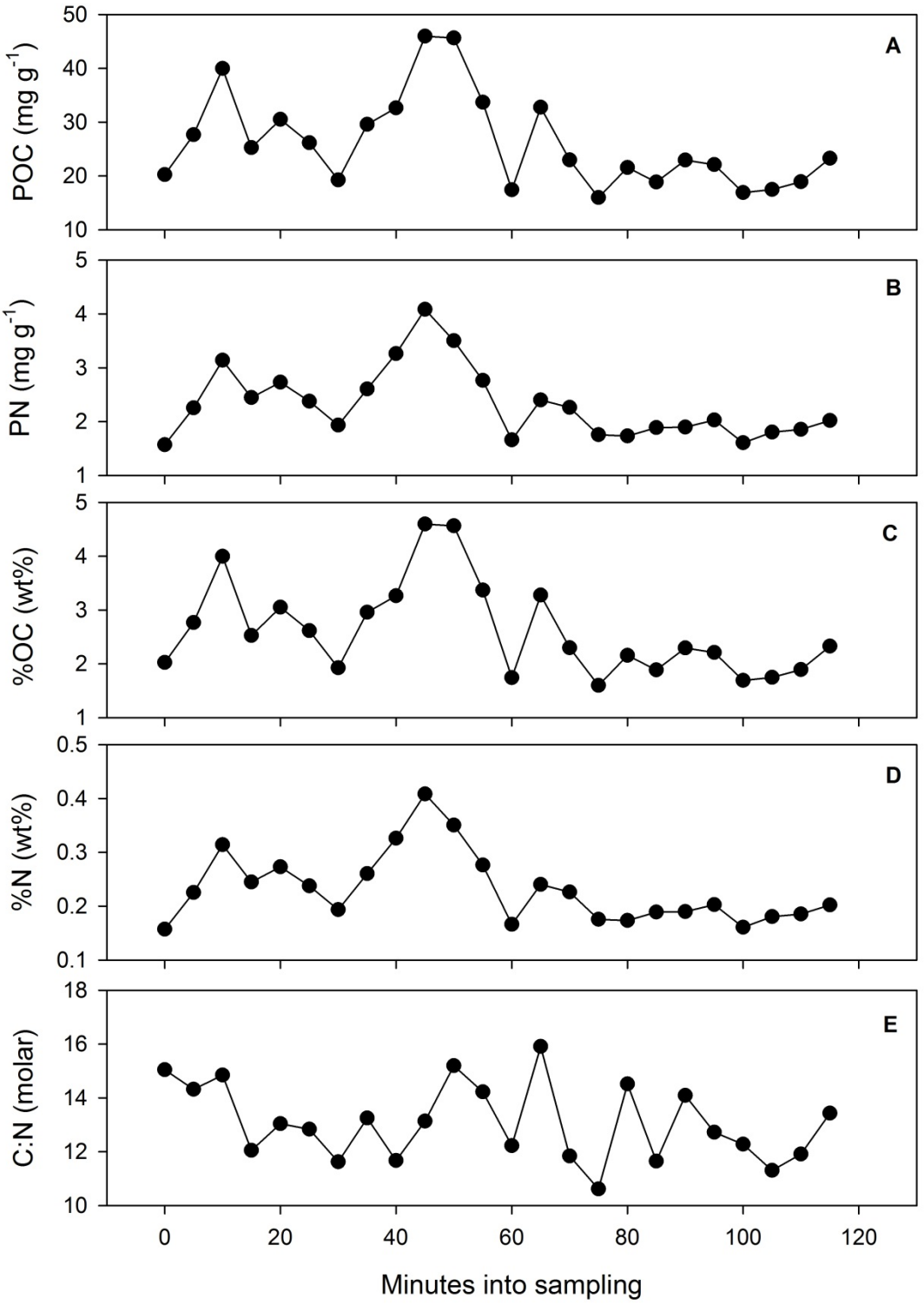

Figure 20. Organic nutrient data from the 7-13-11 rain event. (A) POC, (B) PN, (C) %OC, (D) %N, and (E) C:N.

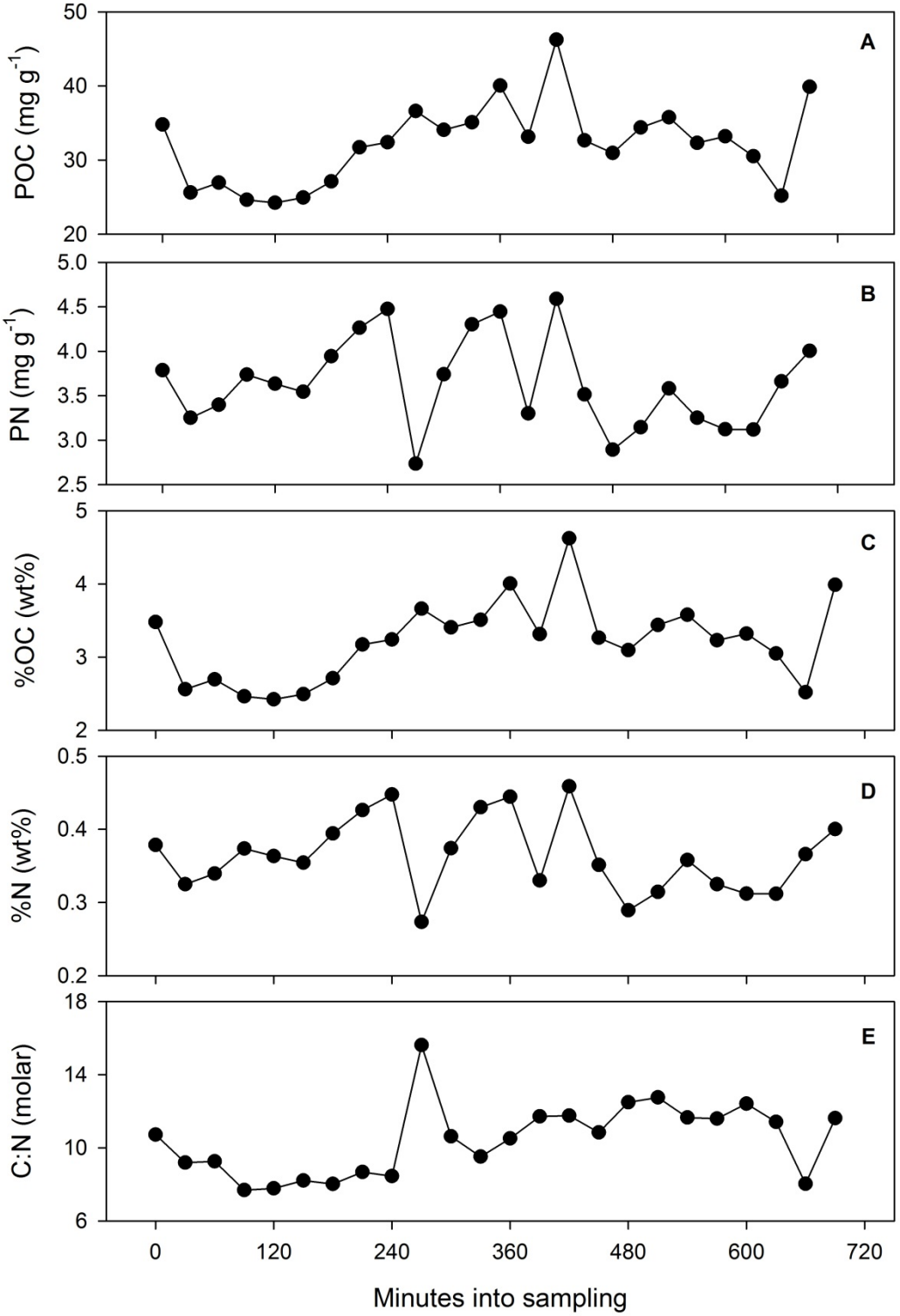

Figure 21. Organic nutrient data from the 3-30-11 tidal cycle sampling. (A) POC, (B) PN, (C) %OC, (D) %N, and (E) C:N.

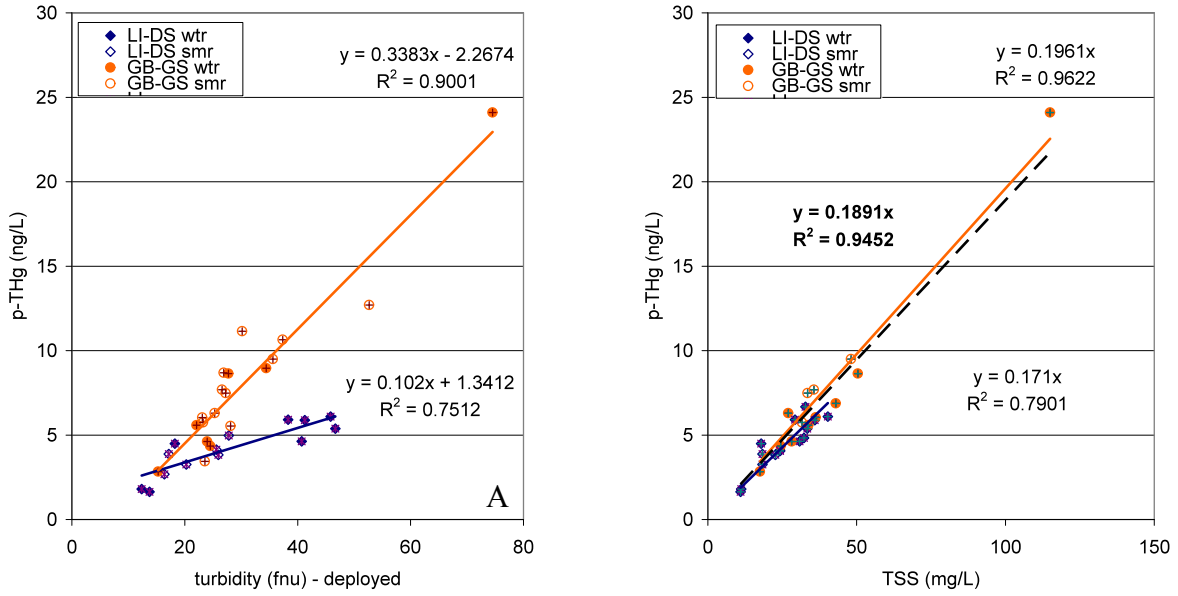

Figure 22. Relationships between particulate total mercury (pTHg) and (A) turbidity measured in situ by the deployed instrument package and (B) total suspended sediment (TSS) concentration measured in the lab.

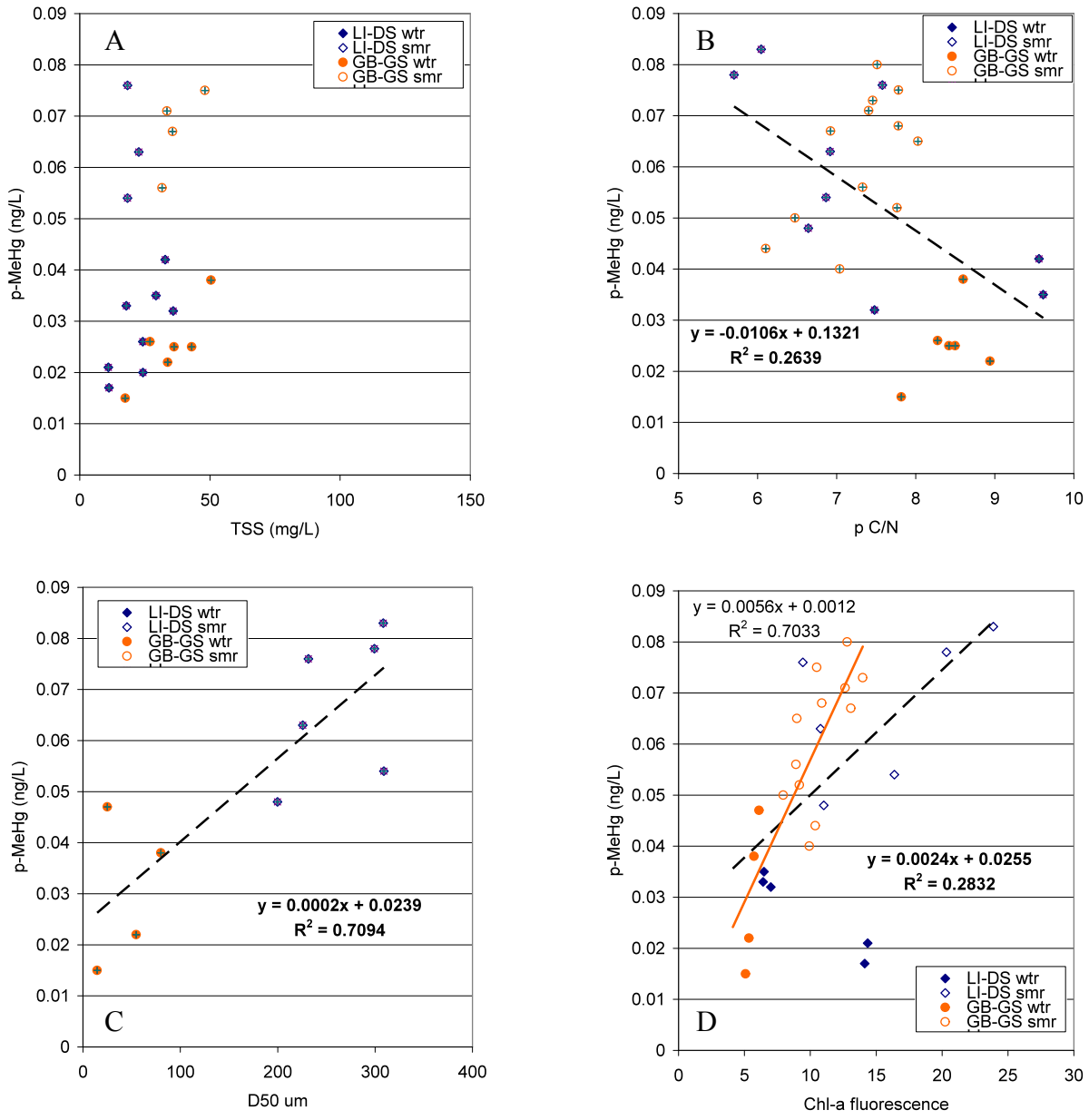

Figure 23. Relationships between pMeHg and (A) TSS and (B) particulate organic carbon to organic nitrogen ratio measured in the lab, and (C) median particle size (D50) and (D) chlorophyll-a fluorescence measured in situ by the deployed instrument package.

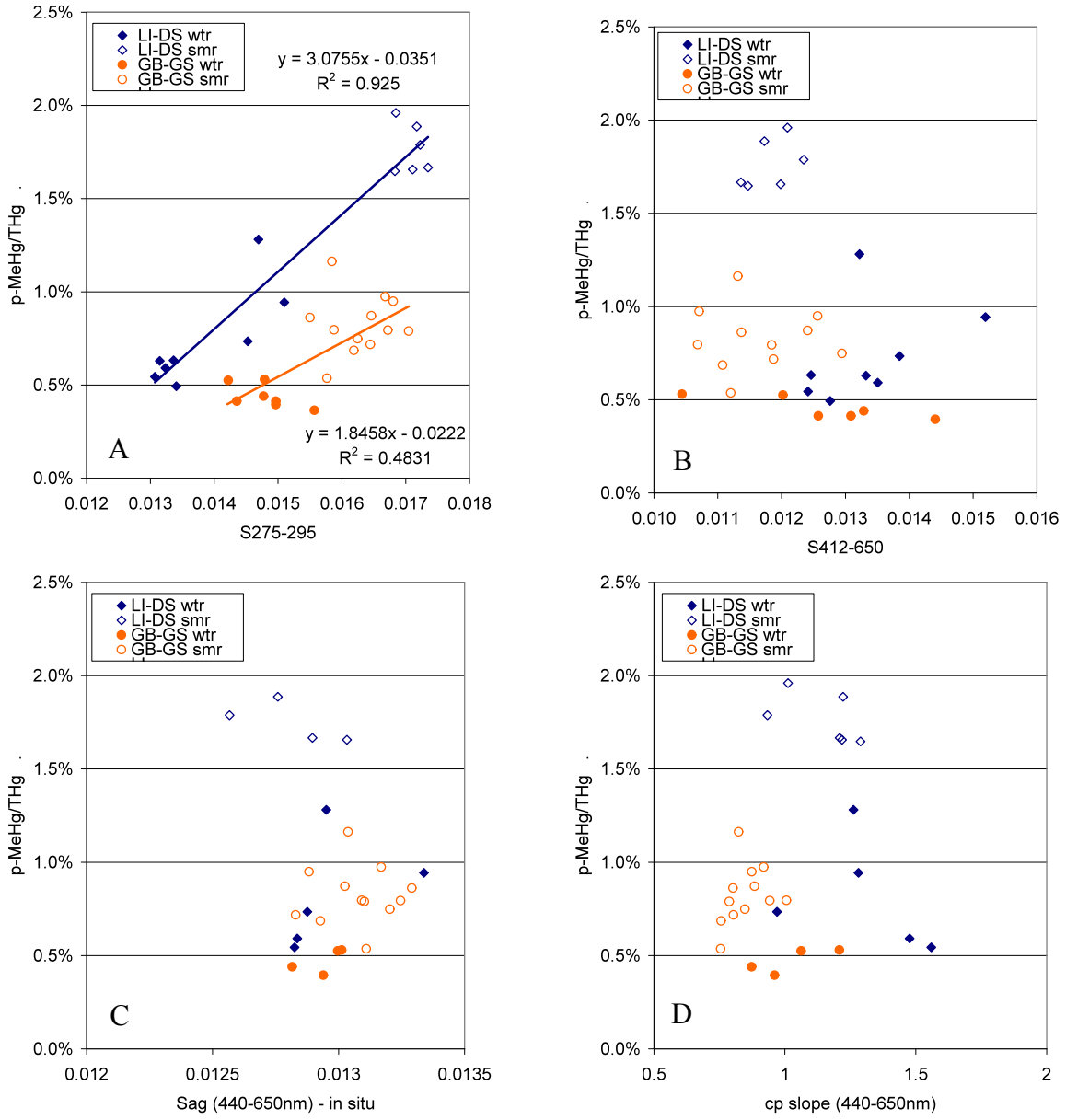

Figure 24. Relationships between the ratio of MeHg to THg in particles to absorption spectral slopes (A) Sag275-295 and (B) Sag440-650 measured in the lab and (C) Sag440-650 , and (D) Scp440-650 measured in situ by the ac9. Higher slopes reflect more bacterial or algal contribution to DOM (Sag) and particle size (cp).

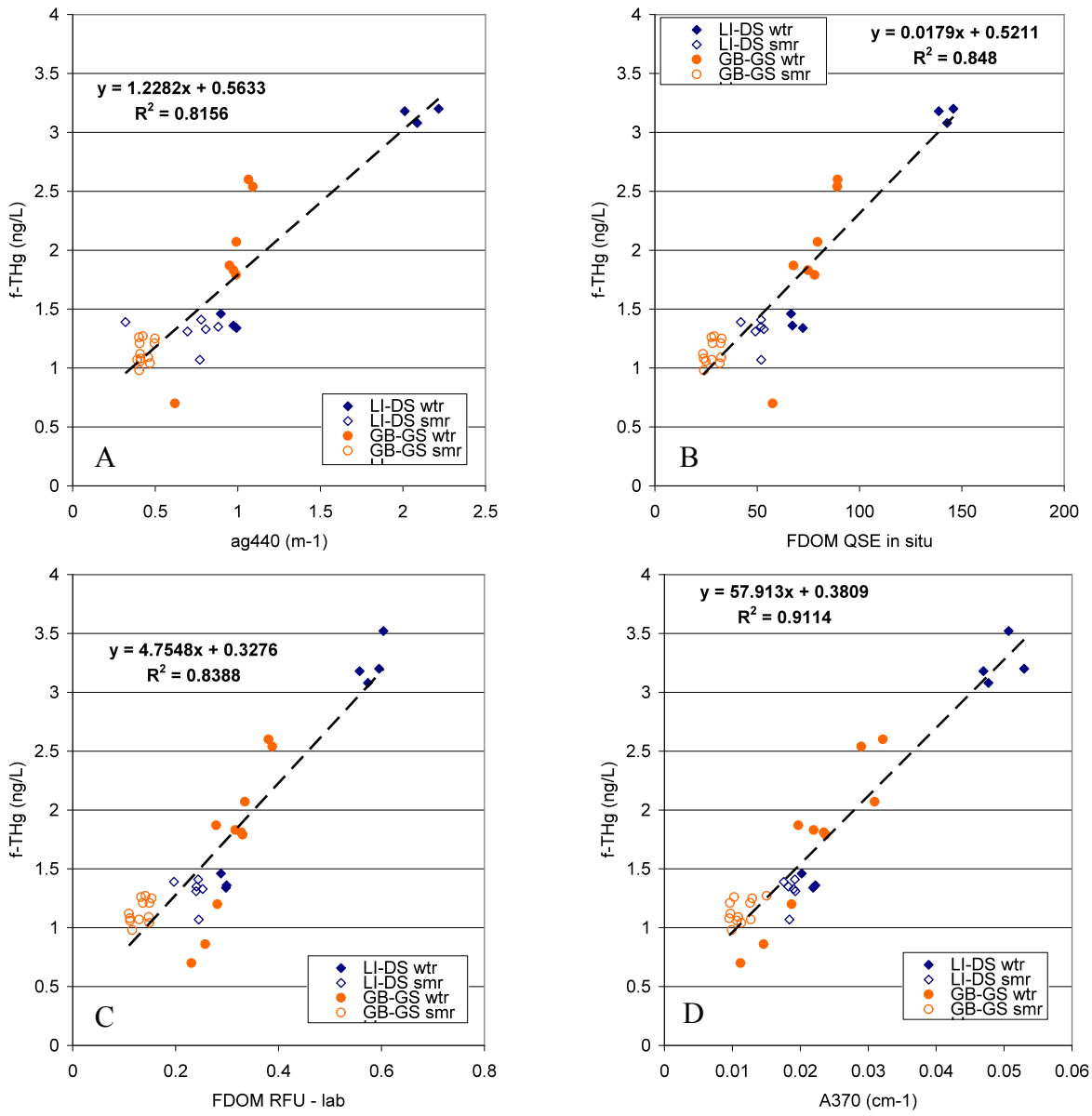

Figure 25. Relationships between fTHg and (A) FDOM and (B) absorption at 440 nanometers (ag440) measured in situ by the deployed instrument package, and (C) FDOM and (D) absorbance at 370 nanometers (A370) measured in the lab.

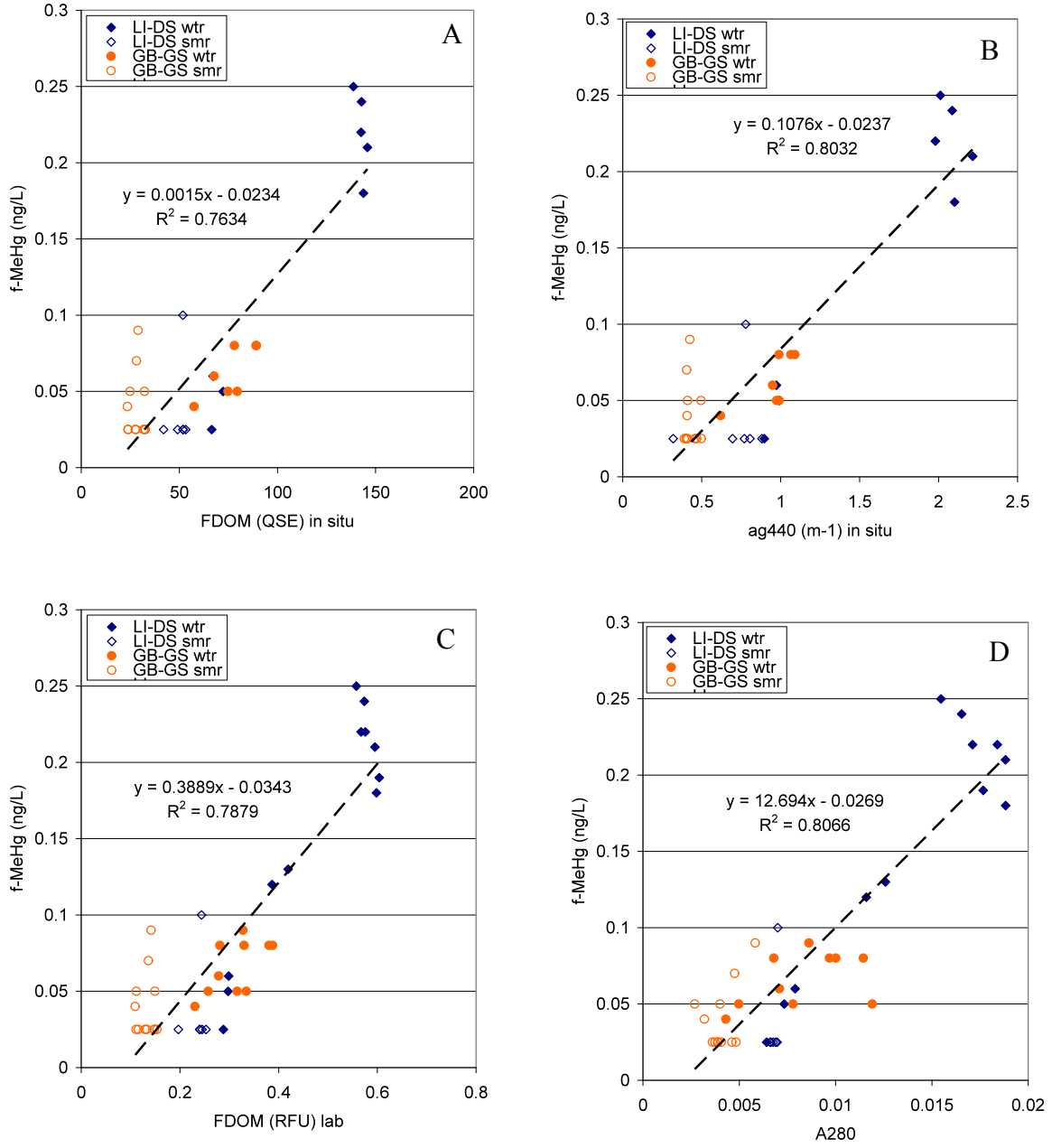

Figure 26. Relationships between fMeHg and (A) FDOM and (B) absorption (ag440) measured in situ by the deployed instrument package and (C) FDOM and (D) absorbance measured at 280 nm (A280) measured in the lab.

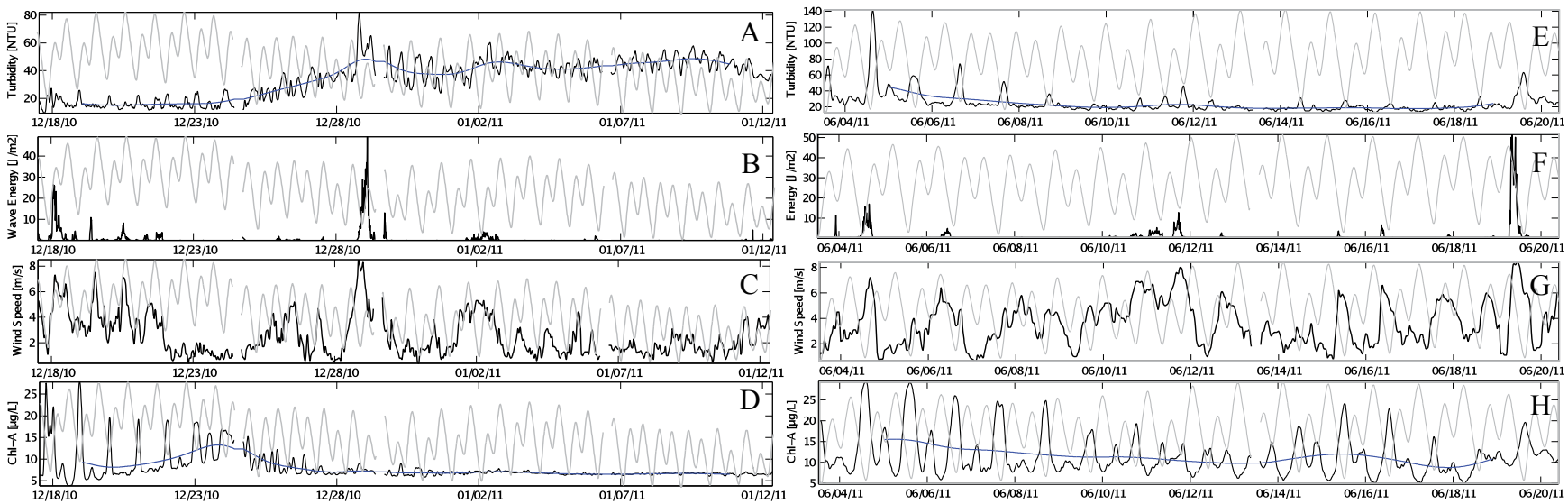

Figure 27. Time series of turbidity, wave energy, wind speed and chlorophyll-a fluorescence measured in situ in winter (A-D, left column) and summer (E-H, right column) deployments at Liberty Island. The gray time series represents water depth at the deployment site. Note differences in scales between winter and summer time series.

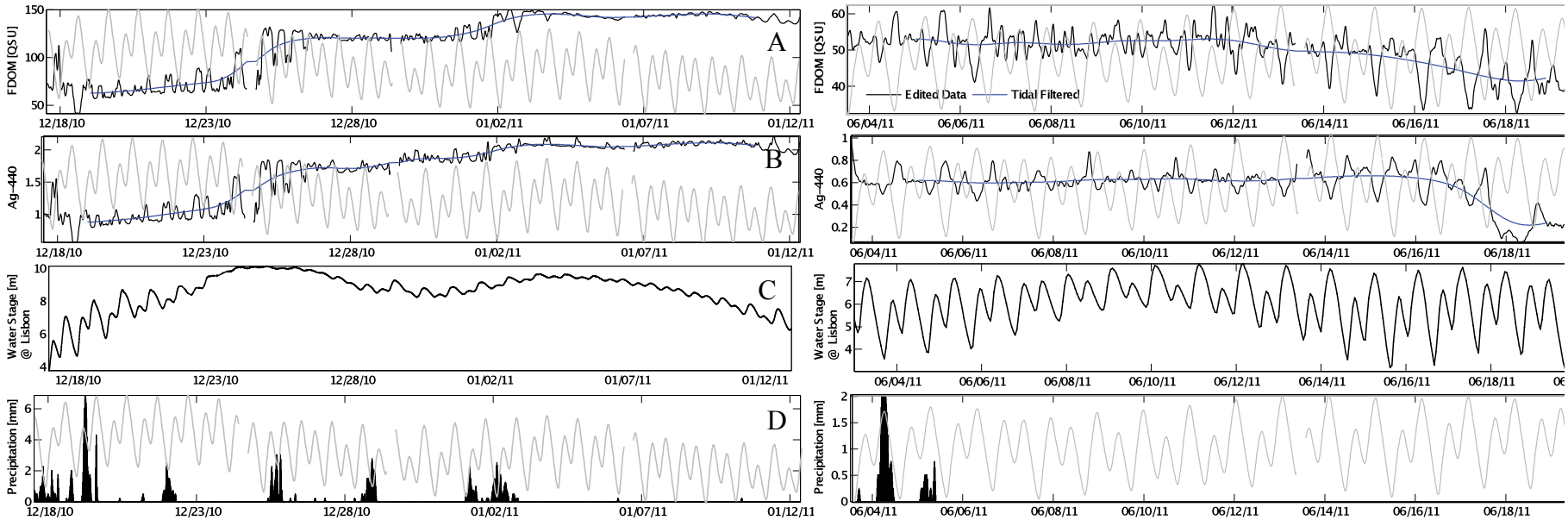

Figure 28. Time series fluorescent dissolved organic matter (FDOM), absorption at 440 nm (ag440), regional water stage measu at Lisbon Weir (US Geological Survey National Water Information System, 2011) and precipitation at the Hastings East/Dixon Cl site in winter (A-D, left column) and summer (E-H, right column) deployments at Liberty Island. The gray time series represents water depth at the deployment site. Note differences in scales between winter and summer time series.

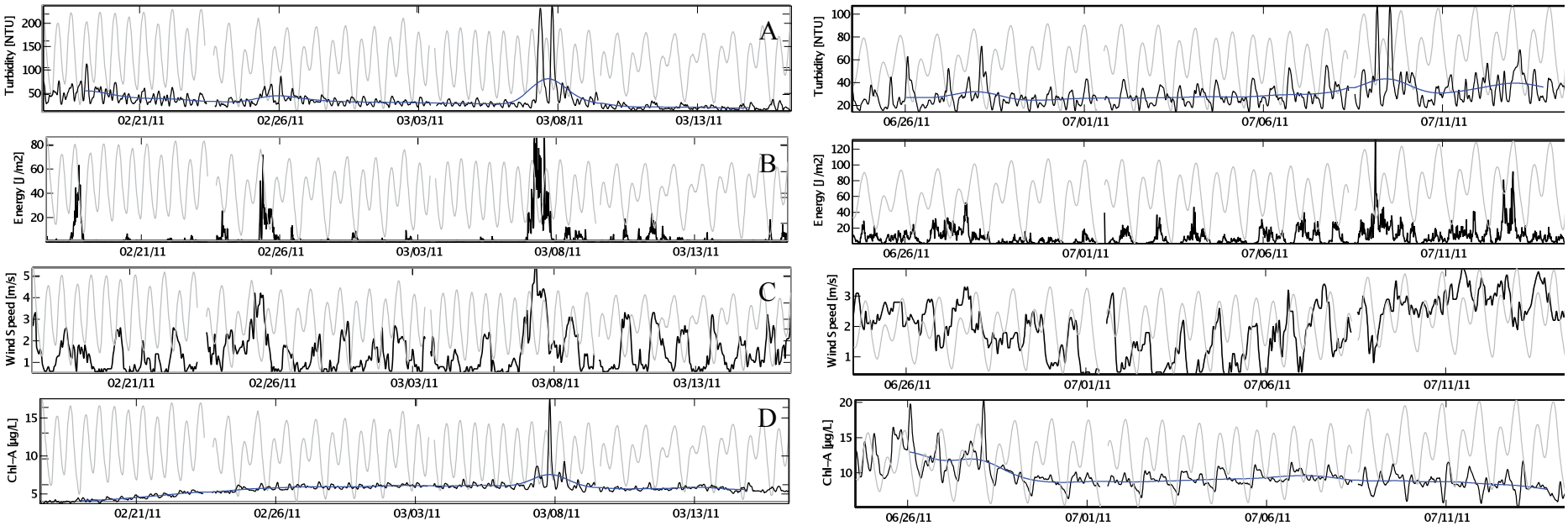

Figure 29. Time series of turbidity, wave energy, wind speed and chlorophyll-a fluorescence measured in situ in winter (A-D, left column) and summer (E-H, right column) deployments at Grizzly Bay. The gray time series represents water depth at the deployment site. Additional time series of optical, hydrodynamic and meteorological measurements are shown in Appendix A. N differences in scales between winter and summer time series.

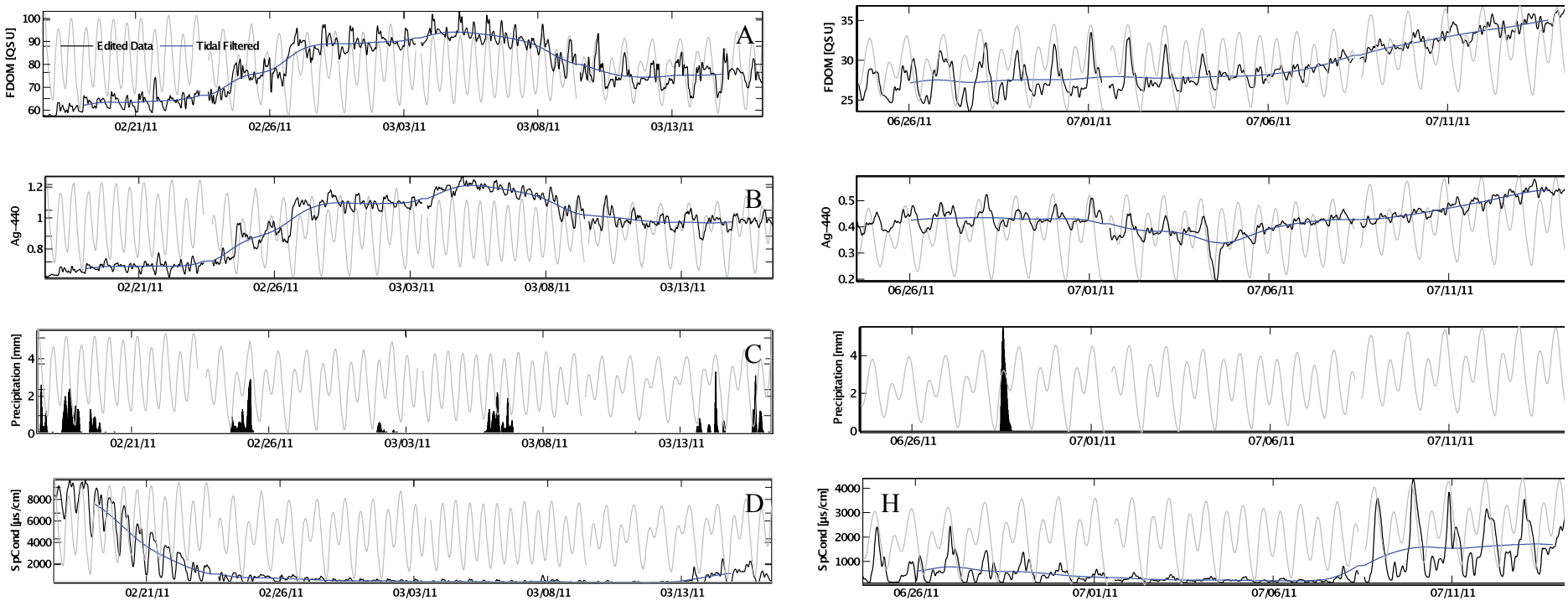

Figure 30. Time series fluorescent dissolved organic matter (FDOM), absorption at 440 nm (ag440), specific conductance and precipitation at the nearby CIMIS site in winter (A-D, left column) and summer (E-H, right column) deployments at Grizzly Bay. T gray time series represents water depth at the deployment site. Additional time series of optical, hydrodynamic and meteorologic measurements are shown in Appendix A. Note differences in scales between winter and summer time series.

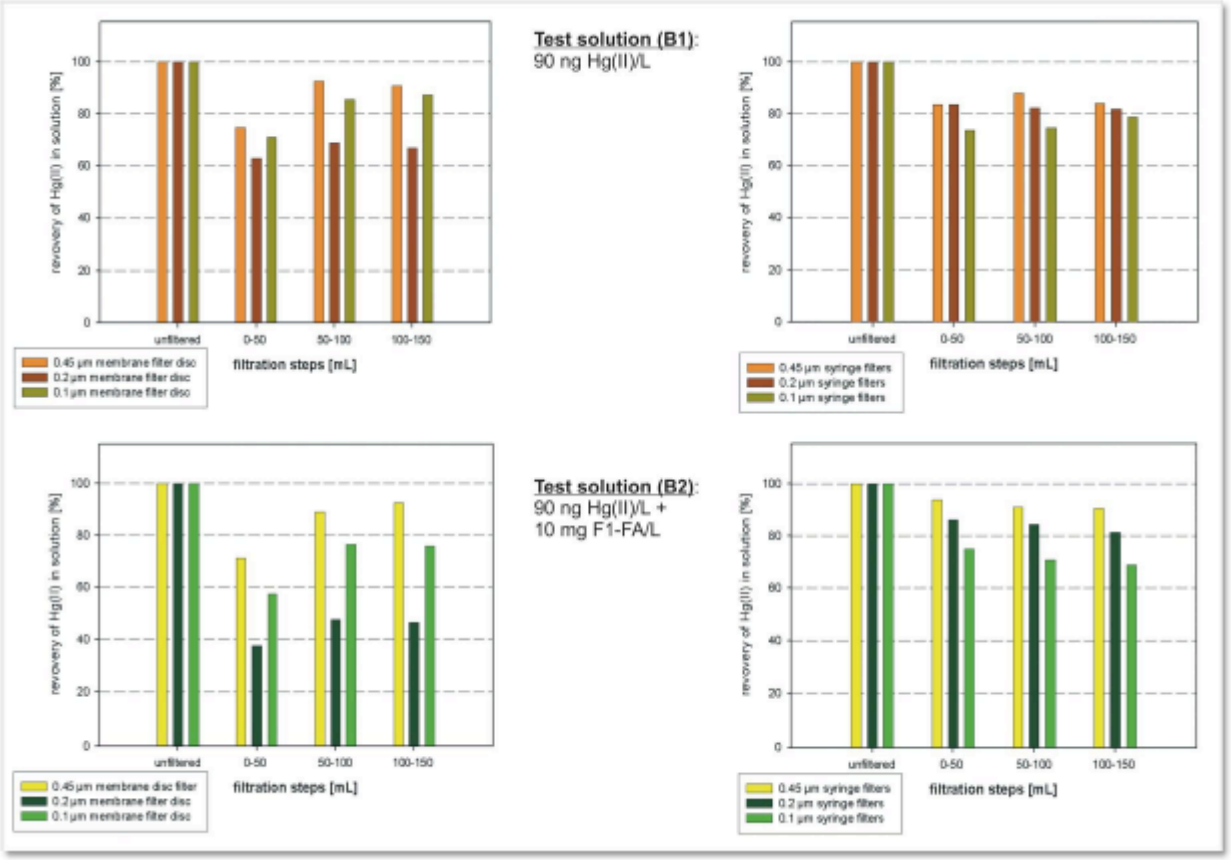

Figure 31. Hg(II) results for membrane filter discs and Acrodisc® syringe filters.

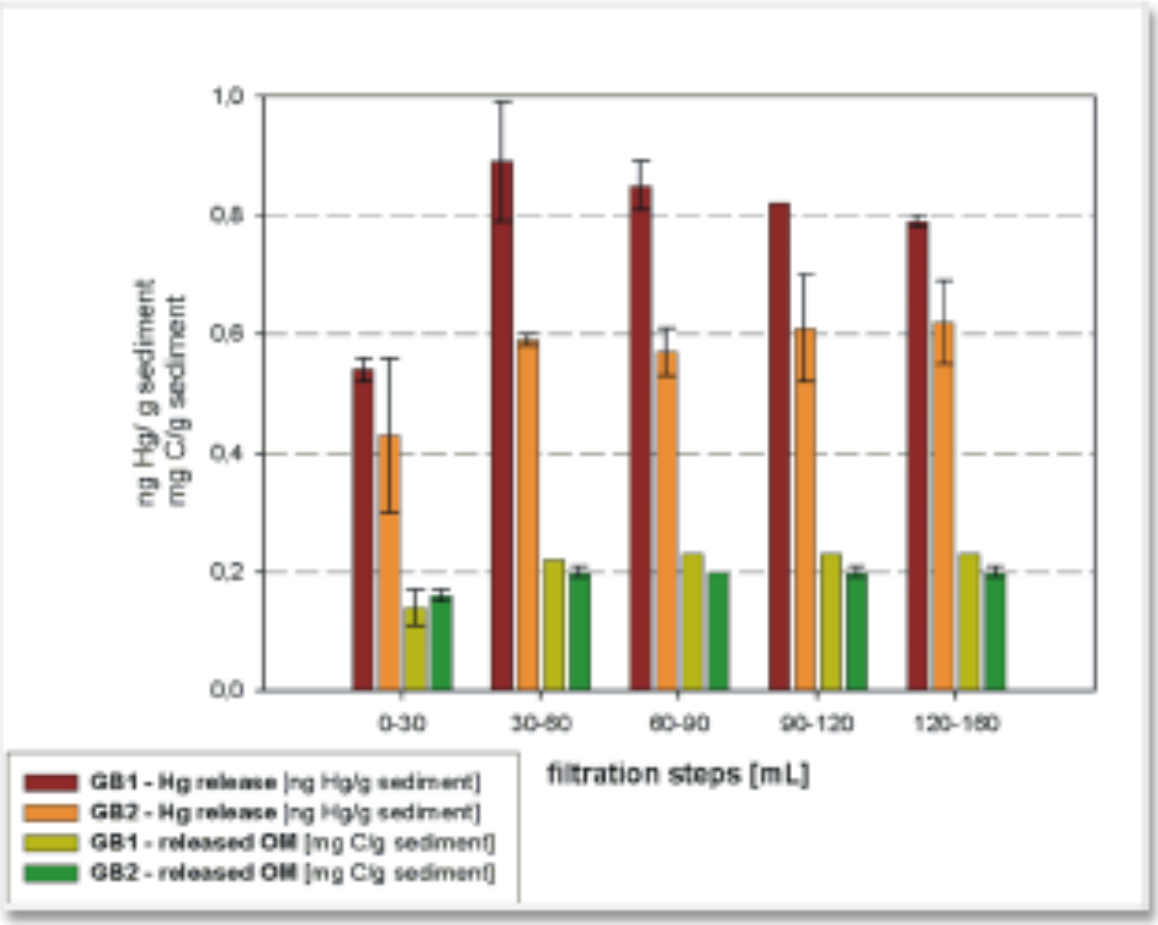

Figure 32. Filter-clogging test for composite samples GB1 and GB2. Vertical bar charts show the mean results for released mercury and organic matter (based on weighed in sample amount for the batch solution) for each filtration step with respective standard deviations of duplicate samples displayed as error bars.

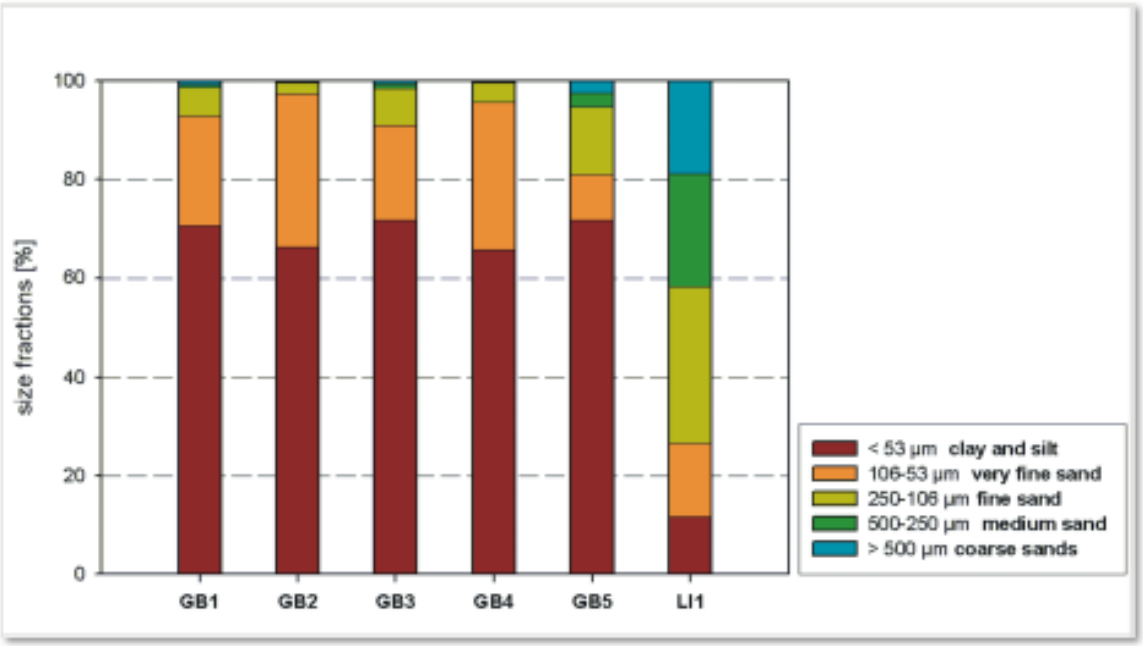

Figure 33. Classification of collected sediment samples. Classification is based on the USDA system (Jackson, 2005).

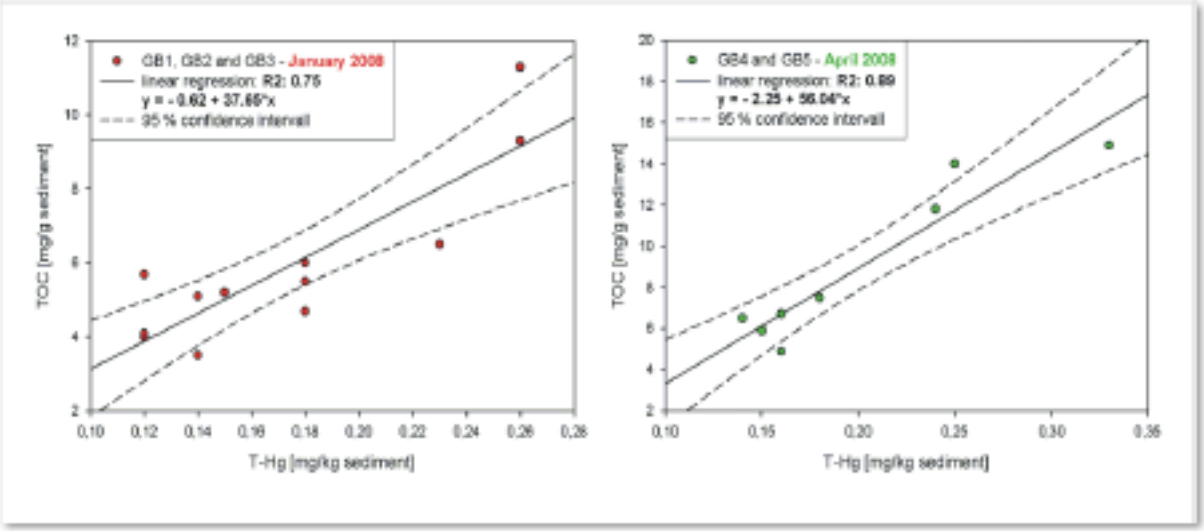

Figure 34. Correlation between TOC and T-Hg concentration of composite samples and size fractions.

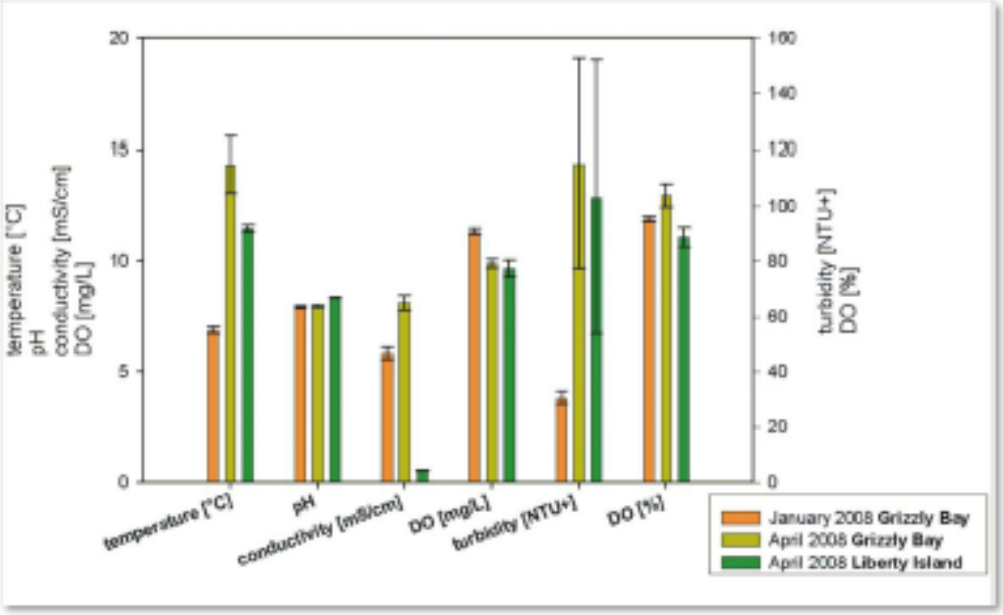

Figure 35. Averaged field water parameters from Grizzly Bay and Liberty Island. Standard deviations calculated from duplicate samples are displayed as error bars.

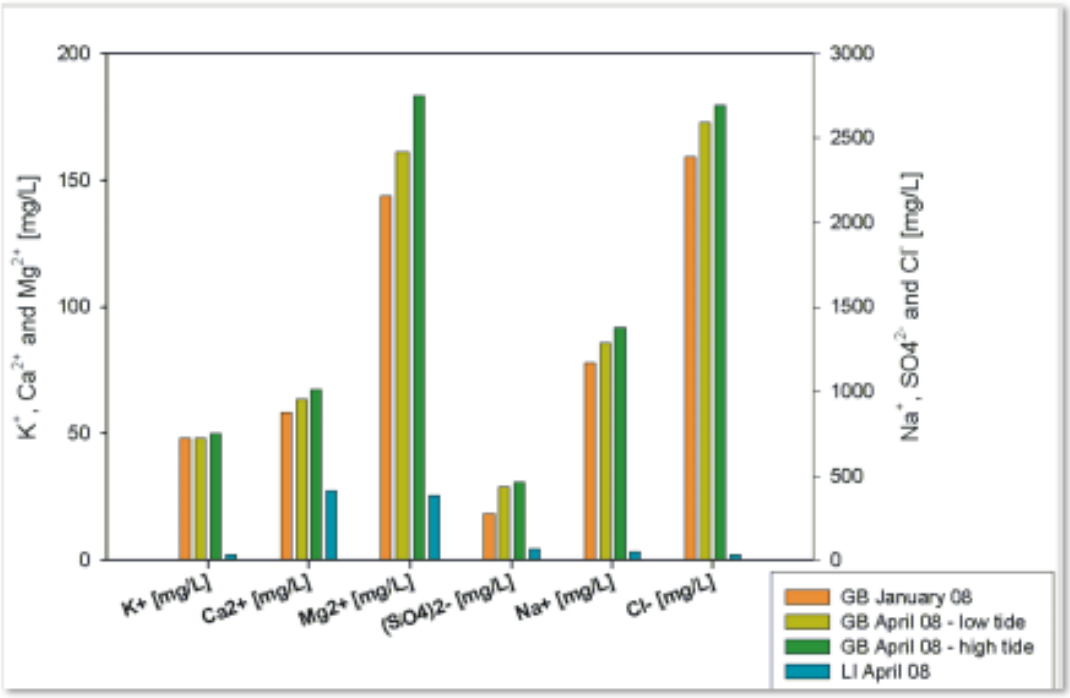

Figure 36. Cation and anion data from Grizzly Bay and Liberty Island water.

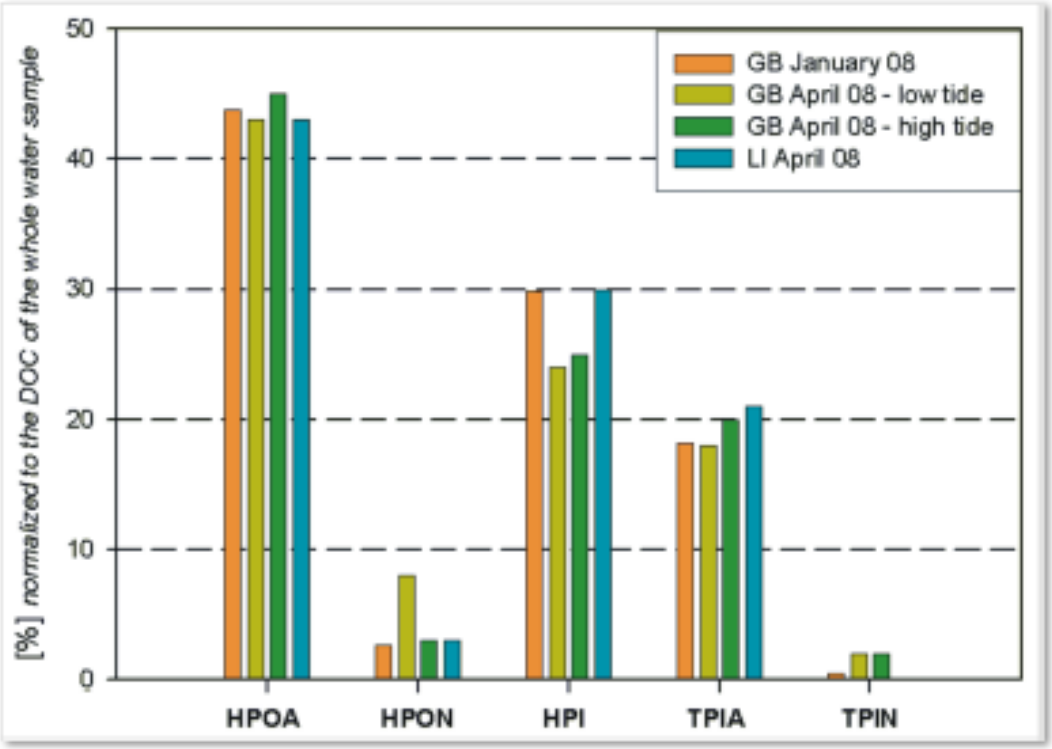

Figure 37. DOC fractionation for Grizzly Bay and Liberty Island water. Percentage distribution of all isolated fractions based on the DOC measured for the whole Grizzly Bay and Liberty Island water. Abbreviations: HPOA = hydrophobic organic acid fraction, HPON = hydrophobic organic neutral fraction, HPI = hydrophilic fraction, TPIA = transphilic organic acid fraction, TPIN = transphilic organic neutral fraction.

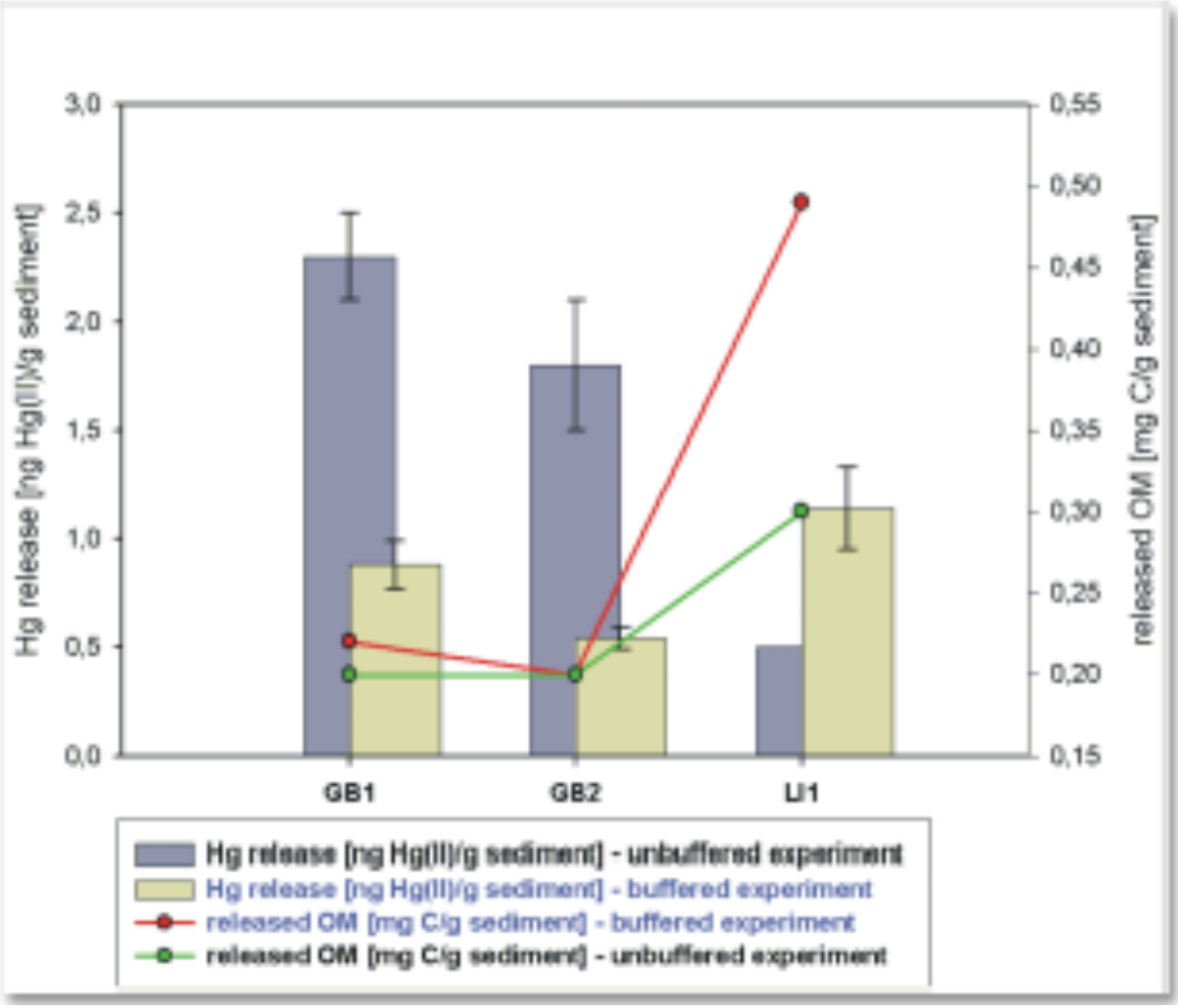

Figure 38. Mercury and OM release from unbuffered and buffered batch experiments. Received results from Grizzly Bay and Liberty Island sediment samples are blank corrected, averaged and the calculated standard deviations of duplicate samples are displayed as error bars.

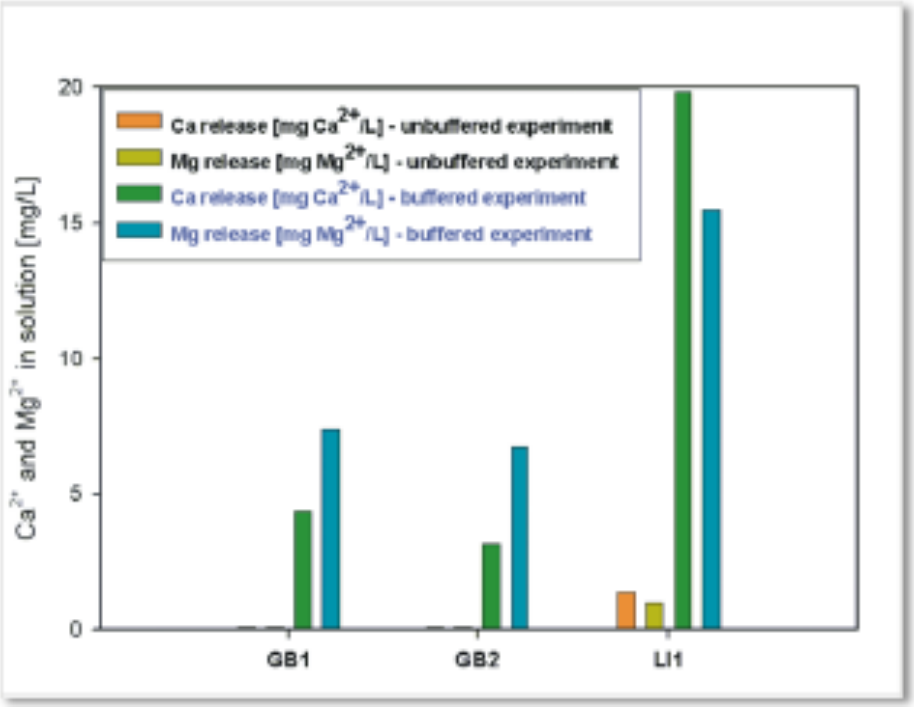

Figure 39. Ca and Mg concentration in solution of unbuffered/buffered batch experiments Received results from Grizzly Bay and Liberty Island sediment samples are blank corrected.

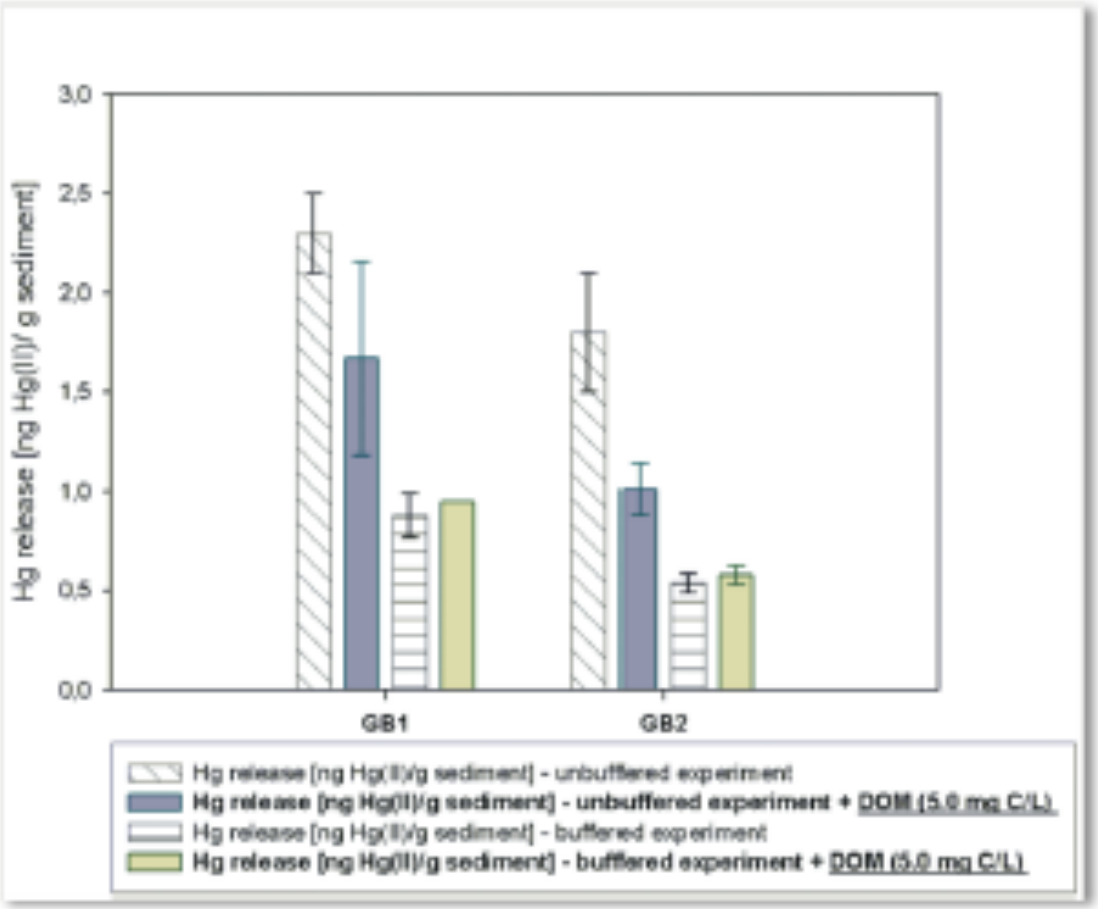

Figure 40. Comparison of mercury release from unbuffered and buffered extractions with and without additional DOM (F1-FA, 5 mgC l-1). Received results from Grizzly Bay sediment samples are blank corrected, averaged and the calculated standard deviations of duplicate samples are displayed as error bars.

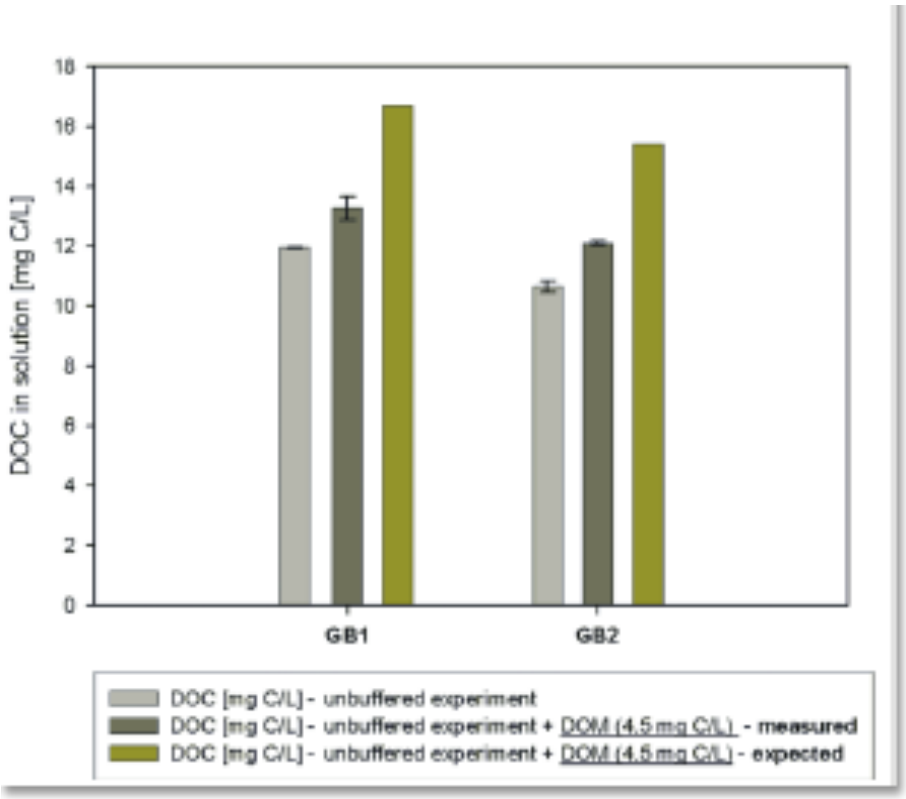

Figure 41. DOC concentration in solution for the unbuffered batch experiment with and without additional DOM and a soil to liquid ratio of 20 g/200 ml. Received results from Grizzly Bay sediment samples are averaged and the calculated standard deviations of duplicate samples are displayed as error bars. For better comparison, the expected DOC concentrations for the unbuffered experiments with additional DOM are displayed as well.

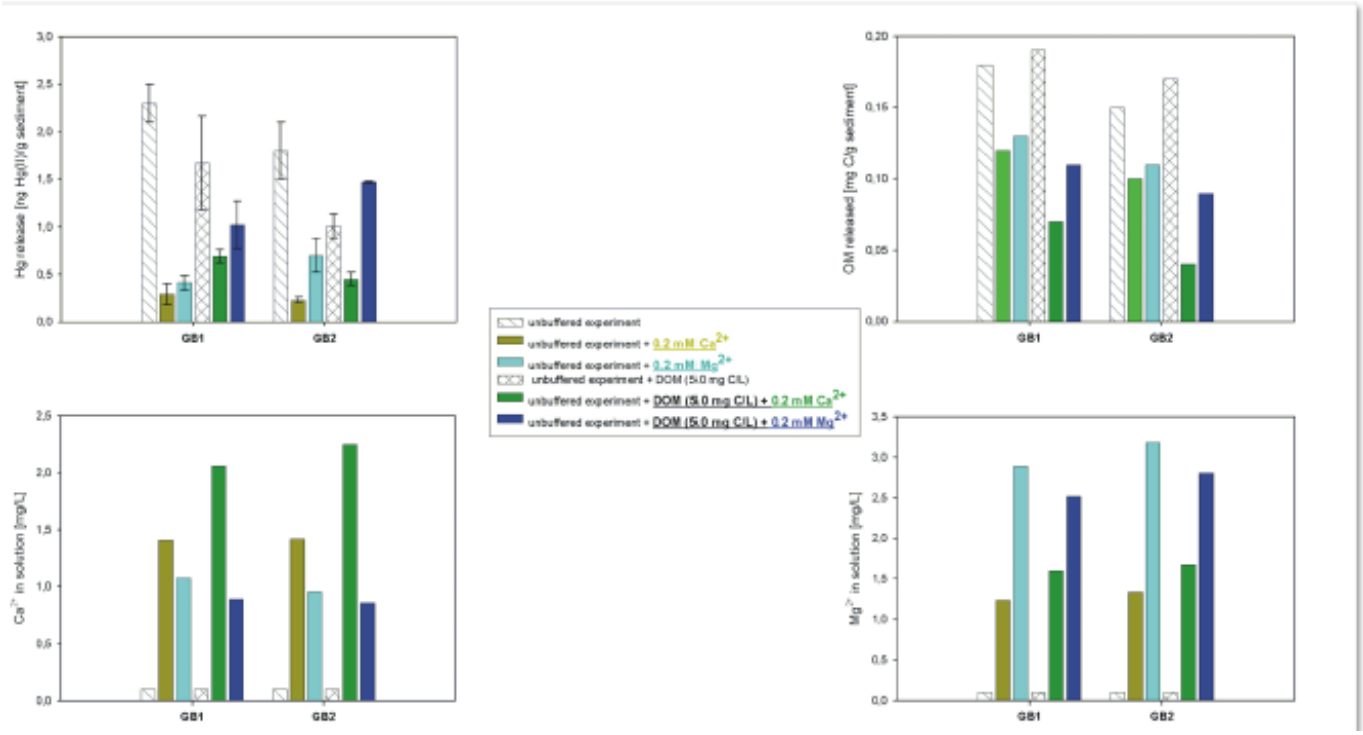

Figure 42. Mercury and OM release, Ca and Mg concentration in solution from unbuffered batch experiments in the presence/absence of DOM, Ca- or Mg.

Received results from Grizzly Bay sediment samples are blank corrected, averaged and the calculated standard deviations of duplicate samples are displayed as error bars.

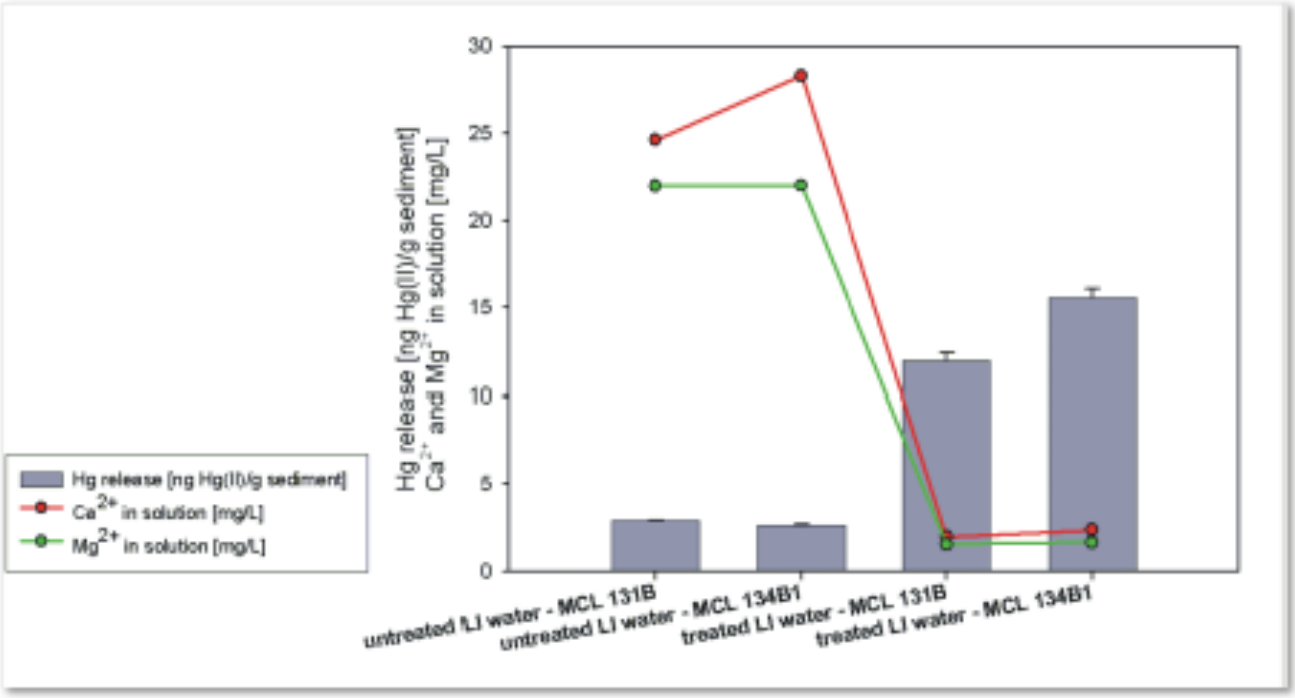

Figure 43. Comparison of mercury release from MCL 131B/MCL 134B1 in experiments with untreated and treated Liberty Island (LI) water Received results from MCL 131B and MCL 134B1 (Coastal Range, Northern California) are blank corrected, averaged and the calculated standard deviations of duplicate samples are displayed as error bars.

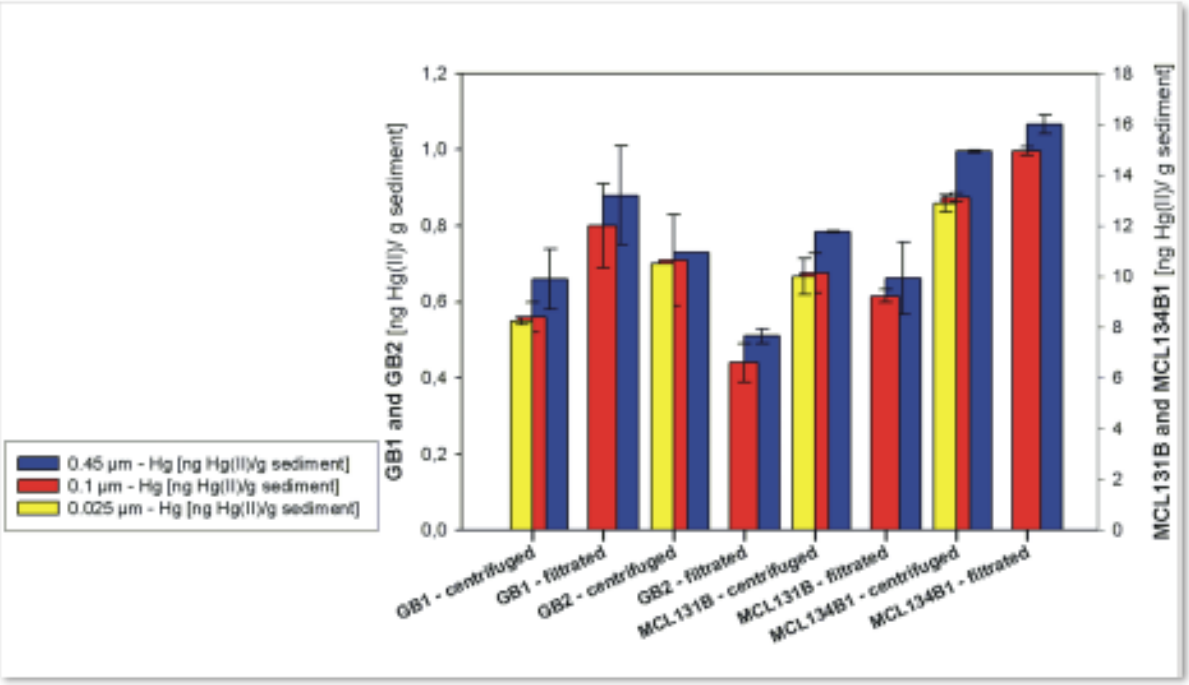

Figure 44. Mercury results from filtration and centrifugation in various size fractions Received results from buffered batch extraction experiments (without additional DOM) are blank corrected, averaged and the calculated standard deviations of duplicate samples are displayed as error bars.

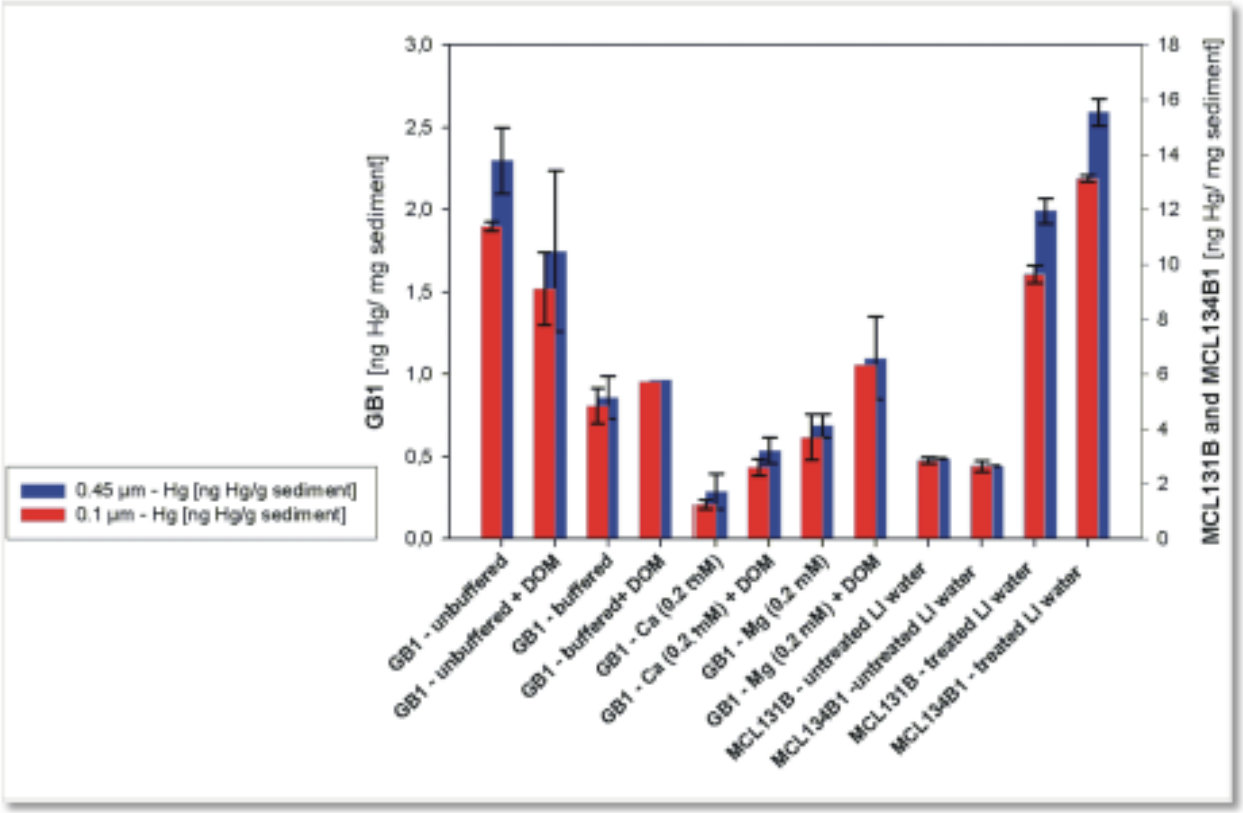

Figure 45. Mercury results of 0.45 and 0.1 µm filtration steps from selected batch experiments. Concentrations are blank corrected, averaged and standard deviations of duplicate samples are displayed as error bars.

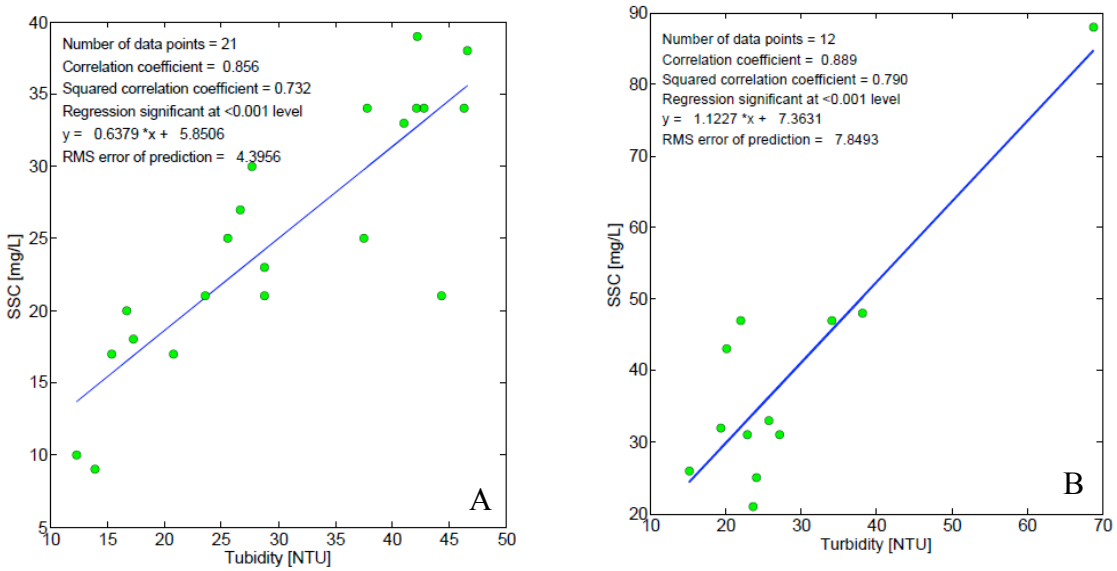

Figure 46. Calibration Plots for Turbidity to SSC for *(A)* Liberty Island data record and *(B)* Grizzly Bay.

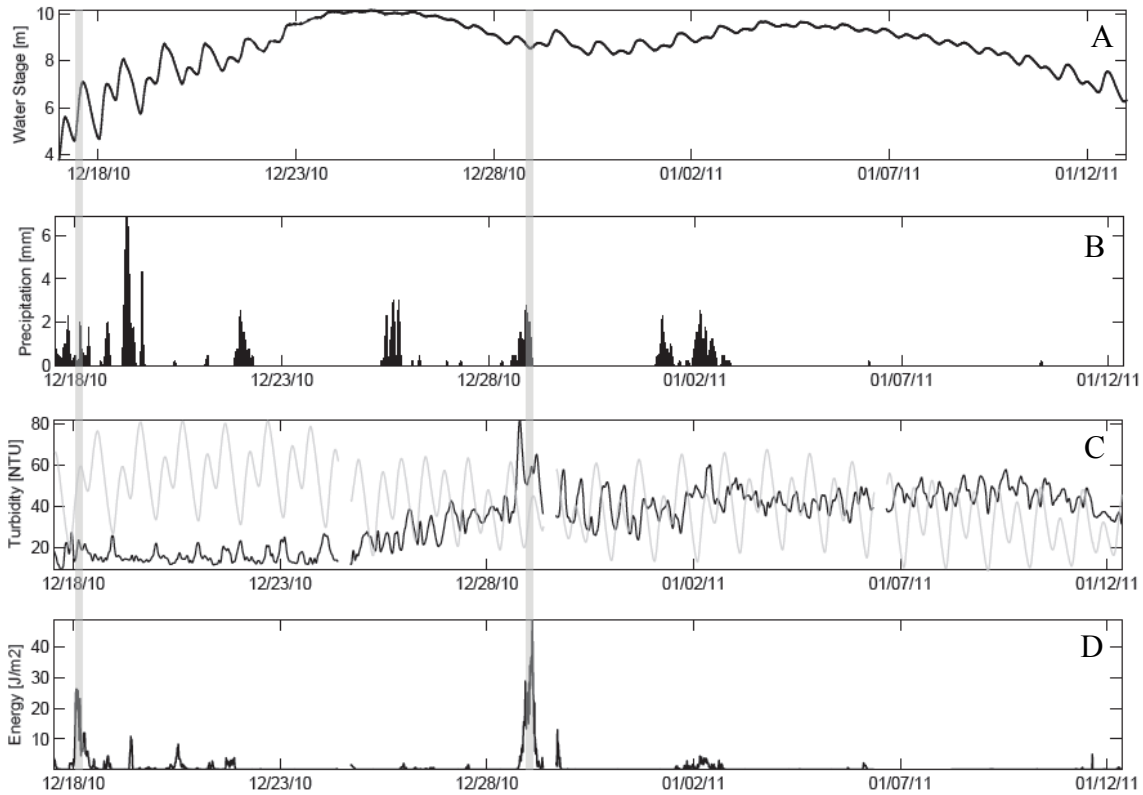

Figure 47. Hydrodynamic data for the LIW measurement period *(A)* Regional hydrology represented by water stage at Yolo at Lisbon, dashed line is stage at 8.5 *(B)* Precipitation at CIMIS station # 120, *(C)* Tidal variations in depth (grey line) and turbidity (black line), and *(D)* Energy contained in surface waves. Gray bands indicate significant wind events. In *A*, the water stage is taken at Yolo at Lisbon, approximately 23 km to the north/northwest of the measurement location. Yolo Bypass is inudated when the water stage is above 8.5 ft.

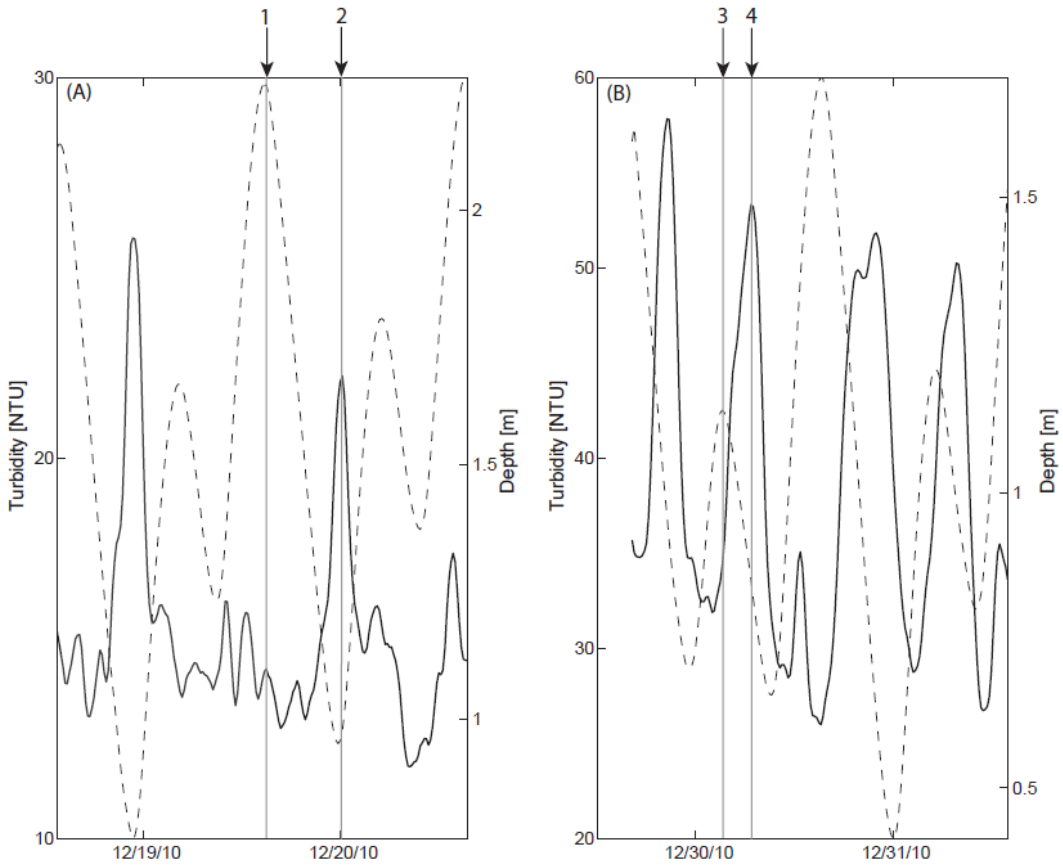

Figure 48. Plots of turbidity (solid line) and water depth (dashed line) for two time periods *(A)* prior to and *(B)* after the influence from the Yolo Bypass runoff. The numbered lines 1-4, refer to time at the start of the ebb tide (1&3), and those of max concentration (2 &4).

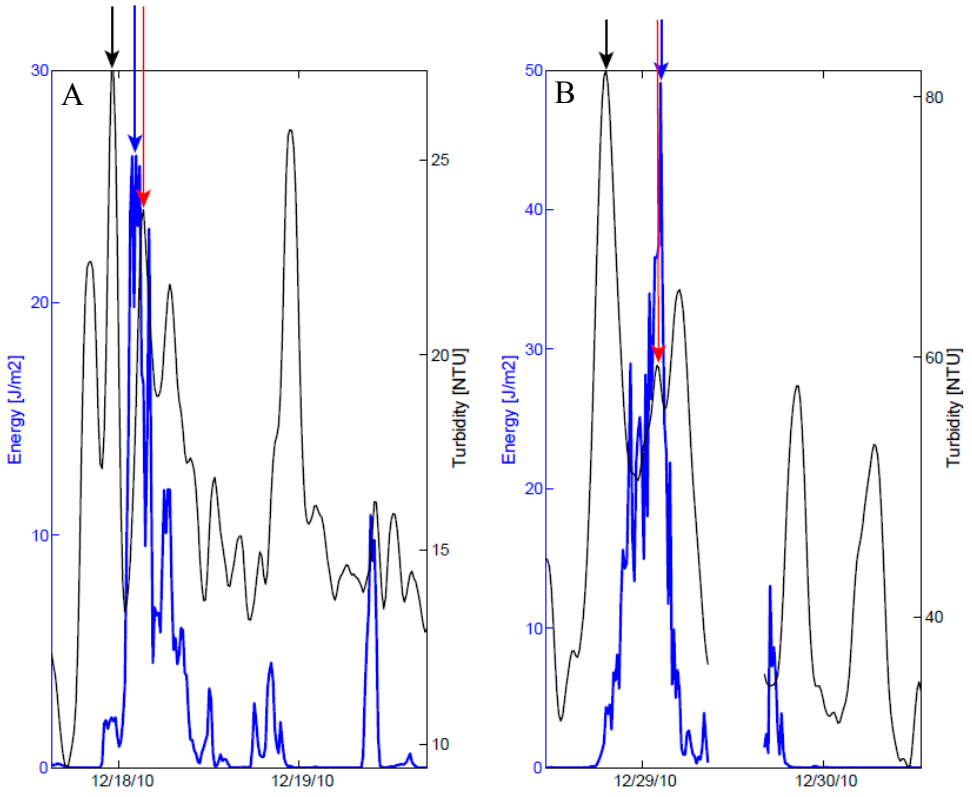

Figure 49. Two significant surface wave energy events as indicated in Figure 2.1.1 on *(A)* Dec. 18, 2011, and *(B)* Dec. 29, 2011.

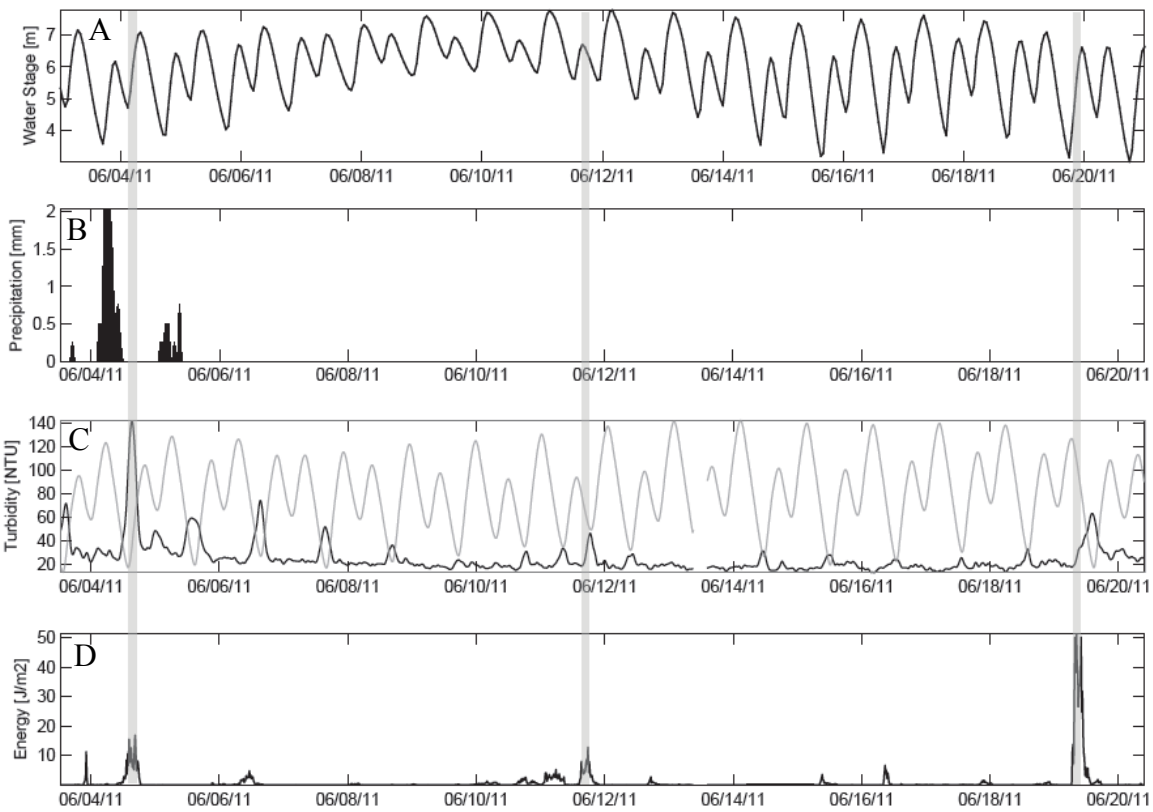

Figure 50. Hydrodynamic data for the LIS measurement period *(A)* Regional hydrology represented by water stage at Yolo at Lisbon *(B)* Precipitation at CIMIS station # 120 *(C)* Tidal variations in depth (dashed line) and turbidity (black line), and *(D)* Energy contained in surface waves. Gray bands indicate significant wind events.

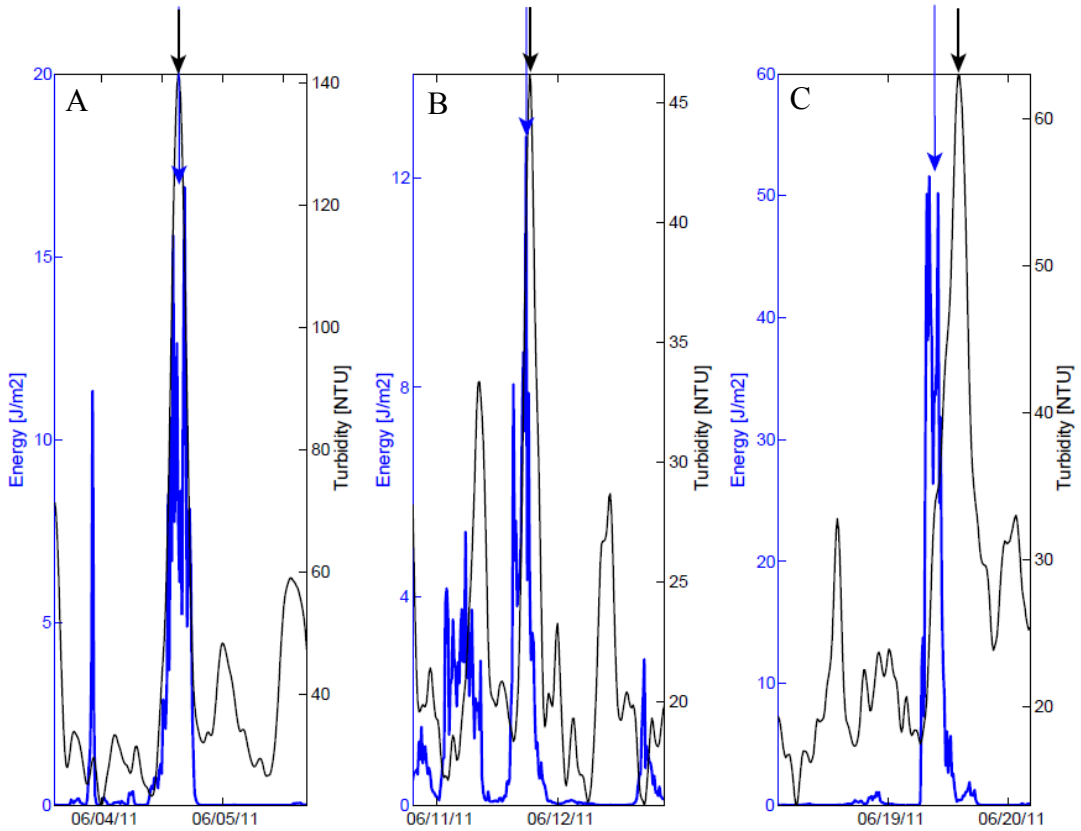

Figure 51. Three surface wave energy events as indicated in Figure 50 on *(A)* June 4, 2011 *(B)* June 11, 2011 and *(C)* June 19, 2011.

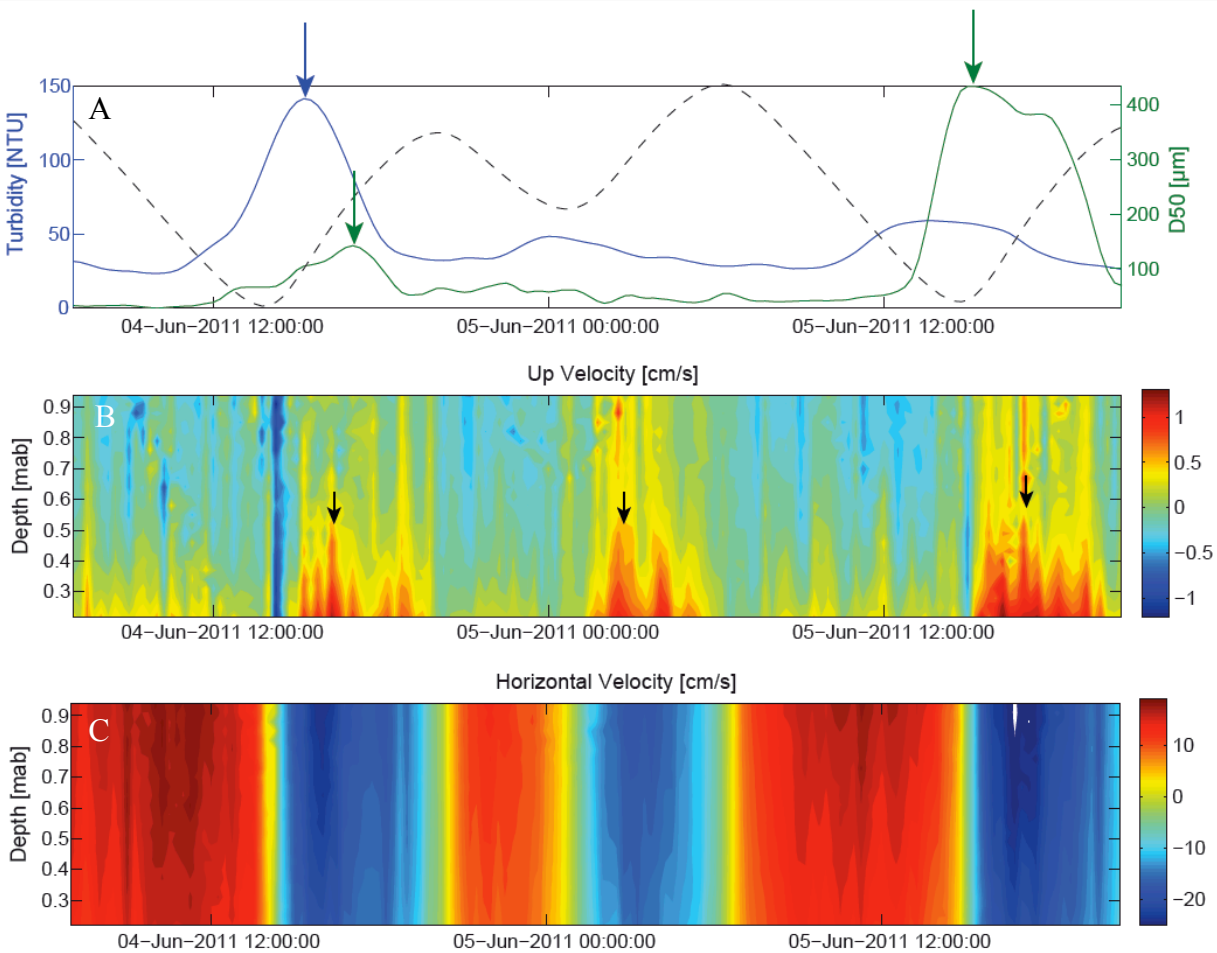

Figure 52. Shows a 36 hour period for the first wind event *(A)* The relation between turbidity (blue line) and D50 (green line) with depth (dashed line) shown for reference *(B)* Vertical profile of the up component of velocity, and *(C)* Vertical profile of the horizontal component of velocity, note that negative velocity corresponds to the flood direction.

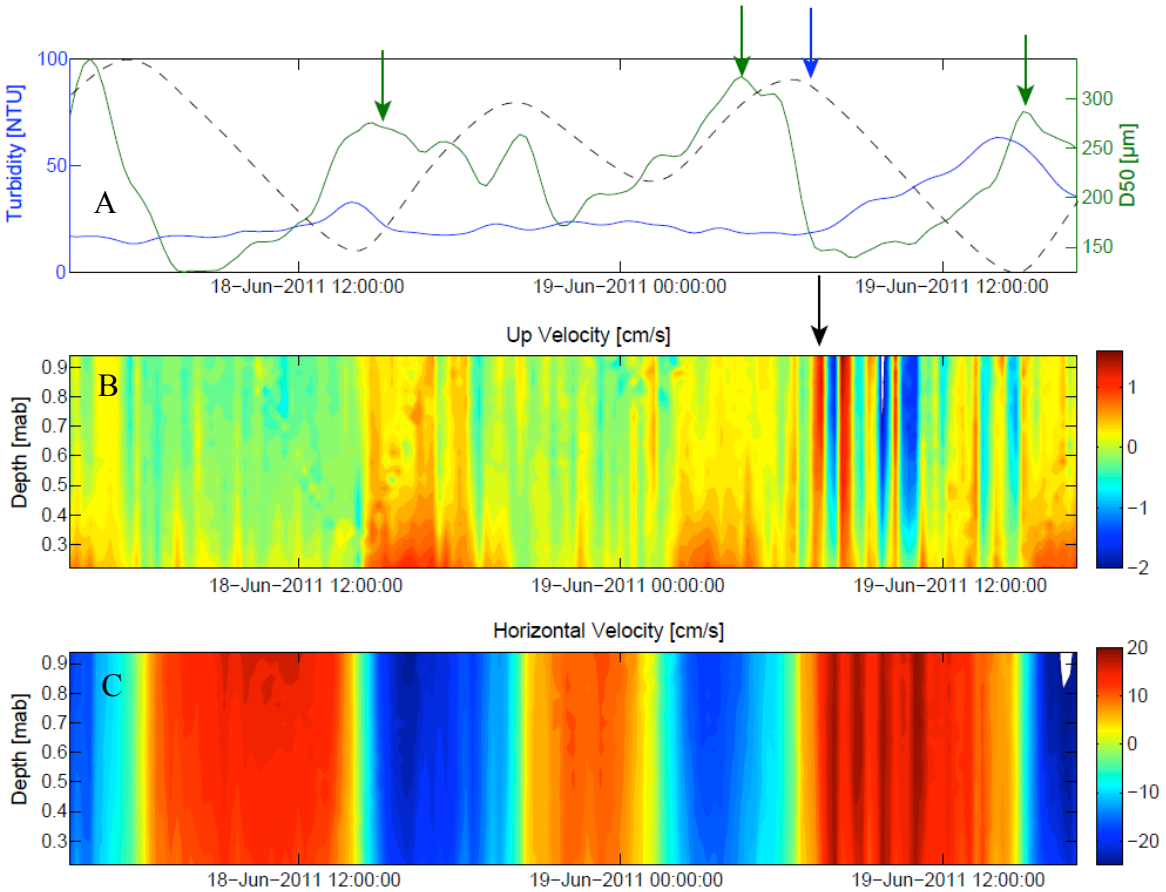

Figure 53. Shows a 36 hour period for the third wind event *(A)* The relation between turbidity (blue line) and D50 (green line) with depth (dashed line) shown for reference *(B)* Vertical profile of the up component of velocity, and *(C)* Vertical profile of the horizontal component of velocity, note that negative horizontal velocity corresponds to the flood direction.

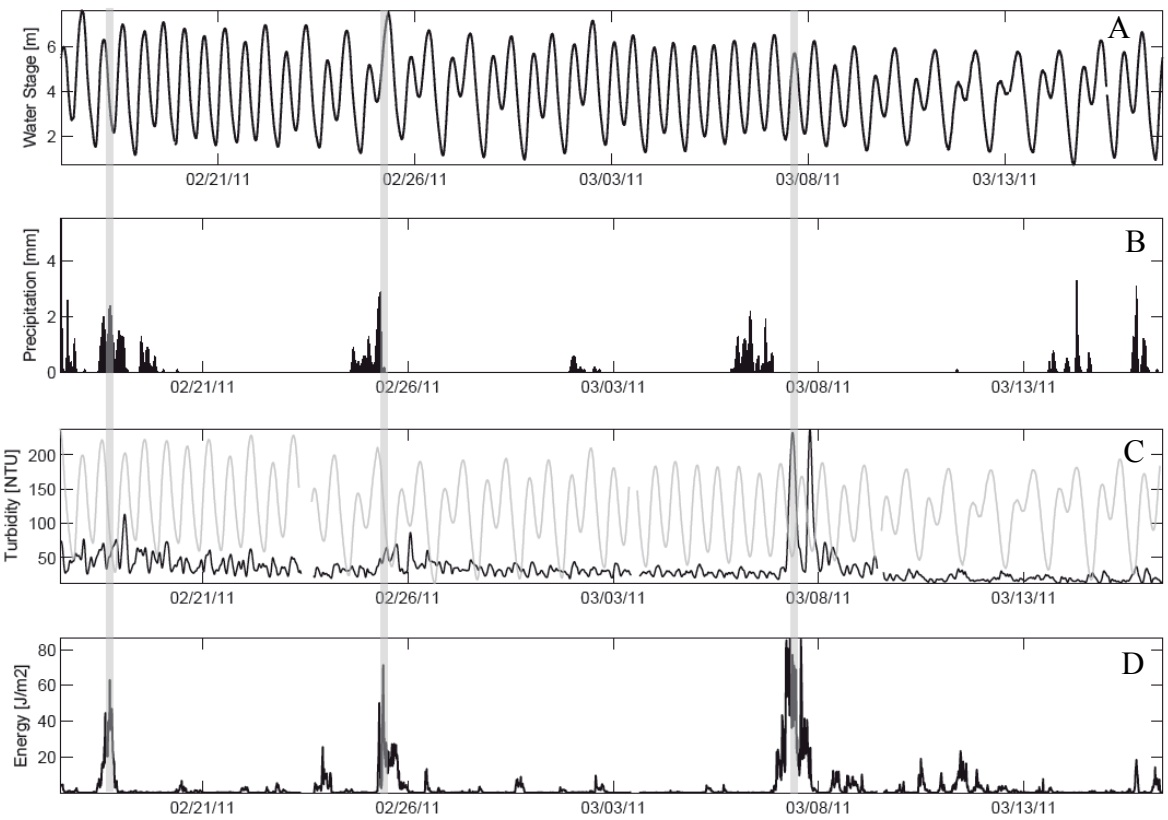

Figure 54. Hydrodynamic data for the GBW measurement period *(A)* Regional hydrology represented by water stage at Montezuma Slough at Hunter Cut *(B)* Precipitation at CIMIS station # 170 *(C)* Tidal variations in depth (gray line) and turbidity (black line), and *(D)* Energy contained in surface waves. Gray bands indicate significant wind events.

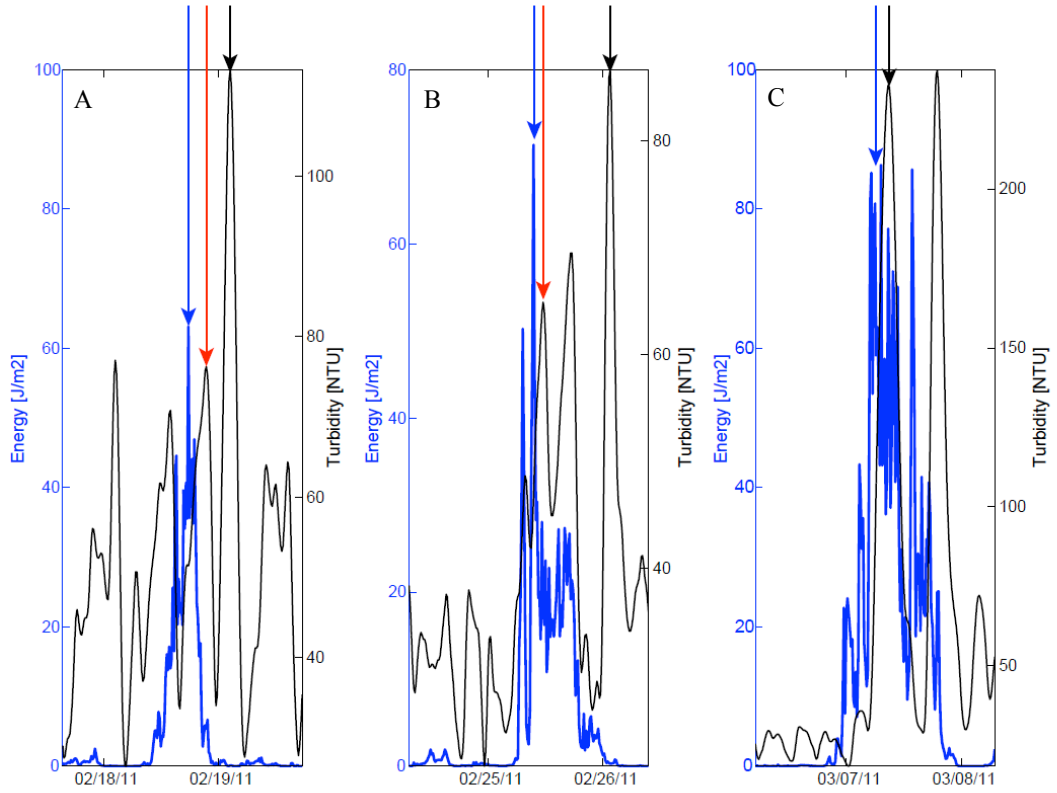

Figure 55. Three surface wave energy events as indicated in Figure 2.1.8 on *(A)* February 18, 2011 *(B)* February 25, 2011 and *(C)* March 7, 2011.

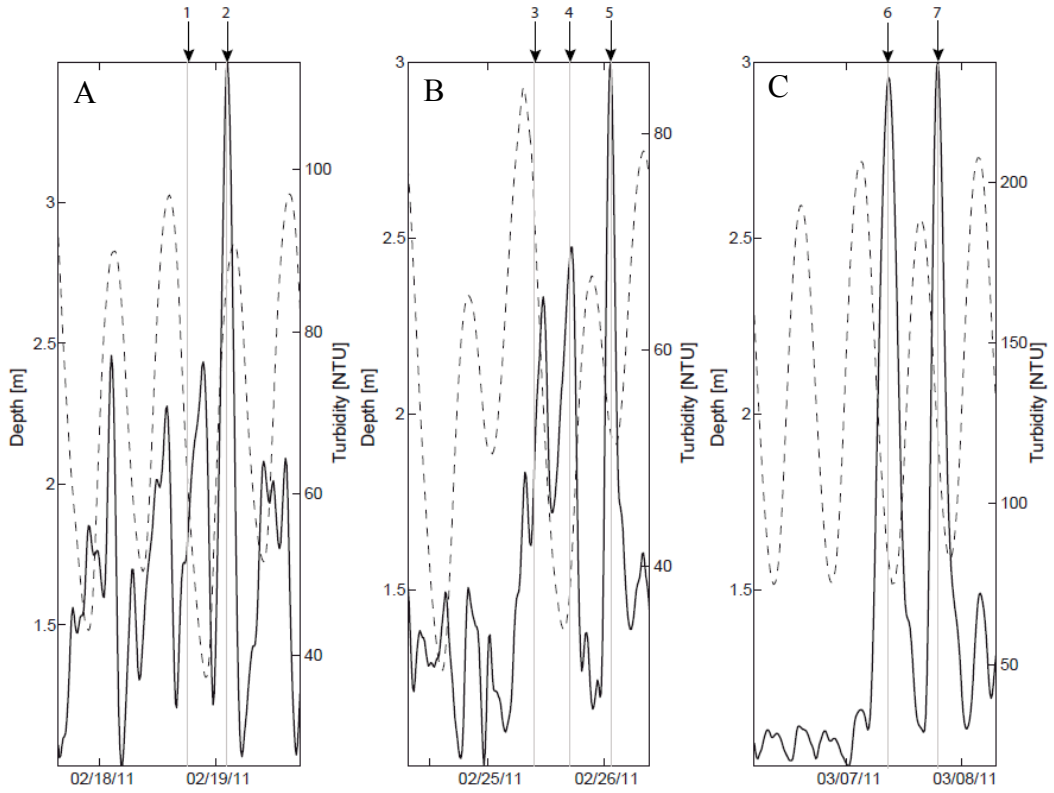

Figure 56. Three surface wave energy events as indicated in Figure19 with depth (dashed line) and turbidity (solid line) on *(A)* February 18, 2011 *(B)* February 25, 2011 and *(C)* March 7, 2011.

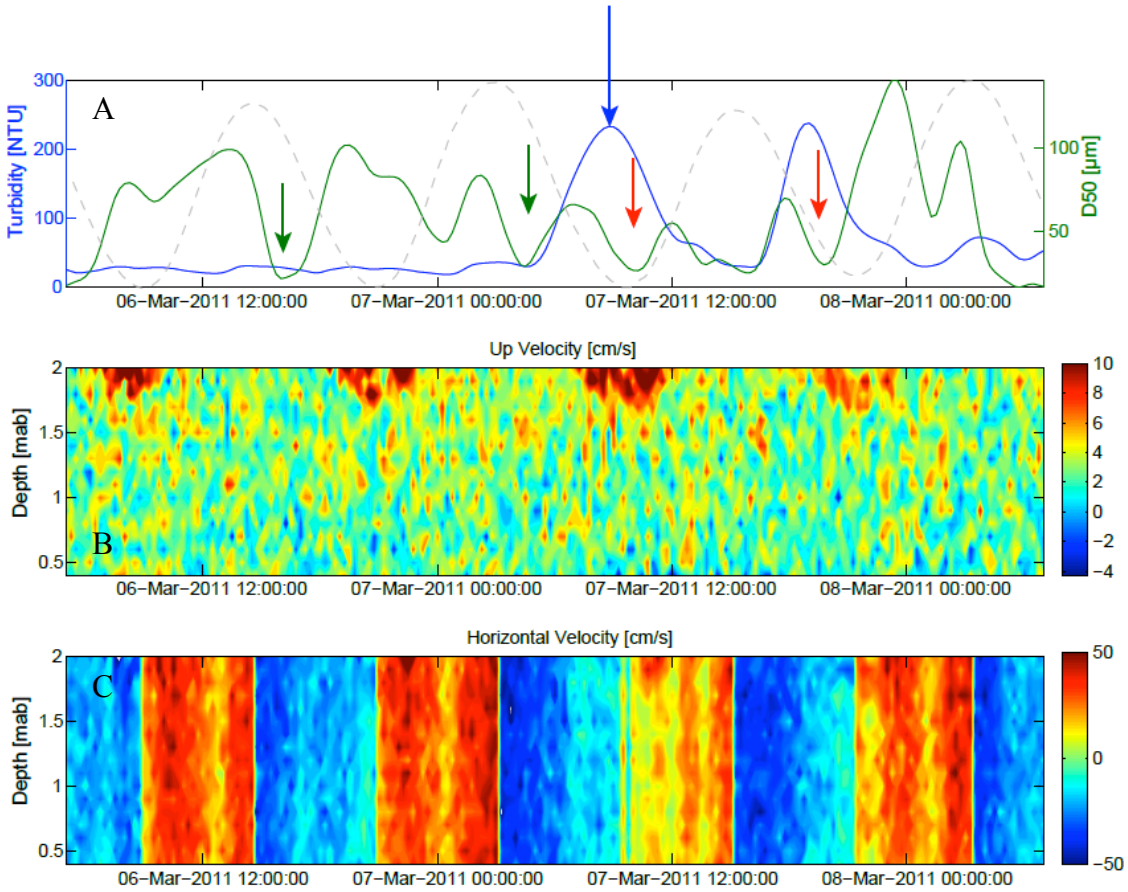

Figure 57. Shows a 48 hour period for the third wind event *(A)* The relation between turbidity (blue line) and D50 (green line) with depth (dashed line) shown for reference *(B)* Vertical profile of the up component of velocity, and *(C)* Vertical profile of the horizontal component of velocity, note that negative velocity corresponds to the flood direction.

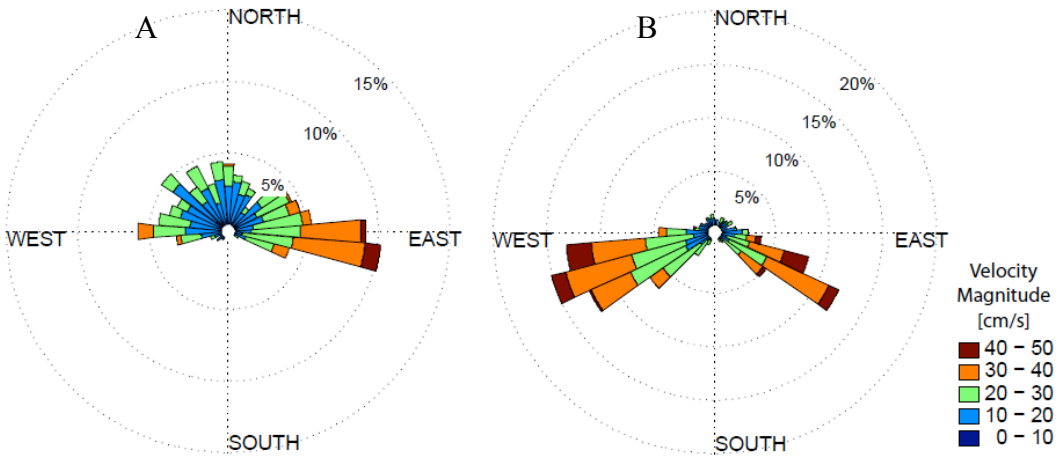

Figure 58. Velocity Vector plot for Grizzly Bay, time period March 3 – 16, 2011 for *(A)* the ebb tide and *(B)* the flood tide. Note that the direction is direction from.

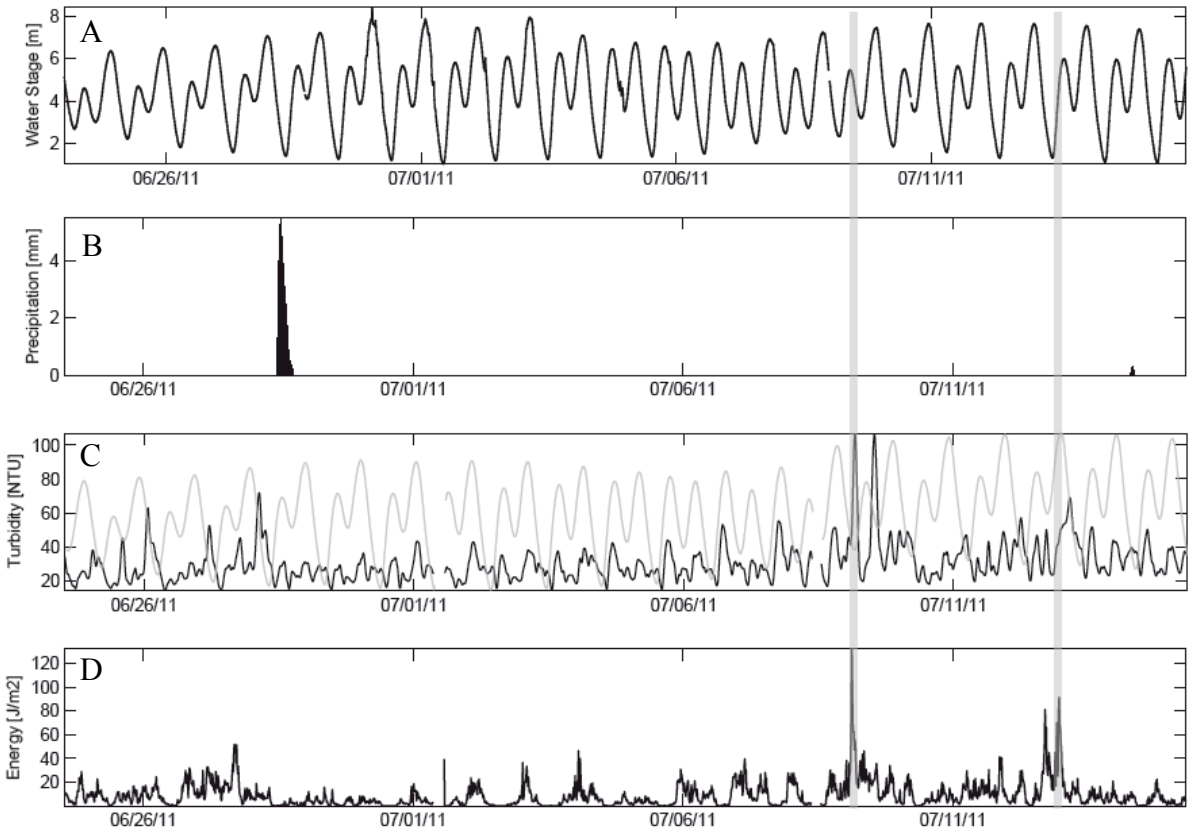

Figure 59. Hydrodynamic data for the GBS measurement period *(A)* Regional hydrology represented by water stage at Montezuma Slough at Hunter Cut *(B)* Precipitation at CIMIS station # 170 *(C)* Tidal variations in depth (gray line) and turbidity (black line), and *(D)* Energy contained in surface waves. Gray bands indicate significant wind events.

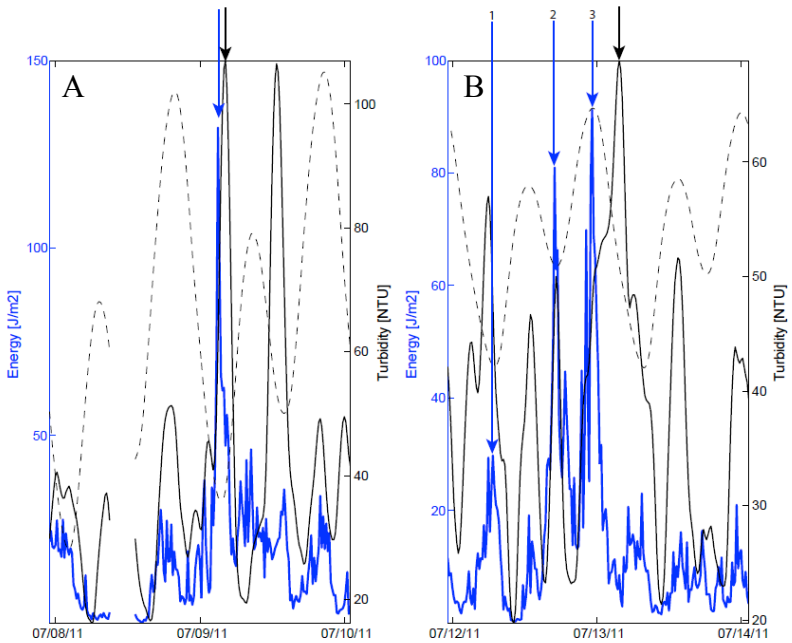

Figure 60. Two surface wave energy events as indicated in Figure 25 with energy (blue line), turbidity (black line), and depth (dashed line) on *(A)* July 9, 2011 and *(B)* July 12, 2011

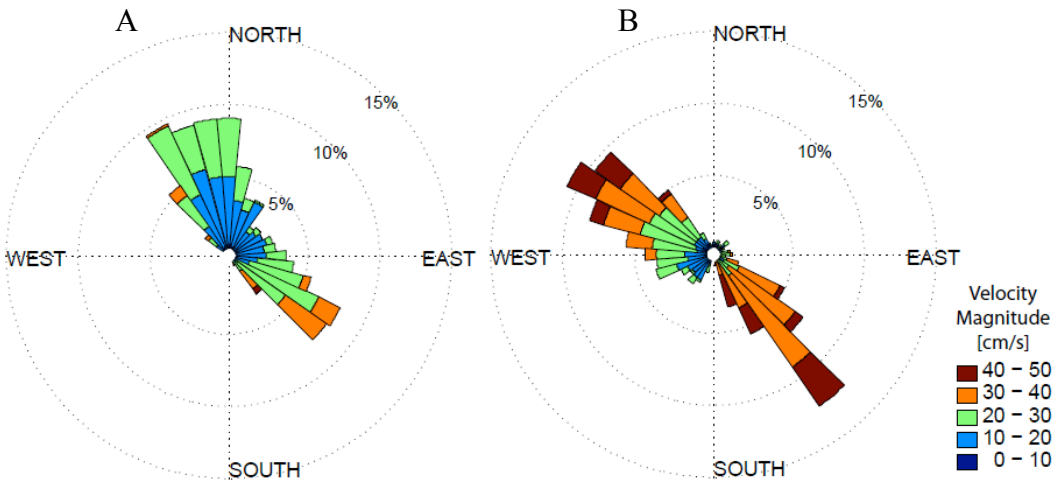

Figure 61. Velocity Vector plot for Grizzly Bay, time period July 1 – 15, 2011 for *(A)* the ebb tide and *(B)* the flood tide. Note that the direction is direction from.

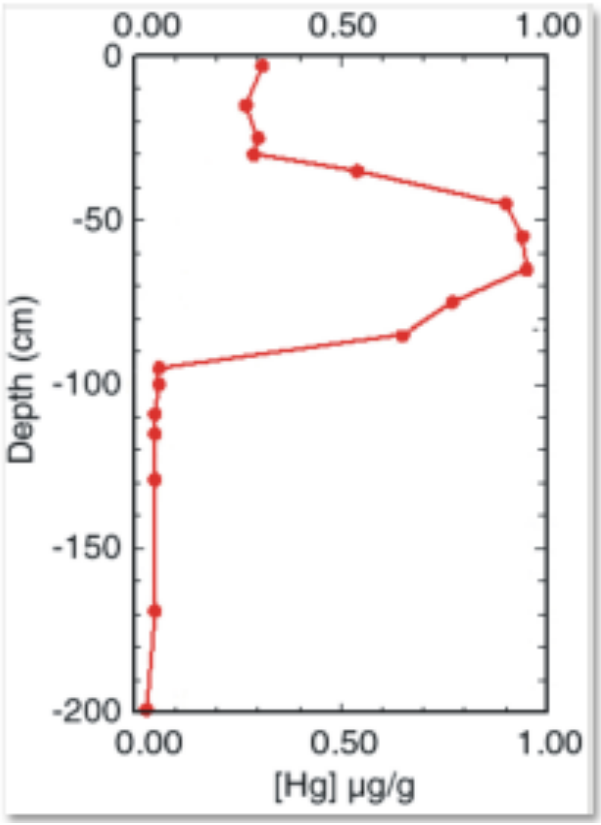

Figure 62. Downcore trend of mercury concentration for Grizzly Bay Modified after Hornberger et al. (1999). Total mercury concentration [in µg g-1 dry weight] in sediments (< 64 µm) was obtained by extractions with aqua regia.

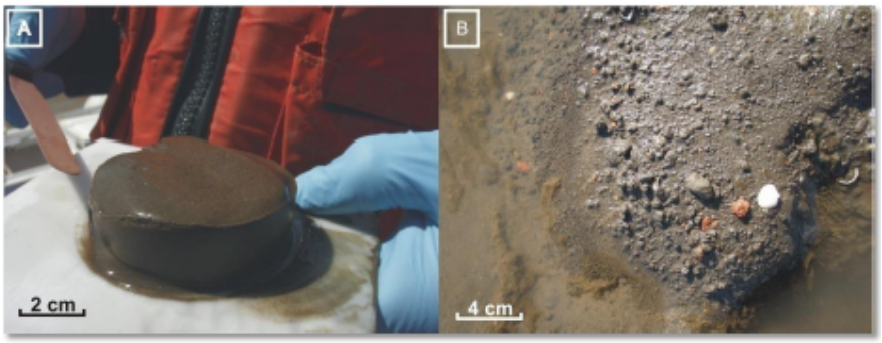

Figure 63. Sediment samples at Grizzly Bay (A) and Liberty Island (B) in April 2008 Red particles on figure B are brick debris.

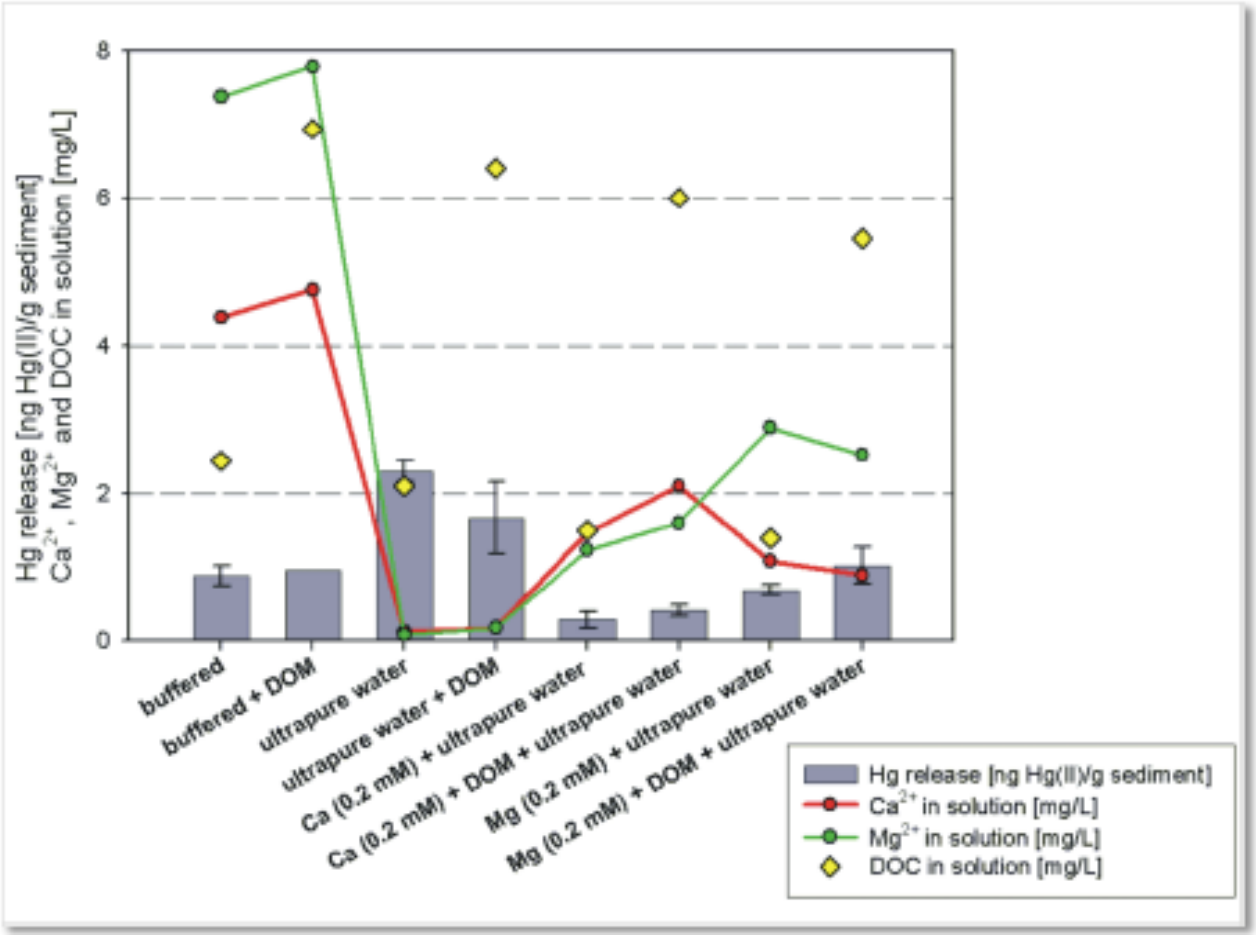

Figure 64. Results from batch extraction experiments with composite sample GB1 The mean mercury release is displayed for the 0.45 µm filtration step with respective standard deviations of duplicate samples (error bars).

Tables

Table 1. Established sampling grids for each field session

Site and date of sampling [mm/dd/y]	Sampling grid (sketch – not at scale)	Sampling depth [cm]	No. of samples per section	No. of sections	Total amount of samples
Grizzly Bay 01/23/2008	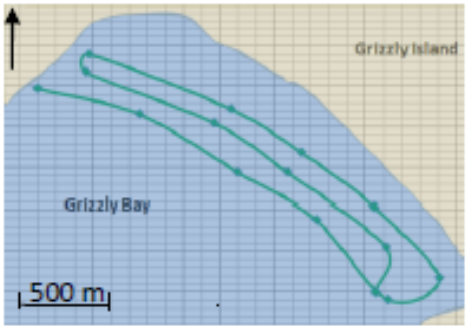	0 - 2 2 - 4	5 3	3 3	15 9
Grizzly Bay 04/07/2008		0 - 2	5	3	14
Liberty Island 04/08/2008	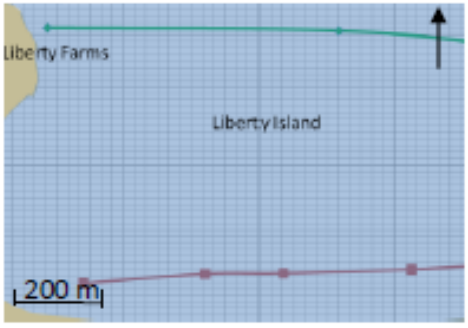	0 - 2	3/5	2	8

Table 2. Overview of all prepared composite samples and associated sample ID´s

Sampling site	Preparation of composite sample	Samples taken for preparation of composite samples	Initial sample code with date of sampling [mm/y]	ID	Performed analyses		
					1	2	3
Grizzly Bay	40 g sediment material was taken from all collecting sites of the respective sections of the grid (Tab. 1) and combined to get a composite sample	samples collected from all sections with the sampling depth: 0-2 cm	G.B.4_6.1cs (01/08)	**GB1**	X	X	X
		samples collected at the closest section to Grizzly Island with the sampling depth: 0-2 cm	G.B.6.1cs (01/08)	**GB2**	X	X	X
		samples collected from all sections with the sampling depth: 2-4 cm	G.B.4_6.2cs (01/08)	GB3	X		
		samples collected at the closest section to Grizzly Island with the sampling depth: 0-2 cm	G.B.6.1cs (04/08)	GB4	X		
		samples collected at the farthest section to Grizzly Island with the sampling depth: 0-2 cm	G.B.4.1cs (04/08)	GB5	X		
Liberty Island		samples collected from all sections with the sampling depth: 0-2 cm	L.I.2.1cs (04/08)	**LI1**	X	X	X

Table 3. Particle size ranges used for characterizing sediments in this study

Particle size range [µm]	Corresponding USDA size fractions (Jackson 2005)
> 1180	very coarse sand (> 1000 µm)
1180 - 500	very coarse sand (> 1000 µm) and coarse sand (1000 – 500 µm)
500 - 250	medium sand (500 – 250 µm)
250 - 106	fine sand (250 – 100 µm)
106 - 53	fine sand (250 – 100 µm) and very fine sand (100 – 50 µm)
< 53	very fine sand (100 – 50 µm), silt (50 – 2 µm), clay (< 2µm)

Table 4. Temperature-time-program for total mercury analyses with the DMA-80

Step	Temperature [°C]	Time [min:s] - liquids	Time [min:s] - solids
1 - drying	200	02:00	00:30
2 – ramp to decomposition temperature	650	01:30	01:30
3 - decomposition	650	03:00	03:00

Table 5. Selective extraction steps to determine biogeochemically relevant mercury fractions.

Extraction step	Extractant	Mercury (Hg) fraction	Typically removed mercury species
F3	1M KOH	organo-chelated mercury	CH_3Hg, Hg-humics, Hg_2Cl_2
F4	12M HNO_3 (trace metal grade)	strong complexed, elemental mercury	Hg(0), Hg_2Cl_2, Hg in amorphous organo-sulfur, Hg–Ag amalgams, crystalline Fe/ Mn oxides
F5	aqua regia –HCl:NO_3 (10:3) (both trace metal grade)	mercuric sulfide	HgS, HgSe

Table 6. Chemical characterization of the F1-FA isolate

Modified after RAVICHANDRAN *et al.* *(1998)*.

		F1-FA isolate
Ash-free elemental composition [wt%]	C	52.94
	O	4.37
	H	39.67
	N	1.43
	S	1.60
Quantitative ^{13}C-NMR analysis [% of total C]	Aliphatic I [0-62 ppm]	43.4
	Aliphatic II [62-90 ppm]	15
	Acetal [90-110 ppm]	5.4
	Aromatic [110-160 ppm]	20.1
	Carboxylic [160-190 ppm]	13.8
	Ketone [190-230 ppm]	2.2
	SUVA [L·mg of C^{-1}·m^{-1}]	4.17

Table 7. Information to additional sediment samples from McLaughlin Reserve, CA, USA

Modified after Süß (2006).

Sample ID	MCL131B	MCL134B1
Geographical position	38°86'29''N -122°37'24''W	38°86'21''N -122°36'98''W
Date of sampling [mm/dd/y]	05/31/2005	05/31/2005
Soil type and sampling zone	sandy silt loam, B-horizon: 26 - 60 cm	sandy loam, B1-horizon: 45 - 67 cm
Site information	UC Davis McLaughlin Reserve, fluvent at distal end of point bar, transitional wetland vegetation	UC Davis McLaughlin Reserve, wetland sediment, vegetation: cattails and willow
T-Hg [µg Hg/g] of sediments	36 ± 4.1	8.8 ± 0.5
Sequential extraction data		
F1 – water soluble Hg	0.3 ± 0.0	0.3 ± 0.0
F2 – "stomach acid" soluble Hg	0.1 ± 0.0	0.0 ± 0.0
F3 - organo-chelated Hg	84.6 ± 0.1	0.2 ± 0.0
F4 - strong complexed Hg	4.2 ± 0.3	3.3 ± 0.4
F5 - Hg sulfide	10.08 ± 0.2	96.2 ± 0.4
TOC [%] of sediments	0.8	2.6

Table 8. List of conducted batch extraction experiments

Performed separation techniques (chapter 2.3.2) are marked with an "X" in the right column of this table. Abbreviations: I = ionic strength; MF = membrane filtration; C = centrifugation.

No.	Basic conditions				Additions	Used sediment samples	Separation	
	Sediment input [g]	1 M pH-buffer [mL]	3 M I-stock [mL]	UPW [mL]			MF	C
Buffered batch extraction experiments								
0A	1.00	2.00	4.70	193.3		MCL131B/ 13481	X	X
						MCL131B/ 13481	X	
0B	2.00	2.00	4.70	193.3		G81/ 2	X	
						G81/ 2	X	X
						U1	X	
Unbuffered batch extraction experiments								
1A	2.00			200.0		G81/ 2	X	
						U1	X	
1B	20.00			200.0		G81/ 2	X	
DOM - batch extraction experiments using F1-FA-stock solution (100 mg C/L)								
2A	2.00	2.00	4.70	173.3	20.0 mL F1-FA-stock	G81/ 2	X	
2B	2.00			180.0	20.0 mL F1-FA-stock	G81/ 2	X	
2C	20.00			180.0	20.0 mL F1-FA-stock	G81/ 2	X	
Calcium - batch extraction experiments using 1M $Ca(NO_3)_2 \cdot 4H_2O$-stock solution								
3A	2.00			199.9	40.0 µL Ca-stock	G81/ 2	X	
3B	2.00			179.9	40.0 µL Ca-stock, 20.0 mL F1-FA stock	G81/ 2	X	
3C	1.00				200.0 mL Liberty Island water: untreated[1], after cation-exchange column[2]	MCL131B/ 13481[1]	X	
						MCL131B/ 13481[2]	X	
Magnesium - batch extraction experiments using Mg-stock solution (10,000 mg/L)								
4A	2.00			199.9	9.7 µL Mg-stock	G81/ 2	X	
4B	2.00			179.9	9.7 µL Mg-stock, 20.0 mL F1-FA stock	G81/ 2	X	

Table 9. Maximum particle size in suspension after centrifugation

Centrifugation is carried out with a Sorvall superspeed centrifuge and a small rotor (50 mL). According to the manufacturer, calculation is made considering a density difference between particle and solution of 1.5 $\frac{g}{cm^3}$ and a temperature of 25°C.

Particle size [µm]	Speed [rpm]	Centrifugation time [min]
0.45	1000	45
0.10	6000	20
0.025	14.000	60

Table 10. Ranges of raw and normalized total leachable metals concentrations during wind event, rain event, and tidal cycle measurement for Grizzly Bay. Elements marked with an asterisk were normalized to the upper continental crust composition (Rudnick and Gao, 2004) instead of the North American Shale Composite. Shaded rows indicate that normalized values are higher than 1.

	Rain event		Wind event		Tidal cycle	
Element	**Raw (ng g^{-1})**	**Normalized**	**Raw (ng g^{-1})**	**Normalized**	**Raw (ng g^{-1})**	**Normalized**
Y89	16372-25526	0.468-0.729	11146-16835	0.318-0.481	16357-23977	0.467-0.685
Zr90	4825-19686	0.024-0.098	4328-7332	0.022-0.037	3964-7896	0.020-0.039
Yb173	1327-2037	0.428-0.657	942-1428	0.304-0.461	1442-2497	0.465-0.806
Rb85	20291-39690	0.162-0.318	24434-32901	0.195-0.263	35644-60604	0.285-0.485
Sr88	66895-131843	0.471-0.928	34255-67864	0.241-0.478	43608-318989	0.307-2.246
Nb93	670-1024	0.052-0.079	735-1077	0.057-0.083	1048-1799	0.081-0.138
Cd111	43-135	0.001-0.005	16-187	0.001-0.006	19-2180	0.001-0.073
Sn118*	820-1828	0.391-0.871	537-2671	0.256-1.272	1843-8107	0.877-3.861
Cs133	1707-3359	200.817-395.203	2134-2977	251.041-350.276	3096-5046	364257-593.607
Ba137	128426-281235	0.202-0.442	124769-250919	0.196-0.395	178342-473173	0.280-0.744
La139	11359-18021	0.366-0.581	9321-13083	0.301-0.422	12376-19193	0.399-0.619
Ce140	28304-44160	0.422-0.659	21420-29373	0.320-0.438	28913-44443	0.432-0.663
Pr141*	3260-4905	0.459-0.691	2771-3787	0.390-0.533	3704-5709	0.522-0.804
Nd146	14196-20332	0.518-0.742	11890-16170	0.434-0.590	15707-24008	0.573-0.876
Sm149	3211-4712	0.573-0.841	2744-3734	0.490-0.667	3685-5538	0.658-0.989
Eu151	776-1172	0.646-0.976	639-1162	0.532-0.968	871-6458	0.726-5.382
Gd157	2709-4932	0.521-0.948	2821-3841	0.543-0.739	3971-10197	0.764-1.961
Tb159	486-744	0.572-0.875	406-560	0.477-0.659	563-3186	0.663-3.748
Dy163*	2817-4175	0.722-1.071	2144-3105	0.550-0.796	2960-4818	0.759-1.235
Ho165*	550-834	0.662-1.071	405-586	0.488-0.706	578-877	0.696-1.056
Er167*	1507-2302	1.507-2.302	1100-1616	1.100-1.616	1605-3033	1.605-3.033
Lu175	178-291	0.388-0.632	126-224	0.274-0.488	197-2377	0.429-5.167
Hf178	105-289	0.017-0.046	82-222	0.013-0.035	115-1162	0.018-0.184
Ta181	11-21	0.010-0.019	14-114	0.013-0.104	34-581	0.031-0.184
Pb208	19715-29144	0.986-1.457	14947-25477	0.747-1.274	29603-42793	1.480-2.140
Th232	3185-5496	0.259-0.447	2889-4477	0.235-0.364	3906-6626	0.318-0.539
U238	1189-2057	0.440-0.762	853-1603	0.316-0.594	894-1747	0.331-0.647
Li7*	14675-29752	0.699-1.417	16764-23164	0.798-1.103	20804-35439	0.991-1.688
Al27	12242917-26634548	0.072-0.158	14498884-20546603	0.086-0.122	20044457-26462594	0.119-0.216
Sc45	7320-12928	0.488-0.862	6856-10551	0.457-0.703	9996-18772	0.666-1.251
Ti47	538838-988982	0.077-0.141	653214-878336	0.093-0.125	751313-1157789	0.107-0.165
V51	57954-92134	0.446-0.709	49228-71327	0.379-0.549	72946-121180	0.561-0.940
Cr53	74409-123807	0.595-0.990	61371-118959	0.491-8.123	107829-161048	0.863-1.288
Mn55	1558788-4358850	1.559-4.359	674640-1419222	0.675-1.419	1143138-4070170	1.143-4.070
Fe57	24884974-45457632	0.439-0.802	25997396-37457258	0.459-0.661	45103506-62549694	0.795-1.103
Co59	21285-30425	0.819-1.170	14380-24832	0.553-0.955	22245-38129	0.856-1.466
Ni60	91606-135261	1.579-2.332	62119-630383	1.071-10.869	79175-133582	1.365-2.303
Cu63*	69852-159652	2.495-5.702	32299-82971	1.154-2.963	39541-76953	1.412-2.748
Zn66	88799-201716	32.89-74.71	83374-120299	30.879-44.555	100534-195998	37.235-72.592
Ga69*	3829-8026	0.219-0.459	4645-6594	0.265-0.377	6392-11274	0.365-0.644
Ag107	49.83-504.48	3.51-35.53	39.85-271.97	2.81-19.15	235.75-1183.81	16.60-83.37

Table 11. Mercury and DOC results for Nalgene® Oak Ridge centrifuge tube tests

Results are given as average with standard deviations from duplicate samples. Recoveries in % are normalized to the concentration in the initial solution. The complete data set can be found in the database (Appendix B – Database).

Test solution	Hg [ng Hg(II)/L]	Hg [%]	DOC [mg C/L]	DOC [%]
UPW	0.85 ± 0.36	157.4 ± 66.7	0.23 ± 0.04	100.0 ± 14.3
UPW spiked with 90 ng Hg(II)/L	81.1 ± 7.5	91.1 ± 8.4	0.17 ±0.01	85.0 ± 5.0
UPW spiked with 90 ng Hg(II)/L and 10 mg F1-FA/L	75.2 ± 6.7	69.3 ± 6.5	6.10 ± 0.04	98.4 ± 0.6

Table 12. XRD results for all composite samples from Grizzly Bay and Liberty Island

Minerals are summarized in the corresponding mineral subclasses (bold font) after Strunz & Nickel (2001). "Me:O" indicates the binding ratio between oxides with metals and oxygen in the mineral.

	Mineral subclasses **wt [%]**	**GB1**	**GB2**	**GB3**	**GB4**	**GB5**	**LI1**
Non-clay minerals	**oxides (Me:O = 1:2)** (quartz)	39.8	45.2	42.4	35.3	27.4	15.8
	tectosilicates (kalifeldspar, plagioclase)	26.5	26.3	25.3	26.5	26.6	15.6
	inosilicates (amphibole)	2.8	2.8	2.3	2.5	1.6	0.7
	carbonates (calcite, dolomite)	0.4	0.9	0.5	-	-	-
	oxides (Me:O = 2:3) (hematite, maghemite)	0.4	0.2	0.3	2.8	2.5	-
	hydroxides (goethite)	-	-	-	0.5	0.5	-
Clay minerals	**phyllosilicates** (halloysite, kaolinite, mica (illite, biotite), chlorite, serpentine, smectite)	30.4	24.5	28.8	32.3	41.4	67.9

Table 13. Results for TOC, T-Hg analyses and selected mercury forms (selective extraction steps) of composite samples and corresponding size fractions

Tab. 12: Results for TOC, T-Hg analyses and selected mercury forms (selective extraction steps) of composite samples and corresponding size fractions

Composite samples and size fractions	TOC [mg C/g sediment]	T-Hg [mg Hg/kg sediment]	Mercury forms [%]		
			Organo-chelated Hg	Strong complexed, elemental Hg	Mercuric sulfide
GB1	**5.2 ± 0.0**	**0.14 ± 0.0**	**56.2**	**32.5**	**11.3**
< 53 µm	5.1 ± 0.1	0.14	-	-	-
106-53 µm	3.5 ± 0.1	0.14	-	-	-
106-250 µm	11.29 ± 0.0	0.26	53.2	43.6	3.2
GB2	**4.1 ± 0.3**	**0.12 ± 0.0**	**71.5**	**26.6**	**1.9**
< 53 µm	4.0 ± 0.1	0.12	-	-	-
106-53 µm	5.7 ± 0.6	0.12	-	-	-
106-250 µm	9.3 ± 0.1	0.26	64.7	31.8	3.5
GB3	**5.5 ± 0.0**	**0.18 ± 0.0**	**-**	**-**	**-**
< 53 µm	6.0 ± 0.0	0.18 ± 0.0	-	-	-
106-53 µm	4.7 ± 0.2	0.18 ± 0.0	-	-	-
106-250 µm	6.5 ± 0.1	0.23 ± 0.0	-	-	-
GB4	**6.7 ± 0.3**	**0.16**	**-**	**-**	**-**
< 53 µm	4.9 ± 1.1	0.16	-	-	-
106-53 µm	6.5 ± 0.6	0.14	-	-	-
106-250 µm	14.9 ± 3.6	0.33	-	-	-
GB5	**7.5 ± 0.3**	**0.18**	**-**	**-**	**-**
< 53 µm	5.9 ± 0.1	0.15	-	-	-
106-53 µm	14.0 ± 0.1	0.25	-	-	-
106-250 µm	11.8 ± 0.1	0.24	-	-	-
LI1	**19.4 ± 0.1**	**0.17**	**67.6**	**15.2**	**17.2**
< 53 µm	19.4 ± 0.1	0.18	54.7	13.9	31.4
106-53 µm	18.6 ± 0.6	0.17	-	-	-
106-250 µm	15.1 ± 2.9	0.15	69.8	16.7	13.5
250-500 µm	14.7 ± 0.0	0.16	-	-	-
500-1180 µm	17.9 ± 4.4	0.16	-	-	-

Table 14. Results for DOC, SUVA, and FI for Grizzly Bay and Liberty Island water

ID	DOC [mg C/L]	SUVA at 254 nm [L·mg C^{-1}·m^{-1}]	Fluorescence index
GB January 08	3.5	2.8	1.4
GB April 08 – low tide	3.6	2.8	1.4
GB April 08 – high tide	3.6	3.0	1.4
LI April 08	4.0	2.8	1.4

Table 15. Results for unbuffered batch extraction experiments

Blank corrected mean results are displayed with corresponding standard deviations for released mercury and OM (based on the amount of sediment input), as well as UVA, SUVA and selected cations and anions in solution for GB1, GB2 and LI1.

	GB1	GB2	LI1
Hg release [ng Hg(II)/g sediment]	2.3 ± 0.2	1.8 ± 0.3	0.5 ± 0.0
% released Hg from T-Hg	1.6	1.5	0.3
Released OM [mg C/g sediment]	0.2 ± 0.0	0.2 ± 0.0	0.3 ± 0.0
UVA [cm^{-1}]	0.1 ± 0.0	0.1 ± 0.0	0.1 ± 0.0
$SUVA_{254\,nm}$ [L·mg of C^{-1}·m^{-1}]	3.8	3.7	3.5
Na^+ [mg Na^+/L]	8.9 ± 0.1	7.7 ± 0.1	2.0 ± 0.0
Ca^{2+} [mg Ca^{2+}/L]	0.1 ± 0.0	0.1 ± 0.0	1.4 ± 0.0
Mg^{2+} [mg Mg^{2+}/L]	0.1 ± 0.0	0.1 ± 0.0	1.0 ± 0.0
Cl^- [mg Cl^-/L]	10.5 ± 1.6	9.0 ± 1.0	0.4 ± 0.0
number of replicates	4	4	2

Table 16. Further information to the isolate F1-FA

With the organic matter associated cations and anions calculated from blank solutions of unbuffered batch extraction experiments and based on the amount of added OM.

Isolate	Mercury [ng Hg(II)/mg OM]	Sodium [µg Na^+/mg OM]	Potassium [µg K^+/mg OM]	Chloride [µg Cl^-/mg OM]	Sulfate [µg SO_4^{2-}/mg OM]	Nitrate [µg NO_3^-/mg OM]
F1-FA	0.9	17.4	0.7	17.2	8.4	17.6

Table 17. Water chemistry of Liberty Island water before and after cation exchange column

	Liberty Island water (untreated)	Liberty Island water (after removal of divalent cations)
Na^+ [mg Na^+/L]	53.5	137.0
Ca^{2+} [mg Ca^{2+}/L]	28.0	0.0
Mg^{2+} [mg Mg^{2+}/L]	23.2	0.0
Cl^- [mg Cl^-/L]	38.9	49.5
DOC [mg C/L]	3.7	4.1

Table 18. Correlation coefficients for single variable and multivariable proxies of the mercury species measured in this study.

Measurement	pTHg	fTHg	pMeHg	fMeHg
Depth [m]	0.361452	-0.38814	0.061321	**-0.38925**
Temp [deg C]	0.059134	-0.74412	0.749536	**-0.68187**
SpCond [us/cm]	0.719277	-0.21855	-0.44332	**-0.08981**
pH	-0.57472	0.022641	0.208522	**0.028006**
Turbidity [NTU]	0.800429	0.150451	0.377367	**0.43745**
FDOM [QSU]	-0.19976	0.920853	-0.55356	**0.873339**
Chlorophyll-A [ug/L]	-0.22124	-0.39754	0.484717	**-0.33195**
Filtered Absorption @ 440nm (ag440)	-0.22019	0.903112	-0.48806	**0.897393**
Filtered Attenuation @ 440nm (cg440)	-0.22764	0.871307	-0.42229	**0.85868**
Filtered Scattering @ 440nm (bg440)	-0.13296	0.19437	0.100707	**0.105122**
Particulate Absorption @ 440nm (ap440)	0.484637	0.159381	0.274542	**0.308124**
Particulate Attenuation @ 440nm (cp440)	0.463276	0.170616	0.302507	**0.3349**
Particulate Scattering @ 440nm (bp440)	0.445443	0.171944	0.306876	**0.339464**
ap/cp	0.129511	-0.00142	-0.10475	**-0.03093**
Cp Slope	-0.5942	0.773482	-0.41331	**0.748041**
Bg-440	0.476215	0.161421	0.316328	**0.337135**
A254	-0.27695	0.936187	-0.47541	**0.901657**
SUVA254	-0.05029	0.20706	-0.13004	**0.01857**
Spectral Slope_275-295	0.249514	-0.73736	0.683131	**-0.65235**
Spectral Slope_290-350	0.191723	-0.87855	0.414859	**-0.78148**
Spectral Slope_350-400	0.258091	-0.1722	0.020953	**-0.24581**
Spectral Slope_412-676	-0.03903	-0.08772	0.011713	**-0.14695**

Fluorophore A	-0.26315	0.908987	-0.53587	**0.8743**
Fluorophore C	-0.25287	0.915139	-0.55641	**0.887234**
Fluorophore M	-0.26432	0.905197	-0.5331	**0.880273**
Fluorophore D	-0.24372	0.915714	-0.56466	**0.889563**
Fluorophore B	-0.01242	-0.02226	0.15447	**-0.04623**
Fluorophore T	-0.30452	0.834617	-0.51354	**0.832681**
Fluorophore N	-0.28459	0.897431	-0.52087	**0.87994**
Fluorescence Index	-0.09613	0.335556	-0.56106	**0.315588**
Humic Index	0.009798	0.39426	-0.24788	**0.348086**
Max Wave Height [m]	0.381727	-0.52759	0.452649	**-0.42108**
Energy [J/m2]	0.331432	-0.38542	0.440033	**-0.29625**
Precipitation [mm]	0.742338	-0.23752	-0.41476	**-0.10389**
Solar Radiation [W m2]	-0.09249	-0.45073	0.727001	**-0.50984**
Wind Speed [m/s]	-0.00037	-0.15554	0.490488	**-0.05876**
Wind Dir [deg]	**0.014131**	**0.123977**	**-0.36638**	**0.10966**

Table 19. Comparison of metals concentrations and toxicity guidelines. ERL = effects range low. ERM = effects range median. AET = apparent effects threshold determined for San Francisco Bay. ERL and ERM data are from Long et al. (1995).

Element	ERL (ppm)	ERM (ppm)	Rain mean (ppm)	Wind mean (ppm)	Tidal mean (ppm)
Ag	1	3.7	0.18	0.09	0.52
Cd	1.2	9.6	0.07	0.03	0.25
Cr	81	370	102.76	126.78	133.53
Cu	34	270	113.82	57.69	55.63
Ni	20.9	51.6	115.47	109.43	102.46
Pb	46.7	218	24.96	19.20	35.39
Zn	150	410	142.28	96.92	131.50

Table 20. Total metal content transported by each event, and transport rates, for selected metals.

	Rainy		**Windy**		***Tidal***	
Element	**Total mg L^{-1}**	**Rate µg L^{-1} s^{-1}**	**Total mg L^{-1}**	**Rate µg L^{-1} s^{-1}**	**Total mg L^{-1}**	**Rate µg L^{-1} s^{-1}**
Y89	51.943	7.214	29.452	4.091	63.262	1.464
Cd111	0.176	0.024	0.061	0.008	0.596	0.014
Cs133	5.765	0.801	5.224	0.726	12.398	0.287
Nd146	43.500	6.042	28.664	3.981	60.855	1.409
Pb208	60.285	8.373	39.157	5.439	111.214	2.574
Cr53	249.768	34.690	264.435	36.727	417.847	9.672
Ni60	283.141	39.325	227.762	31.634	329.926	7.637
Cu63	292.539	40.630	117.461	16.314	185.833	4.302
Zn66	337.879	46.928	200.639	27.866	428.650	9.922
Ag107	0.439	0.061	0.191	0.027	1.463	0.034
	g L^{-1}	**mg L^{-1} s^{-1}**	**g L^{-1}**	**mg L^{-1} s^{-1}**	**g L^{-1}**	**mg L^{-1} s^{-1}**
Mn55	7.817	1.086	2.194	0.305	7.615	0.176
Fe57	86.284	11.984	66.488	9.234	169.345	3.920

References

Aiken, G.R., 1992. Chloride interference in the analysis of dissolved organic carbon by the wet oxidation method. Environmental Science and Technology 26(12):2435-2439.

Aiken, G.R. and Malcolm, R.L., 1987. Molecular-weight of aquatic fulvic-acids by vapor-pressure osmometry. Geochimica et Cosmochimica Acta 51(8):2177-2184.

Aiken, G.R., McKnight, D.M., Thorn, K.A., and Thurman, E.M., 1992. Isolation of hydrophilic organic acids from water using nonionic macroporous resins. Organic Geochemistry 18(4):567-573.

Alpers, C.N., Taylor, H.E., and Domagalski, J.L., editors, 2000a. Metals transport in the Sacramento River, California, 1996-1997. Volume 1: Methods and data. U.S. Geological Survey Water Resources Investigations Report 99-4286.

Alpers, C.N., Anteweiler, R.C., Taylor, H.E., Dileanis, P.D., and Domagalski, J.L., editors, 2000b. Metals transport in the Sacramento River, California, 1996-1997. Volume 2: Interpretation of metal loads. U.S. Geological Survey Water Resources Investigations Report 00-4002.

Alpers, C.N., Hunerlach, M.P., May, J.T., and Hothem, R.L., 2005. Mercury contamination from historical gold mining in California. U.S. Geological Survey, USGS Fact Sheet 2005-3014 Version 1.1.: 6 pp.

Benoit, J.M., Gilmour, C.C., Mason, R.P., Riedel, G.S., and Riedel, G.F., 1998. Behavior of mercury in the Patuxent River estuary. Biogeochemistry 40(2-3):249-265.

Bergamaschi, B.A., 2008. Information concerning the sample preparation for total organic carbon determination. USGS California Water Science Center, Sacramento,CA, Contact: bbergama@usgs.gov. 01/2008 - 07/2008.

Bergamaschi, B. A., Fleck, J. A., Downing, B. D., Boss, E., Pellerin, B., Ganju, N. K., Fujii, R., 2011. Methyl mercury dynamics in a tidal wetland quantified using in situ optical measurements. Limnology and Oceanography, 56(4):1355-1371.

Bilinski, H., Kwokal, Z., Plavsic, M., Wrischer, M., and Branica, M., 2000. Mercury distribution in the water column of the stratified Krka river estuary (Croatia): importance of natural organic matter and of strong winds. Water Research 34(7): 2001-2010.

Bird, S.M., Fram, M.S., and Krepeau, K.L., 2003. Method of analysis by the U.S. Geological Survey California District Sacramento Laboratory - Determination of dissolved organic carbon in water by high temperature catalytic oxidation, method validation, and quality-control practices. U.S. Geological Survey, Open File Report 03-366: 13 pp.

Bloom, N.S., Preus, E., Katon, J., and Hiltner, M., 2003. Selective extractions to assess the biogeochemically relevant fractionation of inorganic mercury in sediments and soils. Analytica Chimica Acta 479(2):233-248.

Boss E., W.S. Pegau, M. Lee, M.S. Twardowski, E. Shybanov, G. Korotaev, and Baratange, F., 2004. Particulate backscattering ratio at LEO 15 and its use to study particles composition and distribution. J. Geophys. Res., 109, C1, C0101410.1029/2002JC001514.

Bouse, R.M., Fuller, C.C., Luoma, S.N., Hornberger, M.I., Jaffe, B.E., & Smith, R.E. (2010). Mercury-contaminated hydraulic mining debris in San Francisco Bay. San Francisco Estuary and Watershed Science 8(1).

Brown, C.L. and Luoma, S.N., 1999. Metal trends and effects in Potamocorbula amurensis in North San Francisco Bay. U.S.Geological Survey Water Resources Investigations Report 99-4018.

Brown, L.R., 2003. Potential Effects of Organic Carbon Production on Ecosystems and Drinking Water Quality In: Larry R. Brown, editor. Issues in San Francisco Estuary Tidal Wetlands Restoration. San Francisco Estuary and Watershed Science. Vol. 1, Issue 1 (October 2003), Article 3.

CALFED, 2005. Mercury in Every Mix. Science Action. News from the California Bay-Delta Authority Science Program April 2005: 16 pp.

Cappiella, K., Malzone, C., Smith, R., and Jaffe, B., 1999. Sedimentation and bathymetry changes in Suisun Bay: 1867-1990. U.S. Geological Survey, Open-File Report 99-563: 1 pp.

Chin, Y.-P., Aaiken, G.R., and O'Loughlin, E., 1994. Molecular weight, polydispersity, and spectroscopic properties of aquatic humic substances. Environmental Science and Technology 28(11):1853-1858.

Choe, K.Y., Gill, G.A., and Lehman, R., 2003. Distribution of particulate, colloidal, and dissolved mercury in San Francisco Bay estuary. 1. Total mercury. Limnology and Oceanography 48(4):1535-1546.

Chung, E. G., Bombardelli, F. A., & Schladow, S. G., 2009. Sediment resuspension in a shallow lake. [Article]. Water Resources Research, 45. doi: W0542210.1029/2007wr006585.

Cloern, J.E. and Nichols, F.H., 1985. Time scales and mechanisms of estuarine variability, a synthesis from studies of San Francisco Bay. Hydrobiologia 129:229-237.

Conaway, C.H., Squire, S., Mason, R.P., and Flegal, A.R., 2003. Mercury speciation in the San Francisco Bay estuary. Marine Chemistry 80:199-225.

Conaway, C.H., Ross, J.R.M., Looker, R., Mason, R.P., and Flegal, A.R., 2007. Decadal mercury trends in San Francisco Estuary sediments. Environmental Research 105:53-66.

Coquery, M., Cossa, D., and Sanjuan, J., 1997. Speciation and sorption of mercury in two macro-tidal estuaries. Marine Chemistry 58(1-2):213-227.

Cox, P. A., 1989. The Elements: Their Origin, Abundance, and Distribution. Oxford University Press, Oxford: 207 pp.

Cuetara, J.I., Burau, J.R., and Schoellhamer, D.H., 2001. Hydrodynamic and suspended solids concentration measurements in Suisun Bay, California, 1995. U.S. Geological Survey Water Resources Investigations Report 01-4-86.

Daskalakis, K.D., and O'Connor, T.P., 1995. Distribution of chemical concentrations in US coastal and estuarine sediment. Marine Environmental Research 40 (4):381–398.

Davis, J.A. 1982. Adsorption of natural dissolved organic matter at the oxide/water interface. Geochimica et Cosmochimica Acta 46(11):2381-2393.

Del Vecchio, R. and Blough, N.V., 2004. On the origin of the optical properties of humic substances, Environ. Sci. Technol 38(14):3885–3891, doi:10.1021/es049912h.

DeWild, J. F., Olson, M. L., & Olund, S. D., 2002. Determination of methyl mercury by aqueous phase ethylation, followed by gas chromatographic separation with cold vapor atomic fluorescence detection (Vol. Open-File Report 01–445): U.S. Geological Survey.

Dittman, J. A., J. B. Shanley, C. T. Driscoll, G. R. Aiken, A. T. Chalmers, J. E. Towse, and Selvendiran, P., 2010. Mercury dynamics in relation to dissolved organic carbon concentration and quality during high flow events in three northeastern U.S. streams, Water Resources Research 46:W07522, doi:10.1029/2009WR008351.

Domagalski, J., 2001. Mercury and methylmercury in water and sediment of the Sacramento River Basin, California. Applied Geochemistry 16:1677–1691.

Domagalski, J.L., Dileanis, P.D., Knifong, D.L., Munday, C.M., May, J.T., Dawson, B.J., Shelton, J.L., and Alpers, C.N., 2000. Water-quality assessment of the Sacramento River Basin, California: water-quality, sediment and tissue chemistry, and biological data, 1995-1998. U.S. Geological Survey: Open-File Report 2000-391, http://ca.water.usgs.gov/sac_nawqa/waterindex.html. Access: 11/2008.

Downing, B.D., E. Boss, B. A. Bergamaschi, J. A. Fleck, M. A. Lionberger, N. K.Ganju, D. H. Schoellhamer, and Fujii, R., 2009. Quantifying fluxes and characterizing compositional changes of dissolved organic matter in aquatic systems in situ using combined acoustic and optical measurements. Limnol. Oceanogr.: Methods 7:119–131, doi:10.4319/lom.2009.7.119.

Eberl, D., 2003. User's guide to RockJock: A program for determining quantitative mineralogy from powder x-ray diffraction data. U.S. Geological Survey, Open-File Report 03-78: 39 pp.

Eberl, D., 2008. Information related to quantitative X-ray diffraction analysis. USGS, Boulder, CO, Contact: dderbel@usgs.go. 01/2008 - 05/2008.

Eisma, D., 1986. Flocculation and de-flocculation of suspended matter in estuaries. Netherlands Journal of Sea Research, 20(2-3):183-199.

Flegal, A.R., Conaway, C.H., Scelfo, G.M., Hibdon, S.A., and Sañudo-Wilhelmy, S.A., 2005. A review of factors influencing measurements of decadal variations in metal contamination in San Francisco Bay, California. Ecotoxicology 14:645-660.

Fuller, C.C., Van Geen, A., Baskaran, M., and Anima, R., 1999. Sediment chronology in San Francisco Bay, California, defined by ^{210}Pb, ^{234}Th, ^{137}Cs, and ^{239,240}Pu. Marine Chemistry 64(21):7–27.

Gabriel, M.C., and Williamson, D.G., 2004. Principal biogeochemical factors affecting the speciation and transport of mercury through the terrestrial environment. Environmental Geochemistry and Health 26(4):421-434.

Gartner, J. W., 2004. Estimating suspended solids concentrations from backscatter intensity measured by acoustic Doppler current profiler in San Francisco Bay, California. [Article]. Marine Geology 211(3-4):169-187. doi: 10.1016/j.margeo.2004.07.001.

Gray, J. R., G. D. Glysson, L. M. Turcios, and Schwarz, G. E., 2000. Comparability of Suspended-Sediment Concentration and Total Suspended Solids Data, p. 20. Water-Resources Investigations Report 00-4191. U.S. Geological Survey.

Gray, J. R., and Gartner, J. W., 2009. Technological advances in suspended-sediment surrogate monitoring. [Article]. Water Resources Research 45. doi: 00d2910.1029/2008wr007063.

Gross, T. F., and Nowell, A. R. M., 1985. Spectral scaling in a tidal boundary layer. Journal of Physical Oceanography, 15(5):496-508.

Haitzer, M., Aiken, G.R., and Ryan, J.N. 2002. Binding of mercury(II) to dissolved organic matter: The role of the mercury-to-DOM concentration ratio. Environmental Science and Technology 36(16):3564-3570.

Haitzer, M., Aiken, G.R., and Ryan, J.N. 2003. Binding of mercury(II) to aquatic humic substances: Influence of pH and source of humic substances. Environmental Science and Technology 37(11):2436-2441.

Hayes, M.H.B. and Swift, R.S. 1978. The chemistry of soil colloids. In: The Chemistry of Soil Constituents, (ed. Greenland D. J., Hayes M. H. B.), Wiley-Intersience, New York: pp. 179-203.

Hill, P.S., Boss, E., Newgard, J.P., Law, B.A., & Milligan, T.G., 2000. Observations of the sensitivity of beam attenuation to particle size in a coastal bottom boundary layer. Journal of Geophysical Research 116(C02023), 14. doi: 10.1029/2010JC006539.

Hornberger, M.I., Luoma, S.N., van Geen, A., Fuller, C., and Anima, R. 1999. Historical trends of metals in sediments of San Francisco Bay, California. Marine Chemistry 64:39-55.

Horvat, M., Liang, L., & Bloom, N. S., 1993. Comparison of distillation with other current isolation methods for the determination of methyl mercury compounds in low level environmental samples, part II–water. Analytica Chimica Acta 282:153-168.

Jackson, M.L. 2005. Soil Chemical Analysis-Advanced Course. 2nd ed., rev. Parallel Press, University of Wisconsin-Madison Libraries, Madison, Wis.: 930 pp.

Jaffe, B E., Smith, R.E., and Torresan, L. 1998: Sedimentation and bathymetric change in San Pablo Bay, 1856-1983. U.S. Geological Survey, Open-File Report 98-759: 1 pp.

Jones, N.L., and Monosmith, S.G., 2007. Measuring short-period wind waves in a tidally forced environment with a subsurface pressure gauge. Limnology and Oceanography: Methods 5:317-327.

Jones, N.L., Monosmith, S.G., and Thompson, J.K., 2008. A Note on the Effect of Wind Waves on Vertical Mixing in Franks Tract, Sacramento-San Joaquin Delta, California. San Francisco Estuary and Watershed Science 6(2):11.

Knowles, N., and Cayan, D. R., 2002. Potential effects of global warming on the Sacramento/San Joaquin watershed and the San Francisco estuary. Geophysical Research Letters. 29:91-94.

Krone, R.B., 1977. Sedimentation in the San Francisco Bay System. Fifty-eighth Annual Meeting of the Pacific Division of the American Association for the Advancement of Science, San Francisco State University, San Francisco, California, June 12-6, 1977, San Francisco, California: pp. 85-96.

Lohrmann, Atle., 2001. Monitoring Sediment Concentration with acoustic backscattering instruments. Nortek AS. Sediment concentration with acoustic backscattering instruments/Nortek technical notes/October 15, 2001/Document No. N4000-712.

Long, E.R., MacDonald, D.D., Smith, S.L., and Calder, F.D., 1995. Incidence of adverse biological effects within ranges of chemical concentrations in marine and estuarine sediments. Environmental Management 19:81-97.

Lorke, A., 2007. Boundary mixing in the thermocline of a large lake. Journal of Geophysical Research 112:C09019.

Lu, X.Q., Werner, I., and Young, T.M., 2005. Geochemistry and bioavailability of metals in sediments from northern SFBay. Environment International 31:593-602.

Macalady, D.L., and Ranville, J.F., 1998. The chemistry and geochemistry of natural organic matter (NOM). In: Perspectives in Environmental Chemistry (ed. Macalady D. L.), Oxford Press, New York: 94-137 pp.

McKnight, D.M., Boyer, E.W., Westerhoff, P.K., Doran, P.T., Kulbe, T., and Anderson, D.T., 2001. Spectrofluorometric characterization of dissolved organic matter for indication of precursor organic material and aromaticity. Limnology and Oceanography 46(1):38-48.

Melamed, R., Trigueiro, F.E., and Villas Boas, R.C. 2000. The effect of humic acid on mercury solubility and complexation. Applied Organometallic Chemistry 14(9):473-476.

Mikac, N., Niessen, S., Ouddane, B., and Wartel, M. 1999. Speciation of mercury in sediments of the Seine estuary (France). Applied Organometallic Chemistry 13 (10):715-725.

Mikkelsen, O. A., Hill, P. S., and Milligan, T. G., 2006. Single-grain, microfloc and macrofloc volume variations observed with a LISST-100 and a digital floc camera. Journal of Sea Research, 55(2):87-102.

Milestone SRL. 2007. DMA-80 with terminal 640/1640: MILESTONE DMA-80 USER MANUAL. Milestone SRL, Italy: 135 pp.

Mitchell, C.P.J., and Gilmour, C.C., 2008. Mercury methylation in a Chesapeake Bay salt marsh. Journal of Geophysical Research – Biogeosciences, 113, G00C04, doi: 10.1029/2008JG000765.

Mitsch, W. J. and Gosselink, J.G., 1986. Wetlands. Van Nostrand Reinhold, New York: 539 pp.

Morel, F.M.M. and Hering, J.G., 1993. Principles and applications of aquatic chemistry. John Wiley & Sons, INC., New York - Chichester - Brisbane - Toronto - Singapore: 608 pp.

Nichols, F.H., Cloern, J.E., Luoma, S.N., and Peterson, D.H., 1986. The modification of an estuary. Science 231:5667-573.

NIST, 1999. National Institute of Standards and Technology: Certificate of Analysis. Standard Reference Material® 1944: New York/New Jersey Waterway Sediment. National Institute of Standards and Technology: 17 pp., https://srmors.nist.gov/certificates/1944.pdf. Access: 07/2008.

NWRI, 1984. Certificate of Analysis: WQB-1. A Lake Ontario Sediment for Trace Elements - Environment Canada Analytical Reference Material. National Water Research Institute: 2 pp., http://www.nwri.ca/nlet-lnee/crm-mrc/reference_tables/table5_sediment_te-e.html Access: 07/2008.

NWRI, 1992. Certificate of Analysis: TH-2. A Toronto Harbour Sediment for Trace Elements - Environment Canada Analytical Reference Material. National Water Research Institute: 2 pp., http://www.nwri.ca/nlet-lnee/crm-mrc/reference_tables/table5_sediment_te-e.html Access: 07/2008.

Olson, M. L., and Dewild, J. F., 1999. Techniques for the Collection and Species-Specific Analysis of Low Levels of Mercury in Water, Sediment, and Biota, p. 11. Water Resources Investigations 99-4018-B. US Geological Survey.

Phillips, B.M., Anderson, B.S., Hunt, J.W., Thompson, B., Lowe, S., Hoenicke, R., and Tjeerdema, R., 2003. Causes of sediment toxicity to Mytilus galloprovincialis in San Francisco Bay, California. Archives of Environmental Contamination and Toxicology 45:492-497.

Pullin, M.J., Anthony, C.A., and Maurice, P.A., 2007. Effects of iron on the molecular weight distribution, light absorption, and fluorescence properties of natural organic matter. Environmental Engineering Science 24:987-997.

Ravichandran, M., 2004. Interactions between mercury and dissolved organic matter--a review. Chemosphere 55(3):319-331.

Ravichandran M., Aiken, G.R., Reddy, M.M., and Ryan, J.N., 1998. Enhanced dissolution of cinnabar (mercuric sulfide) by dissolved organic matter isolated from the Florida Everglades. Environmental Science and Technology 32(21):3305-3311.

Ravichandran M., Aiken, G.R., Ryan, J.N., and Reddy, M.M., 1999. Inhibition of precipitation and aggregation of metacinnabar (mercuric sulfide) by dissolved organic matter isolated from the Florida Everglades. Environmental Science and Technology 33(9):1418-1423.

Ritson, P.T., Bouse, R.M., Flegal, A.R., and Luoma, S.N., 1999. Stable lead isotopic analyses of historic contemporary lead contamination of San Francisco Bay estuary. Marine Chemistry 64:71-83.

Rusello, P.J., 2009. A practical primer for pulse coherent instruments, Nortek Technical Note, TN-027, Nortek.

Ryan J.N. and Elimelech, M. 1996. Colloid mobilization and transport in groundwater. Colloids and Surfaces A: Physicochemical and Engineering Aspects 107: pp. 1-56.

San Francisco Estuary Institute (SFEI), 2003. The Pulse of the Estuary: Monitoring and managing contamination in the San Francisco Estuary. SFEI Contribution 74. San Francisco Estuary Institute, Oakland, CA.

San Francisco Estuary Institute (SFEI), 2004. The Pulse of the Estuary: Monitoring and Managing Water Quality in the San Francisco Estuary. SFEI Contribution 78. San Francisco Estuary Institute, Oakland, CA.

Schuster, E. 1991. The behavior of mercury in the soil with special emphasis on complexation and adsorption processes - A review of the literature. Water, Air, and Soil Pollution 56(1):667-680.

Schwarzbach, S.E., T.H. Suchanek, G.H. Heinz, J.T. Ackerman, C.A. Eagles-Smith, T.L. Adelsbach, J.Y. Takekawa, A.K. Miles, D.J. Hoffman, S.E. Wainwright-De La Cruz, S.E. Spring, M.A. Ricca, and T.C. Maurer. 2005. Mercury in birds of the San Francisco Bay-Delta: trophic pathways, bioaccumulation and ecotoxicological risk to avian reproduction. 2005 Annual Report to CALFED, U. S. Geological Survey, Western Ecological Research Center, and U. S. Fish and Wildlife Service, Sacramento Fish and Wildlife Office, 17pp.

Shimadzu 2008. Total Organic Carbon Analyzer - TOC-V series (Model: TOC-V CPH, no. C392-EO58G). Shimadzu Scientific Instruments: 20 pp., www.shimadzu.com. Access: 07/2008.

Singh, S.P., Tack, F.M.G., Gabriels, D., and Verloo, M.G., 2000. Heavy metal transport from dredged sediment derived surface soils in a laboratory rainfall simulation experiment. Water, Air, and Soil Pollution 118:73-86.

Sobczak, W.V., Cloern, J.E., Jassby, A.D., and Müller-Solger, A.B. 2002. Bioavailability of organic matter in a highly disturbed estuary: The role of detrital and algal resources. Proceedings of the National Academy of Science of the United States of America 99 (12):8101-8105.

Spinelli, G.A., Fisher, A.T, and Wheat, C.G., 2002. Groundwater seepage into northern San Francisco Bay: Implications for dissolved metals budgets. Water Resources Research 38(7). Doi: 10.1029/2001WR000827.

Squire, S., Scelfo, G.M., Revenaugh, J., and Flegal, A.R., 2002. Decadal trends of silver and lead contamination in San Francisco Bay surface waters. Environmental Science Technology 36:2379-2386.

Srodon, J., Drits, V.A., McCarty, D.K., Hseih, J.C.C., and Eberl, D.D. 2001. Quantitative X-Ray Diffraction Analysis of Clay-Bearing Rocks from Random Preparations. Clays and Clay Minerals 49(6):514-528.

Stoicheva, T., Amourouxa, D., Wassermanc, J.C., Pointa, D., De Diegod, A., Bareillea, G., and Donard, O.F.X. 2004. Dynamics of mercury species in surface sediments of a macrotidal estuarine-coastal system (Adour River, Bay of Biscay). Estuarine, Coastal and Shelf Science 59(3):511-521.

Süß, E. 2006. Mercury distribution between particulate and dissolved states in wetlands in California, USA. Master Thesis, TU Bergakademie Freiberg, Freiberg Online Geosciences ISSN 1434-7512, Volume 15. 155 pp.

Telliard, W.A. and Gomez-Taylor, M. 2002. Method 1631, Revision E: Mercury in water by oxidation, purge and trap, and cold vapor atomic fluorescence spectrometry. United States Protection Agency, EPA-821-R-02-019: 38 pp. U.S.EPA (2004): TECHNICAL MEMORANDUM: Origin of 1 Meal/Week Noncommercial Fish Consumption Rate in National Advisory for Mercury. United States Environmental Protection Agency: 5 pp.

Torres R., Goni M. A., Voulgaris G.V., Lovell C.R., and Morris J.T., 2004. Effects of Low Tide Rainfall on Intertidal Material Cycling. In The Ecogeomorphology of Tidal Marshes. S. Fagherrazi, M. Marani, L. Blum (eds.). Coastal and Estuarine Studies 59. American Geophysical Union. Pp. 93-114.

Twardowski, M. S., Boss, E., Sullivan, J. M., and Donaghay, P. L. , 2004. Modeling the spectral shape of absorption by chromophoric dissolved organic matter. Mar. Chem. 89: 69–88, doi:10.1016/j.marchem.2004.02.008.

U.S. Geological Survey, 2006. Collection of water samples (ver. 2.0): U.S. Geological Survey Techniques of Water-Resources Investigations, book 9, chap. A4, September 2006; *http://pubs.water.usgs.gov/twri9A4/* (accessed 11/29/11).

Waples. J.S., Nagy, K.L., Aiken, G.R., and Ryan, J.N. 2005. Dissolution of cinnabar (HgS) in the presence of natural organic matter. Geochimica et Cosmochimica Acta 69 (6):1575-1588.

Warner, J.C., Schoellhamer, D.H., Ruhl, C.A., and Burau, J.R., 2004. Floodtide pulses after low tides in shallow subembayments adjacent to deep channels. Estuarine, Coastal and Shelf Science 60:213-228.

Weiner, J.G., Gilmour, C.C., and Krabbenhoft, D.P., 2003. Mercury Strategy for the Bay-Delta Ecosystem: A Unifying Framework for Science, Adaptive Management, and Ecological Restoration. http://calwater.ca.gov/Programs/Science/adobe_pdf/MercuryStrategy_FinalReport_1-12-04.pdf

Weishaar, J.L., Aiken, G.R., Bergamaschi, B.A., Fram, M.S., Fujii, R., and Mopper, K. 2003. Evaluation of specific ultraviolet absorbance as an indicator of the chemical composition and reactivity of dissolved organic carbon. Environmental Science and Technology 37(20):4702-4708.

Wood, M.L., Foe, C., Cooke, J., and Louie, S.J., 2010. Sacramento – San Joaquin Delta Estuary TMDL for Methylmercury. Staff Report. Draft Report for Public Review. Regional Water Quality Control Board – Central Valley Region. February 2010, 233 p.